2015

Design of A Novel Low - Cost, Portable, 3D Ultrasound System with Extended Imaging Capabilities For Point-of-Care Applications

Michail Tsakalakis
Wright State University

DESIGN OF A NOVEL LOW – COST, PORTABLE, 3D ULTRASOUND SYSTEM
WITH EXTENDED IMAGING CAPABILITIES
FOR POINT-OF-CARE APPLICATIONS

A dissertation submitted in partial fulfillment of the
requirements for the degree of
Doctor of Philosophy

By

MICHAIL TSAKALAKIS

B.S., National Technical University of Athens, 2011

2015
Wright State University

WRIGHT STATE UNIVERSITY

GRADUATE SCHOOL

August 21st, 2015

I HEREBY RECOMMEND THAT THE DISSERTATION PREPARED UNDER MY SUPERVISION BY Michail E. Tsakalakis, ENTITLED Design of a Novel Low−Cost, Portable, 3D Ultrasound System with Extended Imaging Capabilities for Point-Of-Care Applications BE ACCEPTED IN PARTIAL FULFILLMENT OF THE REQUIREMENTS FOR THE DEGREE OF Doctor of Philosophy.

_____
Nikolaos Bourbakis, Ph.D.
Dissertation Director

_____
Michael Raymer, Ph.D. Director,
Computer Science & Engineering
Ph.D. Program

_____
Robert E. W. Fyffe, Ph.D. Vice
President for Research and Dean of
the Graduate School

Committee on
Final Examination

_____
Nikolaos G. Bourbakis, Ph.D.

_____
Soon M. Chung, Ph.D.

_____
Yong Pei, Ph.D.

_____
Konstantina Nikita, Ph.D.

_____
Catherine Marco, Ph.D.

I dedicate this dissertation to my beloved wife, Christina Nikolopoulou,

who has been a constant source of support and encouragement during the challenges of

graduate school and life. I am truly thankful for having you in my life.

ACKNOWLEDGMENTS

I would like to thank all the individuals who helped me complete this enriching and exciting doctoral journey. Professor Nikolaos Bourbakis provided constant support and invaluable guidance through the past several years. I appreciate all his contributions of ideas, time, and funding to make my Ph.D. experience productive and successful.

I also wish to thank the Ph.D. committee members, Soon M. Chung, Yong Pei, Konstantina Nikita and Catherine Marco, for their contributions. They all had major positive influence on this Ph.D. work and it was a real pleasure working with them. Moreover, I would like to acknowledge all my colleagues support during the past 3 years, and especially Konstantinos Michalopoulos, Ph.D., for not only being a real friend but also a mentor during this journey.

Last but not least, I would like to express my gratitude to my friends and family, who have always been there for me, bringing out the best in me. Without them, this dissertation would have been an even tougher venture.

ABSTRACT

Tsakalakis Michail. PhD., Department of Computer Science and Engineering, Wright State University, 2015. Design of a novel low-cost portable, 3D Ultrasound System with extended imaging capabilities for point-of-care applications.

Ultrasound Imaging (USI) or Medical Sonography (MS), as it is formally called, has been widely used in biomedical applications over the last decades. USI can provide clinicians with a thorough view of the internal parts of the human body, making use of sound waves of higher frequencies than humans can perceive. USI systems are considered highly portable and of low–cost, compared to other imaging modalities. However, despite those advantages, Ultrasound Systems (US) and especially 3D ones, have not been yet extensively utilized for Point-of-Care (POC) applications, due to numerous restrictions and artifacts that they currently present.

Hardware complexity and real-time requirements are considered to be the major restrictions for portable, 3D (volumetric) USI. Volumetric transducers consist of thousands of piezoelectric elements that make the signaling and the networking of the system extremely complex. Additionally, regions of the internal body require significantly long time to be scanned in the three dimensions. Consequently, real-time applications are considered prohibited. Last, but yet equivalently important, most of the low-cost, portable systems manifest artifacts that degrade the quality of ultrasound image. It is obvious that

researchers' concern and major challenge is to successfully address those problems and manage offset the strong trade-offs that exist.

Given the aforementioned challenge, the current research work presents a novel low–cost, portable 3D Ultrasound system design, composed of four volumetric transducers. The system has been designed for POC applications in a way to manifest extended imaging capabilities. The use of multiple (four), simple 2D phased array transducers is adopted in order for the system to provide enhanced field of view, as well as automatic scanning of the Region of Interest (ROI) (radiologist intervention-free). In order to deal with the high complexity of the system, the transducers were designed with limited number of elements (256 each) and were integrated to a single FPGA board. To compensate for the image degradation caused by transducers of fewer elements, a new image enhancement methodology was proposed. The methodology targets to image de–speckling and image resolution improvement, given the redundant information provided by the multiple transducers. It uses a combination of spatial and frequency compounding techniques along with a Super-Resolution (SR) algorithm. In order to vindicate the selection of the techniques that were used for the proposed methodology, a parametric study regarding the performance of numerous de-noising and SR techniques was conducted. The performance of the methodology was firstly tested using typical 1D phased array transducers and the results in the 2D images offered promising insights its advantages.

Having verified the effectiveness of the proposed methodology for the case of 2D ultrasound images, the methodology was extended to volumetric images. The final de-noised B-mode images manifested increased Contrast Noise Ratio (CNR) and Signal to

iv

Noise Ratio (SNR) compared to various other ultrasound image de-speckling techniques, while at the same time image resolution improvement was observed.

The novel low–cost, portable 3D Ultrasound system design that is proposed, combined with the new image enhancement technique implemented, successfully addresses the existing challenges, in regards to the trade-off between system complexity and image quality. In fact, it not only develops a system of significantly lower complexity but the same time tackles the disadvantages that such a system could have, by integrating in the design the component of image enhancement.

TABLE OF CONTENTS

vii

xi

www.manaraa.com

xii

LIST OF TABLES

xiv

LIST OF FIGURES

xvii

xix

1
INTRODUCTION

1.1   Background and Motivation

During the last few decades, there has been an increasing interest of the scientific community towards continuous, real-time, remote monitoring through medical Point–of–Care (POC) and Personal Health Management (PHM) systems, for healthcare monitoring and diagnostic applications. POC and PHM are acronyms that are used to describe almost the same kind of systems[1], i.e., low-cost, highly portable apparatus that are used for Point–of–Care Testing (POCT). The term POCT refers to medical examination that is performed near to the patient's location [1] and is quite often called bedside testing. POC systems may have the form of portable, wearable and implantable apparatus and contribute to the betterment of today's healthcare system which suffers from fundamental hindrances (highly expensive, slow and inefficient). The main purpose of such systems is to support the vision of citizen-centered healthcare [2] which hopes to the transformation

---

[1] In the current dissertation, only the term POC will be used from now on.

1

of current healthcare system and its extension, beyond the dedicated sites such as hospitals. Additionally, citizen-centered vision targets to increase awareness and involvement of citizens-patients in all stages of care.

Technological advancements in the fields of digital electronics, communications, and information technology, to name but few, have made this vision, reality. These advancements, along with the emerging and continuous evolving POC applications have intrigued a big portion of the scientific community. The number and heterogeneity of such devices and systems regarding both software and hardware components, i.e. sensors, antennas, acquisition circuits, as well as the medical applications that are designed for, is impressive.

1.2   Problem Definition

Despite the plethora of POC systems, currently there are only few able to provide clinicians with the internal view of human organs. It is a matter of fact that the most promising apparatus for portable imaging is considered to be the ultrasound devices. Certain advantages of Ultrasound (US) systems, compared to other imaging modalities such as Magnetic Resonance Imaging (MRI) and Computed Tomography (CT), have rendered them to the first candidate for bedside testing, since they can play a significant role towards low-cost, continuous, remote monitoring.

Although US machines are considered of low-cost and highly portable, there are certain limitations and restrictions that need to be studied and get addressed in order for them to be fully utilized for POCT. Among the most prominent restrictions is a) the system's high complexity, especially for 3D systems, b) the low quality of the generated image, especially

2

in the case of low-cost, highly portable 3D machines, c) the difficulty to produce real-time 3D images (4D Ultrasound Imaging) as well as that d) the outcome highly depends on the radiologist's skills. As a result, it is currently necessary that these weaknesses get addressed in order for the modern healthcare systems to get advantage of the great potential that USI has, in the diagnosis and treatment of serious diseases.

1.3   Research Objectives

The existing flaws that US systems currently present, have highly driven the reasoning of this dissertation. In particular, the research objectives of the current dissertation can be summarized as follows:

- Highlight, study and examine the aforementioned restrictions and limitations that current POC US systems manifest.

- Propose an alternative way of ultrasound examination, independent of the radiologist's skills. That is, a system to be capable of automatic scanning of the volume of interest (VOI) without the guidance of the radiologist. It is worth highlighting that this way of examination is only possible for ultrasound applications where only structural information is required and not functional.

- Propose (define hardware and software components) a novel low-cost, portable 3D ultrasound device for POC applications, capable to provide 3D representation of the internal of the human body without the need of the physical presence of an experienced radiologist on site. This consists of the following lower-level objectives:

3

- ❖ Design 2D phased array transducers, with limited number of active elements, to reduce system's complexity.

- ❖ Develop and introduce a new 3D image processing and analysis methodology that can be applied for the image acquisition process, in order to achieve the best possible image enhancement, given the proposed architecture.

1.4 Methodology

Herein, the proposed approach to tackle the challenges and provide viable solutions to numerous restrictions posed during the design of portable ultrasound systems is described.

Firstly, in order to force the system become capable of automatic region scanning and the final outcome independent of radiologist skills, the use of multiple volumetric transducers is adopted. In particular, four 2D phased array transducers were used in a 2x2 array configuration. In that way, whole VOIs can be automatically monitored without the need of region scanning by an experienced radiologist. The actual design of the system was performed in three distinct parts; a) design of the transducers, b) design of hardware components of the system and c) development of new 3D image reconstruction and a new 3D image enhancement methodology.

Moreover, in order to address the burden of increased complexity that is observed in the case of 2D phased array transducers, the proposed ones were designed to consist of the smallest possible number of active elements. This number, was determined by the capability of the transducers to provide an image of a moderate quality. Transducers that

4

use in total 16x16 = 256 number of elements were used and their performance was then evaluated.

As far as the hardware component is concerned, its design was driven by the need of the system to fulfill certain requirements. Those were the following; portability-miniaturization, cost-effectiveness, low complexity, low power consumption, configurability and scalability. For all the above requirements, the use of a single chip capable to host the analog part (analog front-end) and one FPGA was adopted. The analog part was designed to host 16 independent channels and be responsible of the front-end processes while the mid-end processes were dedicated to the FPGA. Regarding the back-end processes, they were implemented to a regular Personal Computer (PC) and performed off-line.

The selections made in the previous steps have a major drawback. Most of them degrade the quality of the final image produced. Therefore, in order to compensate for the loss of image quality due to these hardware restrictions, two new software-based methodologies were proposed. The first one, is a new 3D image reconstruction method, based on the information provided by multiple transducers. The second one targets at the enhancement of image quality, trying to overcome known artifacts and limitations that exist, such as speckle, low resolution image. A combination of known de–speckling techniques, such as spatial and frequency compounding, with the use of Super-resolution (SR) technique entail the basis of the second methodology.

The use of a simulation tool for ultrasound transducers was critical for the current study, for both the design phase of the system as well as the generation of the simulated ultrasound

5

data, in order to test the validity and effectiveness of the proposed methodologies. In order for the needs of the current study to be addressed, Field II was used, a program for simulating ultrasound transducer fields and ultrasound imaging, using linear acoustics under the environment of MATLAB. The selection of Field II as the primary tool, was based on two critical factors; a) it is publicly available and b) it is widely used. Field II was used to generate the required data (2D and 3D ultrasound images) in order to apply the proposed methodologies. Initially, 2D images were used, in order for the applicability and the effectiveness of the proposed image processing methodology to be tested. In particular, this stage significantly guided the latter development of the final 3D image enhancement technique. The acquired results after applying the proposed methodology were compared to existing techniques and revealed that such a device can deliver clinicians ultrasound images of higher quality, compared to hand-held systems that use stand-alone transducers of the same type.

1.5   Research Contributions

The research contributions of the current dissertation can be summarized as follows:

- Presentation and classification of sensor and biosensor-based systems for POC monitoring applications and proposal of a maturity metric for system's performance evaluation.

- Design of a novel low-cost portable 3D ultrasound system, consist of multiple 2D phased array transducers.

6

- Design of 2D phased array transducer with reduced number of elements for cost and complexity reduction.

- Development of a new 3D image reconstruction methodology based on the information provided by multiple transducers.

- Development of a new 3D image processing methodology for ultrasound image enhancement.

  ➢ Development of a new 3D Super Resolution algorithm

1.6   Dissertation Organization

Chapter 1 acted as an introduction, providing the background and motivation for this study, as well as an overview of the research methodology covering several distinct phases. The rest of the dissertation is organized as follows. In Chapter 2, a brief survey in the field of POC sensor–based wearable and implantable systems is presented, mainly for monitoring applications. In Chapter 3, the technical background of ultrasound imaging systems is discussed along with limitations, artifacts and numerous challenges that currently exist and have attracted the interest of the scientific community. Given the existing limitations of current technologies, Chapter 4 presents a novel low-cost portable 3D ultrasound device with extended capabilities. Chapter 5 identifies all image related artifacts of ultrasound images, and discusses existing techniques for image enhancement. Finally, it proposes a new methodology based on the architecture described in Chapter 4, for ultrasound image enhancement. The aforementioned methodology is implemented in Chapter 6 in the case of 2D images, in order for the previously proposed image

7

enhancement methodology to be tested. Then in Chapter 7, the methodology is implemented for 3D images and are presented and discussed. Finally, Chapter 8 presents the conclusions, contributions and limitations of this research, as well as a discussion on the future challenges.

2

LITERATURE REVIEW

2.1 Introduction

It is generally acknowledged that today's healthcare system suffers from fundamental hindrances, whereas the same time it is considered to be highly expensive, slow, bureaucratic and inefficient. From the other side, the costs in all stages of care monitoring, management, treatment and follow-up of various diseases using current approaches, are continuously rising [3]. Additionally, the major problem of population ageing [4] along with all its consequences, is one of the main factors that has contributed to the inadequacy of the today's healthcare system to address growing needs. Finally, the current methods utilized for management and supervision of chronically ill people are considered outdated. Thus, there is an obvious and urgent need for novel, low-cost, practical and feasible solutions to be found, in order for the current system to be transformed to a faster, efficient, effective and less expensive one.

From the other side, recently a new concept that promotes the customization of healthcare upon the individual's needs has attracted significant attention. Personalized medicine is considered as one of the most emerging approaches for effective treatment and management [5], being driven by the notion that clinicians can deliver more effective and targeted treatment to their patients by monitoring each individual and keeping track of their clinically readable habits. Significant innovations towards individualized medicine are driven by advances in biocompatible materials [6], biomarkers [7] and biosensors [8].

Additionally, the need for remote monitoring is apparent since it can be beneficial not only to the patient but also constitute a great relief to the already bloated healthcare system, as a whole. Remote monitoring includes but is not limited to monitoring of the following groups; a) a frail group of people in their physical setting, in their bedside, b) people in the emergency room or ambulance [9] c) athletes or a group of people who cannot afford or do not have access to hospitals and finally d) people in hostile environments, such as battlefields, and places that have suffered natural disasters [10].

Finally, it is known that different preventive medicine strategies can significantly reduce the overall cost spent in healthcare, depending on the level of prevention. In fact, preventive strategies and methods can considerably contribute to early diagnosis and treatment, or even to disease preclusion.

All the previously discussed issues and notions, i.e., a) shortcomings of healthcare system, b) personalized medicine c) need for remote monitoring and d) preventive medicine, can be supported and enhanced with the use of low-cost, sophisticated POC medical monitors of various physiological and biochemical signals. So far, advancements

10

in certain key technologies have contributed to the burst development of those systems. Evolution in microelectronics and digital electronics have led to the development of low-cost, low-power consumption circuits such as microprocessors, Application Specific Integrated circuits (ASICs) and Field Programmable Gate Arrays (FPFAs) that can provide portable real-time, continuous monitoring solutions for signals acquisition and analysis. Innovations in integrated sensors and Micro-Electro-Mechanical Systems (MEMS) create new challenges that future sensory systems have to address [11]. New wireless communication schemes, such as the Medical Implant Communication Services (MICS) band or Industrial and Scientific Medical (ISM) radio bands, have been reserved for a variety of industrial, scientific and medical applications. Finally, as stated in [12], the illusion of infinite computing resources that cloud computing can offer, can be extremely beneficial for the computational demanding medical applications where huge amount of data need to be stored for further off-line processing.

Given the analysis above and the continuously evolving POC applications, it is currently very important to thoroughly review the state-of-the-art medical devices, as well as assess them in regards to their suitability to be effectively incorporated in the modern healthcare system. Thus, in the following section, a review on presently popular POC systems is presented, whereas details of a maturity evaluation procedure that was conducted for sensor–based systems is further discussed.

2.2 Survey on Health Care Sensor–Based Systems for Point-of-Care Monitoring and Diagnostic Applications

2.2.1 Point-of-Care (POC) Healthcare Monitoring Systems

A high level categorization of POC medical systems is illustrated in Figure 2-1. Although, in the present survey we review only devices that are dedicated to physiological monitoring purposes, it is important to briefly mention others, dedicated to medical intervention.
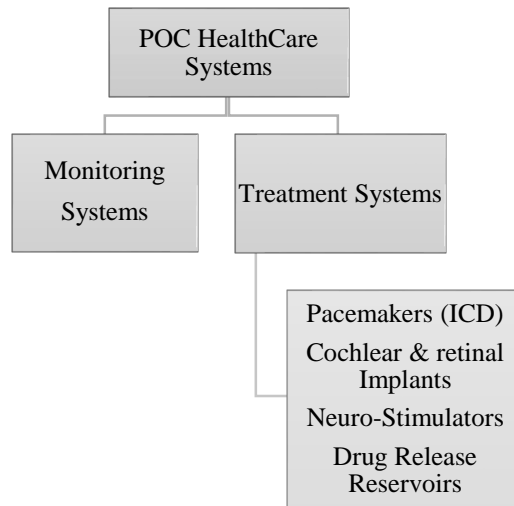
Figure 2-1: High level categorization of POC healthcare systems

Thus, as far as the treatment is concerned, several systems exist. Retinal [13] and cochlear [14] implants rise the expectations of visually and hearing impaired patients. Spinal cord stimulators (SCS) [15], deep brain stimulators (DBS) [16], intravesical stimulators and gastric electrical stimulators are few of the systems extensively used for

the management of neurological disorders. Last but not least, drug release reservoirs [17] can deliver very effective and targeted treatment to groups of people suffering from chronic diseases, cancer and cardiovascular disease (CVD) related disorders.

In the following section, emphasis is given in our area of interest which is the POC monitoring systems, as also shown in Figure 2-2 below.
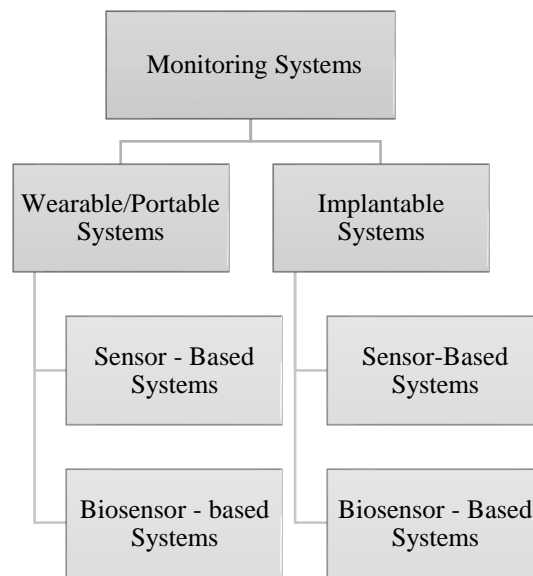
Figure 2-2: High level categorization of POC monitoring systems

2.2.1.1 Wearable/Portable (W/P) Sensor – Based Monitoring Systems

The major categories of such systems are the following: a) *electrocardiogram* (ECG) sensors/platforms for monitoring of cardiac activity and CVD pathologies[18], [19], b) *electroencephalogram* (EEG) sensors/platforms [20] for brain activity screening and brain disorders identification, c) *electromyogram* (EMG) sensors for measuring the electrical activity of muscles for muscular dystrophy, inflammation of muscles, pinched nerves,

13

peripheral nerve damage, d) *blood pressure* sensors for heart related diseases, e) *motion sensors*, such as accelerometers for fall detection and Parkinson related problems [21] and f) *others*, such as for oxygen saturation, temperature and heart rate sensing, that can provide clinicians with valuable complementary information regarding the general health state of the subject. Other systems utilize sensors to capture the electrodermal activity [22] which is highly related to the sympathetic nervous system activity, pulse detection sensor for detecting loss of radial pulse in order to prevent Sudden Cardiac Death (SCD) [23] and g) *ultrasound* sensory systems [24] for internal organs imaging.

2.2.1.2   Implantable Sensor – Based Monitoring Systems

In this category, the Implantable Medical Devices (IMDs) designed for screening and diagnostic applications are examined. The major categories can be divided in: a) *blood flow* sensors [25] usually integrated with vascular prosthetic grafts for early detection of graft degradation or failure, b) *blood pressure* sensors [26][27][28] for heart failure and CVD detection, c) *intraocular pressure* sensors [29] for managing visual related disorders, d) *intracranial pressure* [30][31] sensors for diagnosis or management of neurological disorders such as hydrocephalus and Traumatic Brain Injury (TBI), e) *bladder pressure* [32] sensors for monitoring of the intravesical pressure, that can be informative about kidney's state or detect the manifestation of urinary tract infections, f) *wireless endoscopy pills* [33] that transmit images of gastrointestinal tract (GI tract) and g) *others,* that can measure temperature and oxygen saturation for complementary information.

14

2.2.1.3   Wearable/Portable (W/P) and Implantable Biosensor – Based Systems

Biosensor-based systems are more sophisticated and complex systems, capable of measuring certain biomarkers. Biomarkers are certain substances in human organism such as biomolecules, analytes or biochemical reactions that can be objectively measured and act as indicators of normal or abnormal health state. The main difference between a sensor and a biosensor is that in the latter, there is a bio-recognition element responsible for immobilizing the correct substance to be measured. Measurement of biomarkers is performed in highly equipped laboratories from trained personnel. With the advent of MEMS and the progress observed in biomaterials and tissue engineering, new technologies such as Lab–on–a–Chip (LoC) [34] or System–on–a–Chip (SoC) can enable POC biosensors for monitoring and treatment of outpatients. For instance, glucose meters [35] for managing diabetes and lactate biosensors for CVD management are the two most widely used systems today.

2.2.2   *Maturity Evaluation of Sensor – Based Monitoring Systems*

In this section a comparative study is presented among selected devices that have been proposed in literature. As mentioned above, the focus of this procedure is the sensor-based monitoring systems, both wearable/portable and implantable ones, as shown in Figure 2-3.

15
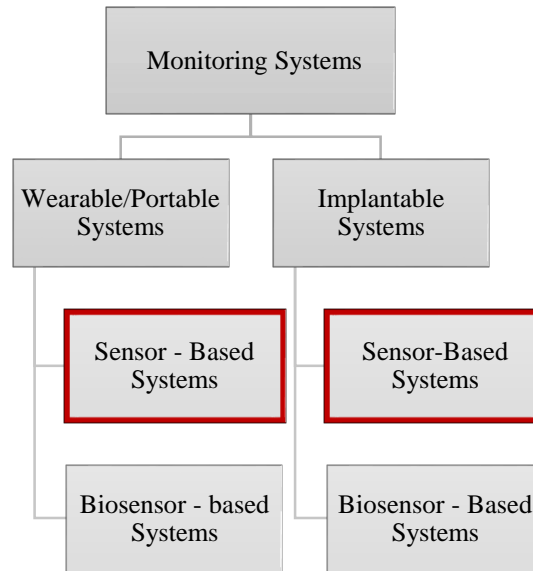
Figure 2-3: Focus area of the maturity evaluation procedure

Each device is evaluated, based on their *"maturity"* to be part of the medical market. All technologies were selected to fulfill certain criteria; a) compose a complete well-described system for a particular application, b) have an impact on the scientific community (most frequently cited papers) and c) provide adequate information, in regards to their performance. At this point, it is worth highlighting that the purpose of the maturity metric is not to criticize or compare each system's performance, but on the contrary, to reveal shortcomings and deficiencies that could be the driving force for further improvements.

A similar methodology to the one presented in [36] was adopted and applied in the two main categories, i.e. wearable/portable and implantable sensor – based devices, for monitoring applications with appropriate modifications.

16

2.2.2.1   Description of the Maturity Evaluation Procedure

This process can be divided into three basic steps: a) feature selection, b) feature weighting and finally c) score assignment and maturity evaluation.

- Step 1: Feature Selection
  The first and most important step for the evaluation of "maturity" was the selection of appropriate features that can fully characterize the performance of a particular device. Wearable/portable devices possess different restrictions compared to implantable devices, thus different features must be selected in each category.

- Step 2: Feature Weighting
  Due to the fact that several parties are involved in the chain, from the early stages of product design, up to the introduction of the product to the market of POC medical systems, it is necessary that their opinion is taken into account, regarding the significance of each feature. Three different groups were taken into consideration, i.e., patients, physicians and manufactures. Values from 1 to 5 (1 = indifferent, 5 = highly interested) were assigned to each feature, given the feedback from each one of the aforementioned groups, in regards to their interest. Then, for each feature i, the average of these values was calculated and used as a weight, i.e., Impact Factor (IF), as shown in (Formula 2-1) below.

$$IF_i = (PP_i + CP_i + MP_i)/3 \qquad (2\text{-}1)$$

In the Formula above, i represents the ith feature, as presented in Table 2-1 and

17

Table 2-2. For instance, i=3 represents the feature *"Ease of Use for Wearable and Biocompatibility for Implantable Devices"*. Last but not least, PP_i, CP_i and MP_i represent the opinion of each one of the groups considered, i.e., patients, physicians and manufactures, regarding the importance of feature i.

Table 2-1: Selected Features for W/P Systems (Step1)

Feature Name	Feature Description	Description
F_1	Accuracy	The ability of the sensor to measure the actual value
F_2	Application's Impact	The importance or the impact of the proposed application in the medical field
F_3	Ease of Use	Patients should feel no discomfort for the whole period they carry the device
F_4	Operational lifetime	Various applications require long term monitoring
F_5	Clinical Evaluation	Performance evaluation to verify system's functionality in real cases
F_6	Reliability	The ability of the device to perform its function not only under normal conditions but also in hostile environments
F_7	Power consumption	The energy that the device is about to consume in order to perform its task
F_8	Portability/ Wearability	System must have low weight and size and be appropriately placed on the body
F_9	Real time Application	The capability of the device to provide real time results
F_{10}	Continuous monitoring	The capability of the device for continuous monitoring
F_{11}	Resolution	The smallest change that sensor can distinguish
F_{12}	Security	Data towards and from the device should be securely transferred
F_{13}	Decision Support	The capability of the device to support diagnosis/decision mechanisms

18

Feature Name	Feature Description	Description
F_{14}	Cost	The overall amount required to produce the system
F_{15}	Size	The overall dimensions of the device

Table 2-2: Selected Features for Implantable Systems (Step 1)

Feature Name	Feature Description	Description
F_1	Accuracy	The ability of the sensor to measure the actual value
F_2	Application's Impact	The importance or the impact of the proposed application in the medical field
F_3	Biocompatibility	The ability of the implant to perform its supposed task without causing damage to the host
F_4	Discomfort	Patients should feel no pain or discomfort for the whole period they carry the device
F_5	Implant's lifetime	The time period from the placement of the device until there is no more functional
F_6	Efficiency	The extent to which time, effort or cost is well used for the intended task or purpose
F_7	Reliability	The ability of the device to perform its function not only under normal conditions but also in hostile environments
F_8	Power consumption	The energy that the device is about to consume in order to perform its task
F_9	Method of Placement	The surgical operation needed for the implant to be placed in the right position
F_{10}	Real time	The capability of the device to provide real time results
F_{11}	Continuous monitoring	The capability of the device for continuous monitoring
F_{12}	Clinical Validation	Tests for the evaluation of the device performance

19

Feature Name	Feature Description	Description
F_{13}	Resolution	The smallest change that the sensor can distinguish
F_{14}	Security	Data towards and from the implant to the external device should be securely transferred
F_{15}	Decision Support	The capability of the device to make certain decisions or interventions
F_{16}	Cost	The overall cost of the device itself and the surgical operation needed for the displacement
F_{17}	Size	The overall dimensions of the implant

- Step 3: Score Assignment and Maturity Evaluation

The final step is to assign to each device involved in the review process, a certain score (F_{ji}) for each feature. For each one of the devices, this score was assessed based on the statements and results provided in the respective literature. The Formula that was used for the final total score calculation, is called maturity and is given in Equation 2-2. This is actually the Normalized Total Score (NTS) for every device evaluated.

$$Maturity_j = NTS_j = (\sum_{i=1}^{n} IF_i * F_{j,i}) / \sum_{i=1}^{n} IF_i \qquad (2-2)$$

In the above, j is the jth system under consideration and can take values from 1 to k, where k is the total number of systems selected. Moreover, i is the ith feature under consideration and can take values from 1 to n, where n is the total number of features. Finally, F_{ji} is the score assigned to device j, with respect to feature i.

20

The average score per feature (FS$_i$) divided by 2 was calculated (using Equation 2-3) as an intention to capture and localize technological shortcomings.

$$FS_i = (\sum\nolimits_{j=1}^{k} F_{j,i}) / 2 * k \qquad (2\text{-}3)$$

For wearable/portable systems n = 6 and k = 15, while for implantable ones n=6 and k=17.

2.2.2.2   Wearable/Portable Sensor – Based Systems

The features that selected in this category to be assessed, are presented in Table 2-1. Moreover, the final maturity score for the considered devices (A[24], B[18], C[19], D[21], E[23], F[22]), As well as the average score of each feature are shown in Figure 2-4 and Figure 2-5.
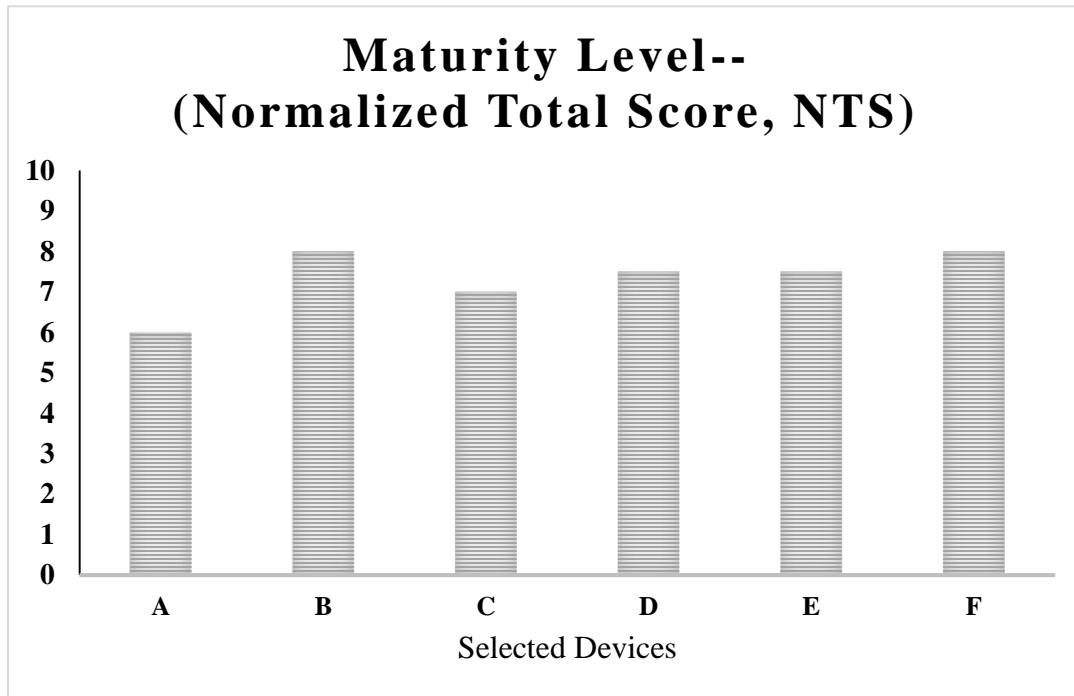
Figure 2-4: Maturity level for w/p systems (using eq. 2-1 and 2-2),
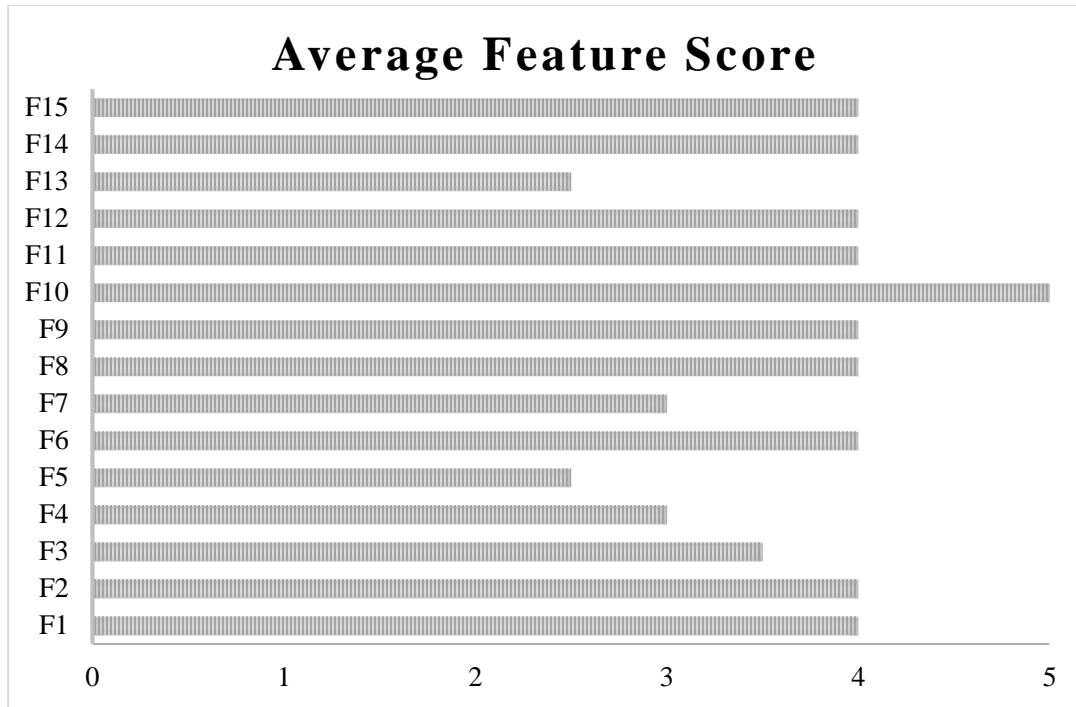
Figure 2-5: Average score per feature for w/p systems (using eq. 2-3)

2.2.2.3 Implantable Sensor–Based Systems

The features that were selected in this category to be assessed, are presented in

Table 2-2. As far as the final maturity score and the average score of each feature for

each one of the devices considered (A[25], B[28], C[32], D[29], E[26], F[31]), are shown

in Figure 2-6 and Figure 2-7, respectively.

22
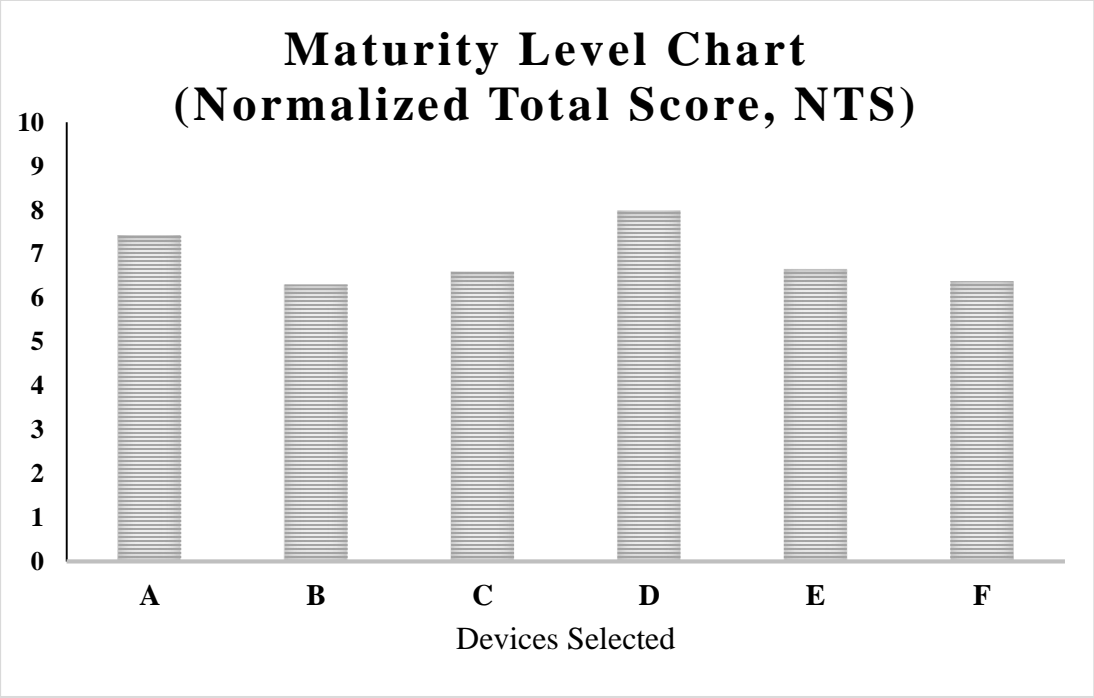
Figure 2-6: Maturity level for implantable systems (using eq. 2-1 and 2-2)

Figure 2-7: Average score per feature for implantable systems (using eq. 2-3)

23

2.2.2.4   Maturity Evaluation Results

As clearly shown in Figure 2-4 and Figure 2-6, none of the reviewed systems achieved the highest possible maturity score. Undoubtedly, despite their evolution during the last decades, there is still room for improvement and respective challenges need to be addressed for prolonged, real-time and ambulatory monitoring in both categories. Moreover, from Figure 2-5 and Figure 2-7, technical characteristics of such systems that require further attention, can be specified and localized. In fact, careful examination of all figures can reveal existing trade-offs and compromises among different technical features.

For w/p systems in particular, the triplet power consumption, operational lifetime and continuous recording is very critical for the designers. The required performance of one of the above directly affects the performance of the other two. For instance, setting a stricter power consumption requirement may result in reducing the operational lifetime of the device, or the continuous monitoring may be impossible. In addition, very few systems support decision making algorithms. Ongoing research is focused on the development of completely autonomous systems with diagnostic capabilities.

From the other side, developing implantable systems is a completely different problem and sets more restrictions and challenges to researchers. Size, power consumption, continuous monitoring and implants' lifetime, are technical features closely related. Ongoing research is focused on reducing the size of implant through different methods of power supply. Energy harvesting and remote transmission of power through inductive link are the main fields of interest. Finally, new biocompatible materials are required not only to ensure the safety of the patient but also for reliable and robust monitoring to be possible.

24

2.2.3 *Discussion on the Survey*

In this section, the state-of-the-art POC systems used in medical applications were discussed and a brief review of sensor-based systems was presented[37]. Concluding, it is important to highlight two important issues; a) the high heterogeneity of systems targeting at the management and monitoring of various diseases as well as b) the number of new features that can be attached to the current healthcare system. Development of POC systems, either simple or more sophisticated can deliver faster and more effective management for a wide range of pathologies. In addition, combination of biosensor-based systems with drug delivery reservoirs can potentially become a very powerful diagnostic and interventional tool. Besides this, the overall expenditures for healthcare and the total cost spent from patients, for medical care can be significantly reduced. In order for these devices to be smoothly embodied in the current system, it is highly recommended that researchers focus their efforts on addressing the issues discussed in the previous section while at the same time, the Food and Drug Administration (FDA) should exhaustively analyze feedback coming from current bearers and revise current regulations and standards accordingly, when necessary.

2.3   Conclusions

As elucidated above, during the last century an inclination towards personalized health care and POC monitoring has been observed. In the previous section a brief survey on wearable and implantable POC systems for monitoring of physiological signals was performed, and the new trends towards a more sophisticated and effective healthcare

25

system were discussed. Moreover, restrictions, limitations and trade–offs that researchers should try to handle during the designing of such systems were highlighted.

The performed survey presented in the previous section, clearly indicates and reveals a lack of reliable, low–cost, POC imaging systems. Although the monitoring of physiological signals, such as ECG, EMG etc., have their own merit in prognosis or prevention of unwanted complications especially for critically ill subjects, there are cases where the numerous complications or failure of internal organs cannot be identified. Moreover, there is a need for low-cost imaging systems in nursing homes (either for elderly people or for people with disabilities), ambulances and emergency rooms, even besides patients' bed. Lastly, it is a matter of fact that the vast majority of earth's population does not have access or cannot afford the high priced imaging modalities, such as MRI, CT or even the high-end US machines located in big hospital centers.

USI systems, as mentioned in the introduction, are considered to be the most promising imaging modality for low cost remote monitoring. The reasons why ultrasonography has attracted the interest of numerous researchers and clinicians and in particular for POC applications, during the last decades are apparent. Ultrasonography is a minimally or a non-invasive technique. In other words, is considered safer than other modalities that make use of ionizing radiation, such as electromagnetic waves, gamma and X-rays which their effects, when interacting with the biological tissues, are still under exhaustive examination. Additionally, the cost of US systems is relative low compared to the previous mentioned modalities. Finally US systems are highly portable devices and as a consequence more easily accessible for the general public.

26

In the following chapter, the principles and fundamentals of medical ultrasound machines are described. Moreover, the state-of-the-art ultrasound systems and in particular for POC applications are presented. Finally, their restrictions and limitations are identified and discussed as to propose a better alternative to the current proposed solutions.

27

3

BACKGROUND OF ULTRASOUND IMAGING SYSTEMS

3.1 Introduction

This chapter consists of four sections which provide the fundamentals of medical ultrasound and some of the major challenges that researchers need to deal with. In the first section, various applications that make use of ultrasound technology are discussed, with an emphasis given to medical ultrasonic applications. In the second one, the typical ultrasound imaging system and its components are presented, as well as the principles of ultrasonic wave generation and their interaction and transmission with and through the biological tissue (the actual medium). Types of various ultrasonic transducers are described in this section, along with the classical beamforming scheme and the image formation procedure for the case of B-Mode 2D ultrasound images. In the third section, certain peculiarities, challenges and limitations of current solutions are presented, with an emphasis on low-cost, portable machines for ambulatory monitoring. Finally, in the last section, a survey on

28

POC ultrasound systems is conducted as to reveal the ongoing research in the field and the different approaches adopted by the researchers.

3.2   Applications of Ultrasounds

In physics, ultrasounds are defined as acoustic waves that oscillate with frequencies higher than the ones that humans can hear (20 Hz – 20 kHz). A wide use of ultrasounds has been observed in various fields, for a wide variety of applications. To name but few, extensive use of ultrasonic waves is observed for non-destructive testing (NDT) or non-destructive evaluation (NDE) [38], [39], for Sounds Navigation and Raging (SONAR) systems, in robotics for object/obstacle detection and measuring distances [40], [41] as well as in numerous medical diagnostic or interventional applications [42], [43]. In medicine, ultrasound is used as diagnostic imaging technique, usually called Ultrasound Imaging (USI) or Medical Sonography (MS) or Ultrasonography that uses acoustic waves, operating in the frequency range of 2 - 20 MHz, for visualization of body structures and various internal organs. US imaging is one of the most widely used methods in medical imaging, along with the Computational Tomography (CT), Magnetic Resonance Imaging (MRI) and X-rays, for prognostic, diagnostic and therapeutic purposes, depending on the oscillating frequency of acoustic waves.

The reasons why ultrasonography has attracted the interest of numerous researchers and clinicians during the last decades, are apparent. Ultrasonography is a minimally and non-invasive technique whereas the acoustic waves that it produces make no use of ionizing radiation. The overall cost is considered to be relatively low, compared to previously mentioned modalities, such as MRI and CT and it is more easily accessible to

29

the general public. Almost every hospital, nowadays, is equipped with machines capable of providing 3D, even 4D (Real-Time 3D) tissue visualization of relatively good quality. Such images can provide physicians with vital information about normal or abnormal functionality of a wide variety of internal organs like lung, pancreas, liver to name but few.

In the first decades from the time that ultrasound was proposed, most of the medical applications were limited to gynecology and obstetrics [42], [44]. Nowadays ultrasound technology is used to identify and monitor a wide variety of pathologies and abnormalities as well as for therapeutic purposes. In therapeutics, efforts have been made to adopt ultrasound for bone-healing [45], thrombolysis (sono-thrombolysis) [46] and in general, to promote gene therapy to specific tissues [47]. Use in dentistry has been also reported [48].

Nevertheless, ultrasound technology is primarily used for diagnosis and monitoring purposes of the internal of the human body. Minimally invasive Intravascular Ultrasound (IVUS) is among the best techniques used so far in artery reconstruction and in the evaluation of atherosclerosis [49]. A wide number of diseases and pathologies associated with many abdominal organs such as lung [50], pancreas [51], liver [43] can be monitored and managed using ultrasound imaging techniques. Abdominal monitoring can be conducted either in hospitals with bulky and expensive machines, providing enhanced quality or with cheaper portable apparatus for POC testing. The present work focuses on the latter systems.

3.3   Typical Ultrasound System

Although there is a heterogeneity in ultrasound systems and methods, as it is also discussed later in this chapter, most of them are composed of three fundamental

30

components, as shown in Figure 3-1. These are the a) ultrasonic transducer(s), b) main board, which is responsible for the acquisition and the processing of the signal and finally, and finally c) the display monitor.

| Transducer | ←→ | Main Board | → | Display Monitor |
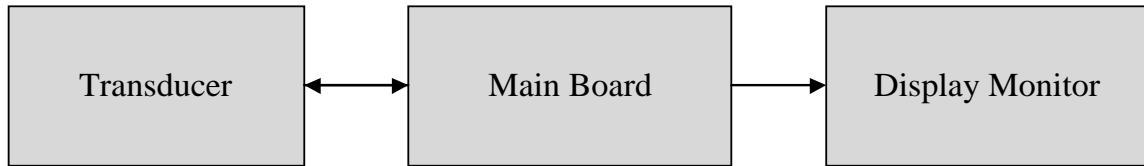
Figure 3-1: Basic Components of an Ultrasound Machine

The main board can be further divided into three parts; the a) front-end, b) mid-end and the c) back-end unit. The front-end unit is responsible for the integration of the transducer to the acquisition board and for the beamforming scheme to be adopted. Its complexity highly depends on the type of the transducer and the number of channels that are used to produce the final ultrasound image. In the mid-end and back-end units, all the appropriate signal and image processing techniques are applied to the raw data. Scan conversion entails the final step of the procedure and transforms the acquired processed data to a 2D readable image [52]. The fundamentals of ultrasounds are presented in the next section, by deconstructing an ultrasound system of typical topology, to its components.

3.3.1 Ultrasound Transducers

As the name indicates, ultrasonic transducer is the hardware component that is responsible for the transformation of the acoustic waves into electrical signal that can be processed by the appropriate circuit. It is the sensory module of every ultrasound system. The principle which most of the ultrasonic transducers are based on, is the piezoelectric effect. The piezoelectric effect, discovered back in 1880 by Jacques and Pierre Curie, refers

31

to the ability of certain materials (mostly crystals and ceramics) to generate electric charge as a result of applied mechanical stress (direct piezoelectric effect). The inverse procedure, which is the generation of mechanical stress when an electrical field is applied, is also feasible and is the basis of the production of ultrasonic waves (inverse piezoelectric effect). The piezoelectric effect is illustrated in Figure 3-2.
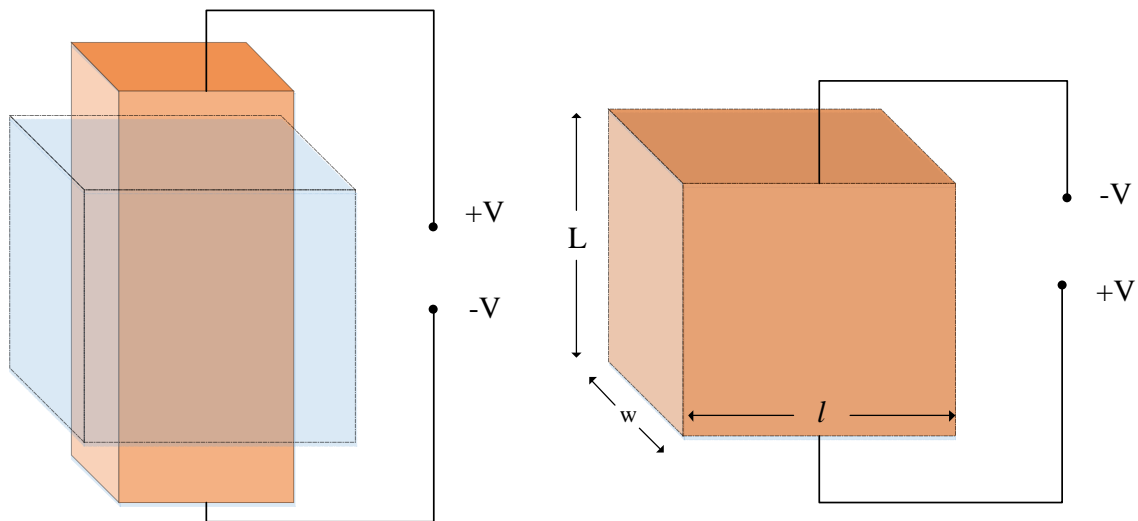
Figure 3-2: Piezoelectric Effect

Each transducer, in all ultrasound applications, consists of at least one piezoelectric element. Combinations of more than one elements may be also used, in order to produce enhanced acoustic signal. The shape and the dimensions of a piezoelectric element, along with the pulse excitation (applied electric field), determine the desired characteristics of the produced acoustic wave.

32

3.3.1.1 Important Characteristics

Different piezoelectric materials manifest different characteristics that are considered to be of great importance and are closely related to the performance of the transducer. The most important among them are the following; natural frequency (f_o), quality factor (Q), thickness (L), width (w) and length (l) of the element (Figure 3-2), as well as sound velocity (c_t) of the material.

Natural frequency (f_o), depends only on the properties of thickness and sound velocity of the piezoelectric material used. The most critical characteristic of a transducer though is considered to be the quality factor (Q) which shows the ability of the transducer to maintain the energy of the vibration internally. The quality factor is defined by the Formula 3-1, below,

$$Q = \frac{f_0}{\Delta f} \tag{3-1}$$

where Δf is the bandwidth, as defined in Figure 3-3.

33

Power Density
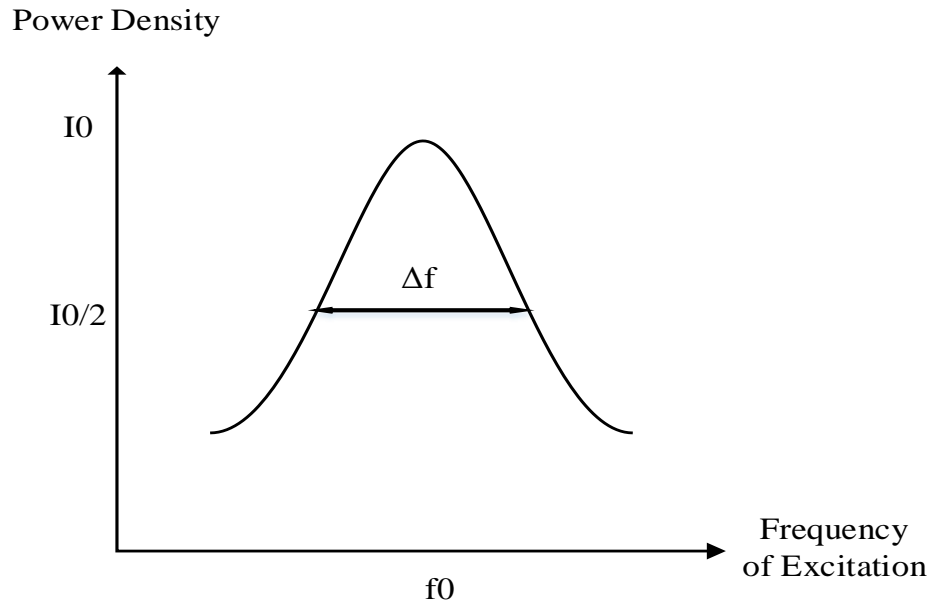
Figure 3-3: Transducer response around excitation frequency

The quality factor is a very important characteristic in ultrasound imaging, especially in systems that use the pulse echo mode. In such systems, the goal is to transmit the energy of the vibration towards the biological tissue and not to maintain it inside the transducer. That is why, for general purpose ultrasound imaging we desire a low quality factor.

In pulse echo mode the excitation of the transducer is achieved by applying a high amplitude pulse that makes it behave like a bell that is struck by a hammer. Such an excitation forces the transducer to oscillate with natural frequency but with an exponential decreasing amplitude (Figure 3-4).

34

Decaying sine function, $y(t) = \sin(wt)*\exp(-at)$
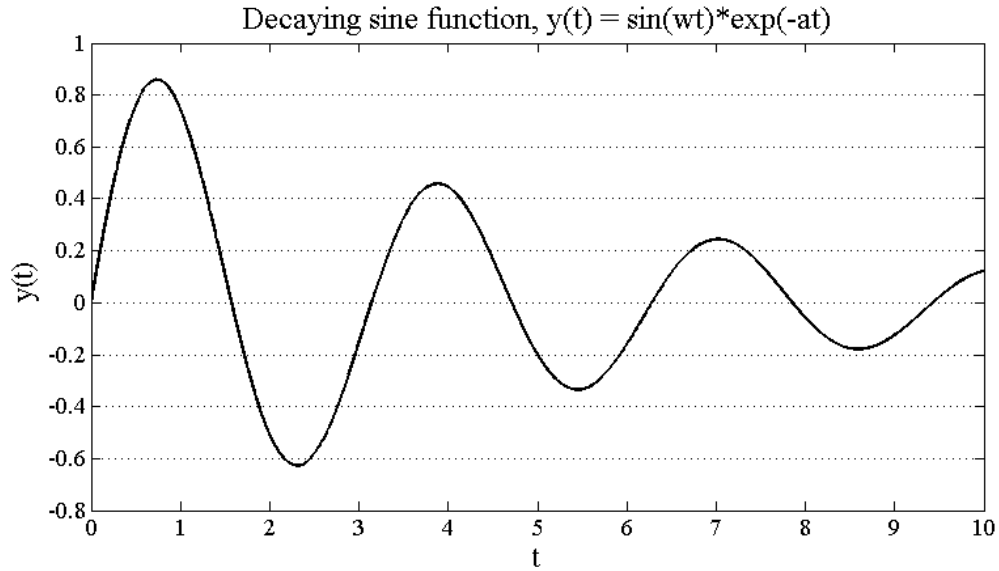
Figure 3-4: Generated sound wave when pulse echo excitation is applied

The larger the quality factor, the slower the exponential decrease (energy that is kept inside the transducer). When such an excitation is applied, the pulse duration (τ), which is the actual time form the generation of pulse until it fades away, is related with the quality factor with the formula:

$$\tau = \frac{Q}{2f_0} \tag{3-2}$$

Pulse duration is one of the most important characteristics, due to the fact that is related to the Axial Resolution (AR) of an ultrasound imaging system, defined in the following Equation:

$$Axial\,\mathrm{Re}\,solution = d = \frac{\tau c}{2} = \frac{Qc}{4f} = \frac{Q}{4}\lambda \tag{3-3}$$

From Equation 3.3, it is clear that low quality factor can lead to short pulse duration

35

and in turn to better axial resolution. The two characteristics explained above constitute the reason why for imaging purposes, piezoelectric materials with low quality factor are preferred. Typical values of quality factor for medical imaging range from 1 to10.

The performance of a piezoelectric transducer can be characterized by f_o and the beam pattern. Beam pattern is actually the amplitude of pressure (created by the sound wave) as a function of spatial coordinates, i.e., how the generated energy is diffused in space. For a circular (disc) transducer that its surface vibrates periodically a) without acoustic lens and b) with acoustic lens (for beam focusing), a simplified beam pattern is given in Figure 3-5. The beam pattern of a transducer, using focusing technique is a highly interesting plot, from where significant information can be derived, such as lateral resolution, focal length, focal size and depth of focus.
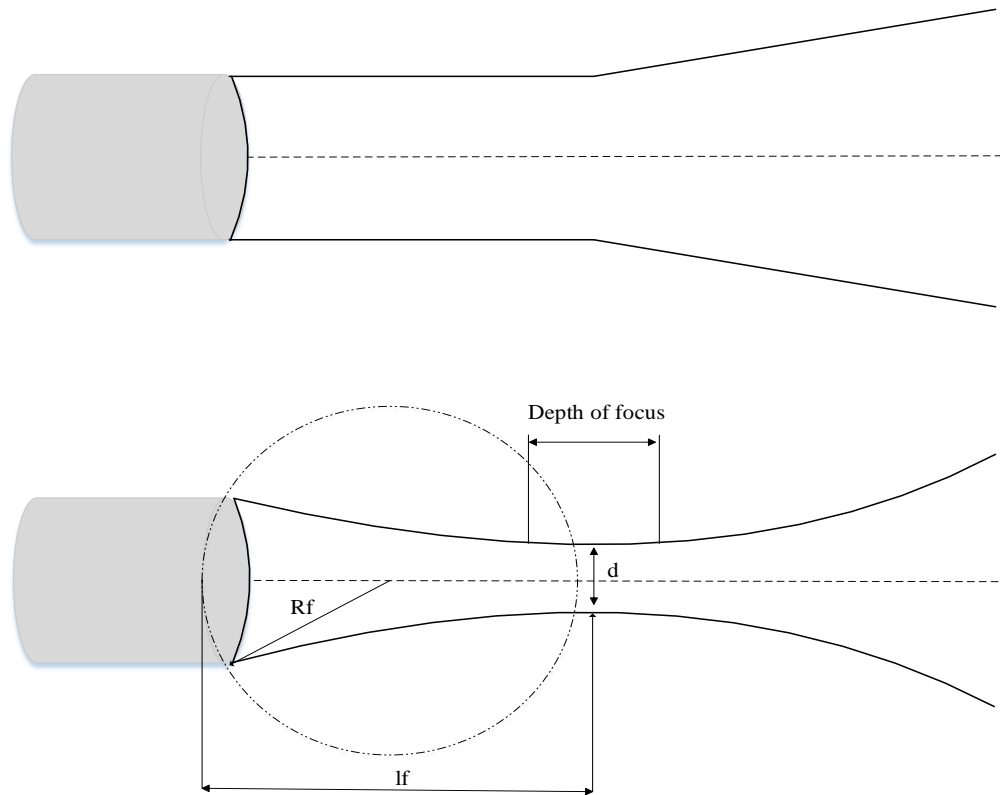
Figure 3-5: Beam profile of simple (upper) and a focused (lower) piston ultrasound transducer

Lateral resolution (LR) is defined as the ability of the system to distinguish two points in the direction perpendicular to the direction of the ultrasound beam. As it is observed from Figure 3-5, lateral resolution is location dependent and is equal to the beam width at that location. Another detail that requires attention is that lateral resolution is optimal at the focal point and degrades as we are moving away from focus. Focal length is actually the location of the focal point, for the described transducer, and is given by the Equation 3-4 below.

37

$$l_f = \frac{R_l}{1 - \dfrac{c_m}{c_l}} \tag{3-4}$$

Focal size, is the beam width at the focal length and thus the lateral resolution of a system that uses a circular element at that location and is given in Formula 3-5:

$$d_c = 2.44\left(\frac{l_f}{D}\right)\lambda \tag{3-5}$$

In this, D is the diameter of the transducer. In the case that a transducer of rectangular type is used, the corresponding beam width at the focal point is given by the Formula 3-6.

$$d_r = 2\left(\frac{l_f}{b}\right)\lambda \tag{3-6}$$

In this case, b is the width of the rectangular transducer.

Finally, Figure 3-5 shows that focusing is not achieved on one single point but instead on a wide zone called focal zone. The width of focal zone is called depth of focus and is described by the formula:

$$depth\ of\ focus = \left(\frac{d^2}{2\lambda}\right) \tag{3-7}$$

Comparing Equations 3-5 and 3-6 with Equation 3-7, it is obvious that focal zone depends on the focal size. In ultrasound imaging, it is very important that LR is kept uniform across the image. As a result, high depth of focus is preferred. On the other hand,

high focal size will result in lower lateral resolution for the imaging system. Therefore, lateral resolution versus depth of focus is another trade–off that researchers need to take under consideration.

In the previous analysis, the most important characteristics of a single element transducer were highlighted. These characteristics play an important role in the designing of the transducer of the proposed system. Most of the aforementioned formulas regarding the transducers characteristics can be modified, in order to describe any type of transducer, according to the application.

3.3.1.2   Types of Ultrasonic Transducers

In this subsection the different types of ultrasonic transducers for medical application are presented. Most of the piezoelectric transducers for medical applications (especially those that are intended for imaging applications) consist of numerous piezoelectric elements, in different array configurations. The geometrical configuration of the elements and the way that they are excited, defines the type of the ultrasonic transducer.

The first criterion for distinguishing ultrasonic transducers, is based on their ability (or inability) to steer or focus the acoustic beam and how they achieve the steering/focusing. According to this, three basic categories for ultrasound imaging can be identified; a) piston transducers, b) linear sequential array transducers and c) linear phased array transducers.

- Piston Transducers

Piston transducers were the first transducers employed for ultrasound imaging [53]. They are composed of only one piezoelectric element, of circular shape. Due to the fact

39

that single element transducers produce sound waves that are transmitted perpendicular in respect to the transducer's surface, the steering is achieved by mechanically rotating the transducer around a fixed axis. In this way, the scanning produces a sector–shape region (Figure 3-6). Although this type of transducer produces a quite acceptable field of view, it was quickly replaced by array transducers, due to the disadvantages of mechanical steering.
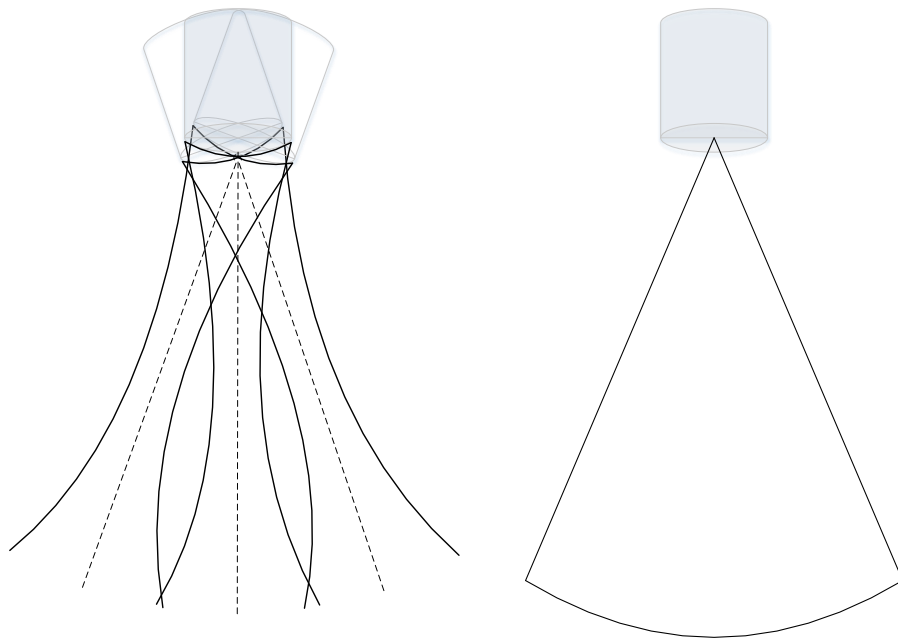
Figure 3-6: Circular piston transducer and its corresponding field of view

- Sequential Arrays

Sequential arrays [54] consist of multiple elements in a row. The typical number of elements varies between 128 and 512, depending on the application. Although sequential transducers do not employ any steering mechanism (the scan lines are directed perpendicular to transducers surface), the large number of elements gives them the capability to produce an image with a field of view proportional to the number and the width of the elements (Figure 3-7). As we examine later, we may have linear or curved

40

sequential transducers.

In this category, two important characteristics can be identified. The first one is that the scanning procedure involves no mechanical steering (moving parts) whereas the second is the great advantage that array transducers manifest, the capability to focus the beam electronically, on different desired locations and depths, producing an ultrasound image of higher quality. Electronic focusing of a sequential array transducer is achieved by activating multiple neighboring elements with appropriate delays, so that the produced waves can positively contribute to the desired location (focal point). As far as the main disadvantage of this category is concerned, this is due to the fact that in order to increase the FOV of a transducer, more elements should be added to it. That, not only increases the average cost per transducer but also dramatically increases the total complexity of the whole ultrasound system.
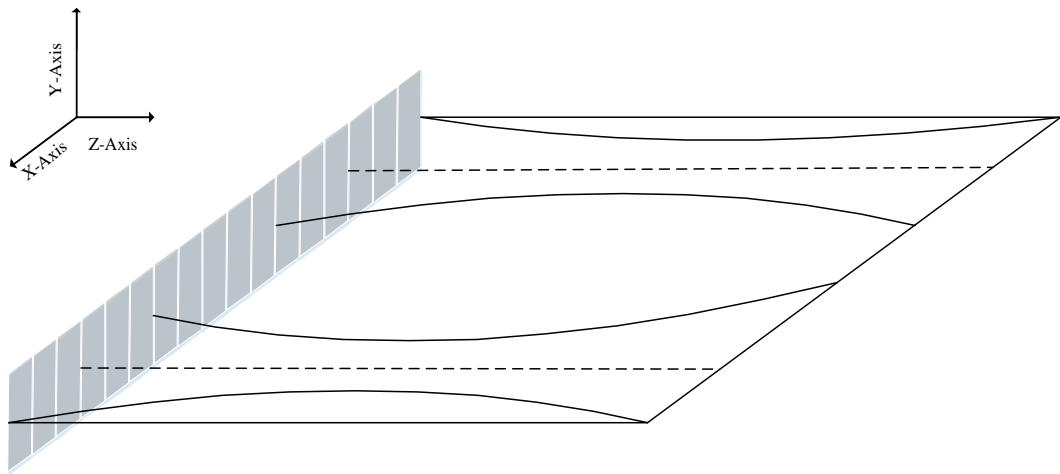
Figure 3-7: 1D linear array transducer and its corresponding field of view

41

- Phased Arrays

In order to overcome the disadvantage of limited FOV of sequential array transducers, phased array transducers were proposed. Phased array [54] transducers operate in a similar manner with the linear sequential array ones, with the only difference that they can also steer the beam towards any desired direction. Thus, instead of emitting sound waves perpendicular in respect to the elements surface, the sound waves can be transmitted towards a different direction (Figure 3-8).

Using the same concept with sequential transducers, steering and focusing of phased arrays can be achieved by electronically delaying the excitation of neighboring elements during transition. The scanning of region of interest produces a sector – shape region and is illustrated in Figure 3-8. Such a transducer can impressively improve the quality of ultrasound images using a technique called dynamic receive focusing [55]. Although phase array transducers require more complex systems to operate in the desired way compared to sequential array transducers, they present the advantage of improved field of view, without requiring to increase the total number of elements.
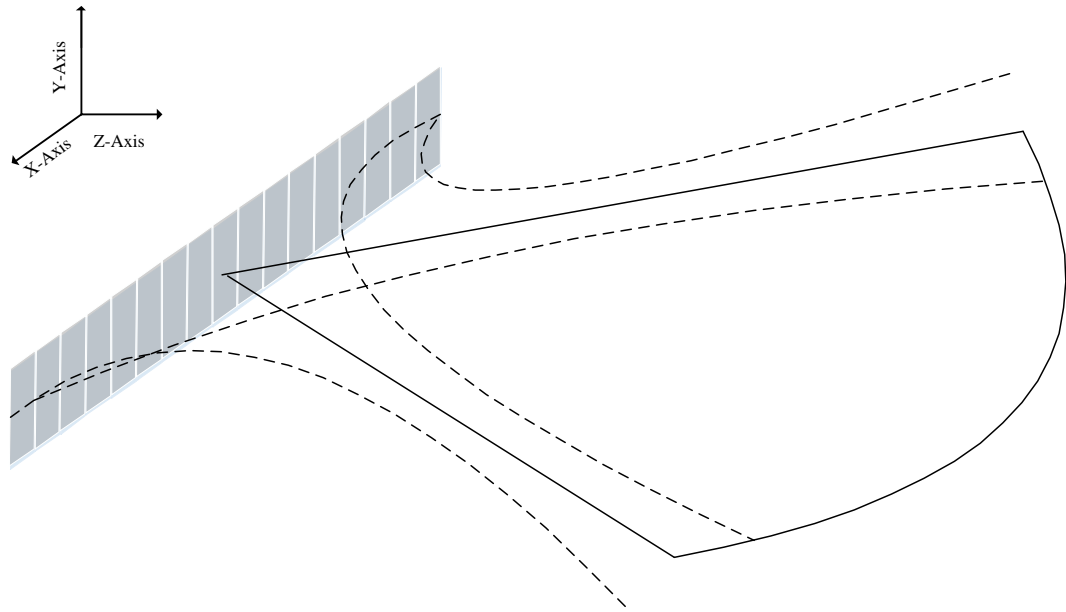
Figure 3-8: 1D phased array transducer and its corresponding field of view

So far, we have examined the major categories of ultrasonic transducers, with respect to their capability to steer and focus the beam. However, ultrasonic transducers can be also classified with respect to the geometrical configuration of their elements (1D grid, 2D grid, annular grid, etc.). Taking under consideration both classification schemes, the most commonly used transducers for medical applications are identified and presented. Those are the a) linear (1D) arrays, b) curvilinear arrays, c) 1D phased array transducers, d) 1.5D phased array transducers and e) 2D arrays (rectangular or annular).

- <u>1D Linear Array Transducers</u>

The firsts transducers widely used in hospitals for ultrasound imaging were the 1D linear array transducers, exactly the way they were described above. They consist of a wide

43

number of piezoelectric elements (up to 512) in a 1D array structure (Figure 3-7). Each time, an acoustic beam needs to be created, a predefined number of elements is activated and the beam can be focused straight ahead but cannot be steered. The result of scanning is a rectangular 2D image of the region of interest to be formed in the screen. Linear sequential arrays were the first array type transducers that replaced pistons transducers for imaging purposes by N. Born 1971. The main drawback of this type of transducers lies in the inherent fact of the reduced field of view which is equal to the footprint of the transducer. They were primarily used in applications of small depth monitoring.

- Curved Array Transducers

The second type is the curvilinear or curved array transducers [56]. This type belongs to the second category of transducers (linear sequential arrays) and operates in a similar manner with the previously discussed type (1D linear arrays). That is, they present the electronic focusing but they lack the electronic steering property. Primary distinction from linear array transducers (and at the same time a great advantage) is that the elements are manufactured to follow a curve shape (Figure 3-11, d) instead of straight line. This curvature offers a significantly better field of view. Curved array transducers are used for general purpose applications and for internal organ monitoring in the abdominal region. The image produced is a 2D plane image of a sector – shape surface (Figure 3-11, d).

- 1D Phased Array Transducers

1D phased array transducers belong to the third category (phased array transducers) and present the same configuration with 1D linear arrays (Figure 3-8). Typical number of elements for 1D phased array transducers are usually in the range of 64–256. Although

44

they are usually composed of fewer number of elements compared to 1D linear array, are considered to be more complex, due to the fact that they incorporate electronic steering mechanisms. Another characteristic that contributes to the increased complexity of phased array transducers id the fact that they make use of all the elements, during transmission and reception. 1D phased array transducers can steer the beam only in the azimuthal plain. As described in the previous section, they produce a sector shape image but with enhanced image quality especially if technique such as dynamic receive focusing is adopted. In favor of the advent of technology, phased array transducers are becoming more popular than curved arrays although there are more complex. Lastly, it is worth mentioning that 1D phased arrays are widely used in cases where there are obstructions such as bones and the scanning should be done through a small opening (cardiac activity monitoring) [57].

- 1.5D Phased Array Transducers

1.5D transducers is a combination of 1D phased array and 2D phased array transducers [58]. Their structure is similar to the 2D arrays, in the essence that they contain elements in both directions but with the difference that in the elevation direction, they contain only a limited number of those (usually less than 10). In that way, they provide a steering capability only in the azimuthal direction and the surplus of elements in the elevation direction is used to improve the quality of the image by improving the strength of the pulse-echo signal.

- 2D Phased Array Transducers

This type of transducers belongs to the third category as well. The elements are placed in a 2D shape (Figure 3-9 and Figure 3-10) and are extended in both azimuthal and

45

elevation direction [59]. The remarkable advantage of this configuration is that the scanning of the ROI can be done in both the elevation and azimuthal direction, producing a 3D representation of the region of interest. Transducers that can generate a 3D image are called volumetric transducers. Despite the potential and revolution that such transducers may bring to ultrasound imaging, they still have not yet been fully integrated in the current ultrasound machines. The major drawback of 2D phased array transducers resides in the fact that the cost for both the acquisition system and the transducer itself is radically increased. The complexity of the circuitry present the same behavior. That is due to the fact that they are composed of thousands of elements (up to 64,000). In addition, the scanning time for a whole region of interest in many cases is prohibitive for real-time applications. Advancements in DSPs, FPGAs and in the power consumption requirements of digital circuits in the last decade will play a primary role in the establishment of 2D ultrasound transducers for most numerous applications especially for monitoring organs in the abdominal region.
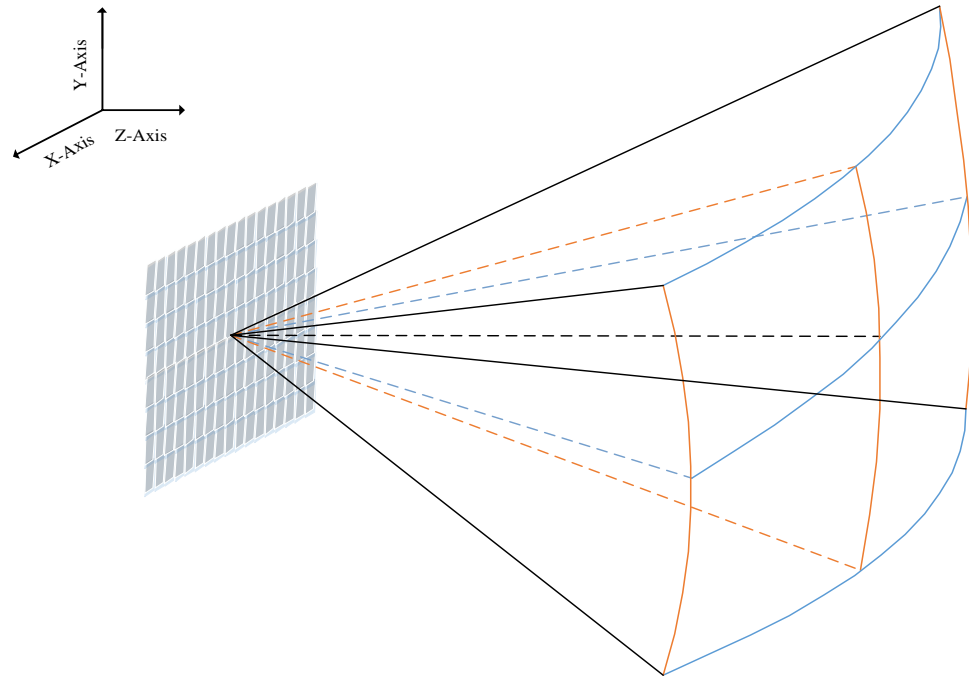
Figure 3-9: 2D phased array transducer and its corresponding field of view.
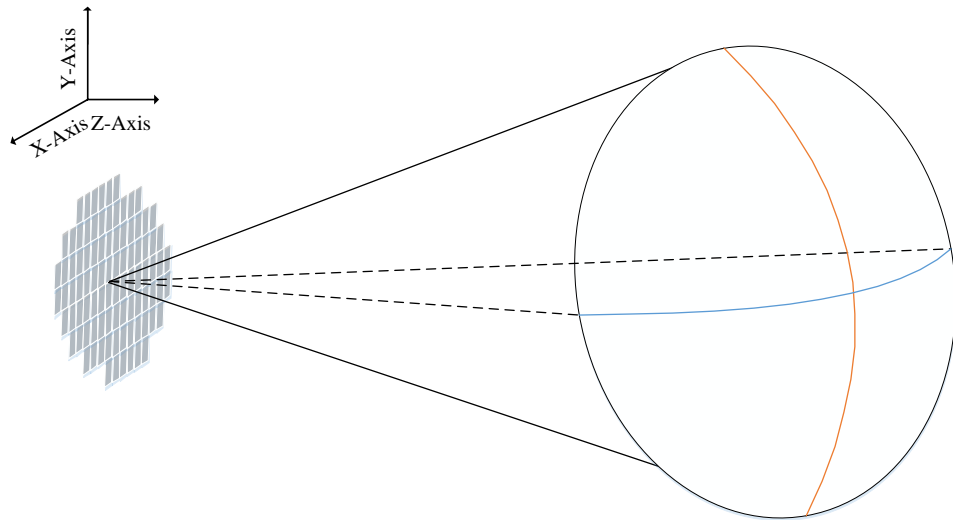
Figure 3-10: 2D circular phased array transducer and its corresponding field of view.

47

- Volumetric Transducers

Real-time volumetric imaging is one of the challenges in medical ultrasound that have attracted the attention of many researchers. 3D images may hold more information in comparison to multiple 2D slices of the ROI, and can be used in various applications such as surgery planning. The first transducers that were capable of capturing the whole volume of the questioned organ were the mechanical scanners. These are usually 1D array transducers with the capability of mechanically rotating the orientation of the array in different angles. In this way, the clinician was able to acquire 2D plane images for different angles and thus covering a whole volume of interest. The appropriate software was responsible through image processing and image analysis techniques for the final outcome to be generated. In this case though, the accuracy and the quality of the obtained 3D representation highly depends on the stability and the skills of the radiologist.

Modern volumetric ultrasound transducers [60] are the 2D phased arrays described above. As elucidated, the fundamental advantage of phased arrays over the mechanical scanners is the competence of electronic steering and the ability of beam focusing in the desired (predefined) focal point. The whole scanning procedure of the 3D ROI is conducted automatically and the image in most of the systems is produced in almost real time. An exhaustive research in the capabilities and the potential of 3D ultrasound scanners can be found in [61].
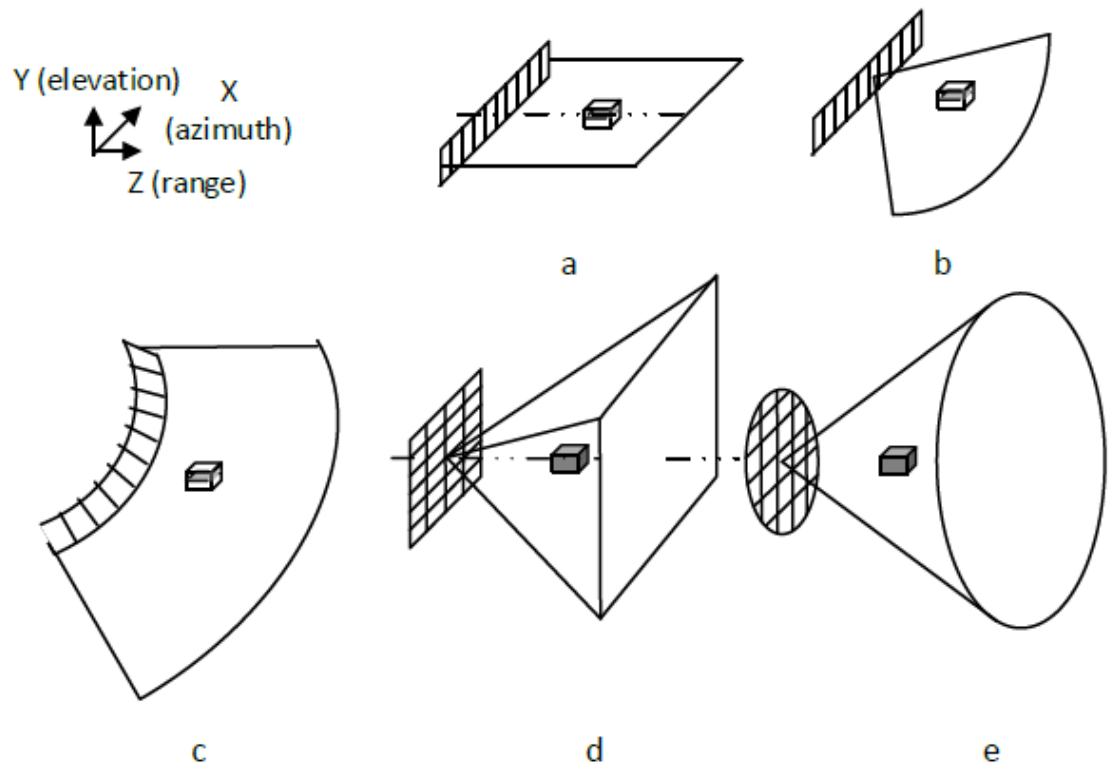
Figure 3-11: Different types of transducers and the region that can monitor: a) linear arrays, b) 1D phased arrays, c) curved arrays d) 2D phased arrays (square) and e) 2D phased circular arrays

In Figure 3-11, the different types of ultrasound transducers that mentioned above are depicted. So far, we described ultrasonic transducers that are using piezoelectric elements and are based in the piezoelectric effect to produce the ultrasound waves. Recently, researches proposed the use of a different type of transducers that use a completely different philosophy in the generation and the recording of sound waves. Following we describe this type of transducers.

- Capacitive Micro-Machined Ultrasound Transducers, CMUTs

Recently, the use of capacitive micro-machined Ultrasonic transducers was proposed

49

instead of piezoelectric elements, as the future in ultrasound imaging delivering new expectations in the field. Researches are still in progress in order to determine the success of theirs use as the fundamental component of the probe and the benefits that can attach to ultrasound systems in contrast to conventional PZT elements. One of the most imperative characteristic of the CMUT is that the can be easily integrated with electronic circuits while at the same time offering enhanced bandwidth leading to a better axial resolution and can be easily fabricated [62].

3.3.2 Acquisition Circuit

The most significant module of an ultrasound system is the acquisition circuit (or main board). The acquisition circuit may be composed of different hardware components, such as FPGAs, DSPs, ASICs, etc. In the acquisition circuit three main processes are performed, as shown in Figure 3-12, that are required for signal acquisition and signal processing (before the final ultrasound image is formatted and presented in the display monitor), as well as for image processing techniques (for image formation and image quality improvement). These processes are the front–end, mid–end and back–end units and compose the ultrasound image formation chain.

Figure 3-12: High level representation of the processes performed in the acquisition circuit

3.3.2.1   Region Scanning and Beamforming Schemes: Front – End

The front-end part of the acquisition board is responsible for the beamforming scheme. In this section, the ROI scanning and image formation procedure, using a typical ultrasound transducer and beamforming scheme is described.

The term beamforming, is referred to the algorithmic steps that are used for scanning the ROI in a predefined manner, as well as the way that the raw data are collected and processed by the system, in order to produce the desired image. A beamforming algorithm considers a) the number of elements that are activated during transmission, in order to produce a sound beam with a specific profile b) the delays to be assigned in those elements, in order to steer or focus the beam to the desired predefined point and c) the corresponding number of elements and delays during reception. Beamforming is the process of using electronic circuits for the multiple sound waves to steer and focus the overall beam in a specific focal point (transmit beamforming) and at the same time to record the echo sound waves coming from multiple directions and correspond them to the correct point from where they are really coming (receive beamforming).

Most of the modern transducers described in the previous section like the 1D and 2D phased arrays (either rectangular or annular), as well as the CMUT use different beamforming techniques to produce the final B-Mode image. B–Mode image is the standard ultrasound grayscale image of a typical ultrasonographer. The letter B stands for Brightness. A wide variety of beamforming schemes have been adopted, based on the type of transducer utilized, the type of image (2D or 3D), and the application itself. Herein, the image formation procedure, of a classical 2D B-Mode ultrasound image is described. For

51

this particular case, 1D phased array transducers are used, as they are the most frequently implemented.

Before we go deeper into the description and the analysis of the beamforming, it is important to address few more issues. Firstly, we would like to explain the way in which a particular region of interest is scanned by the transducer. Supposedly, we have the case of Figure 3-13 where the whole region is scanned by sending sound waves towards predefined directions with the ultimate goal to cover the whole ROI.
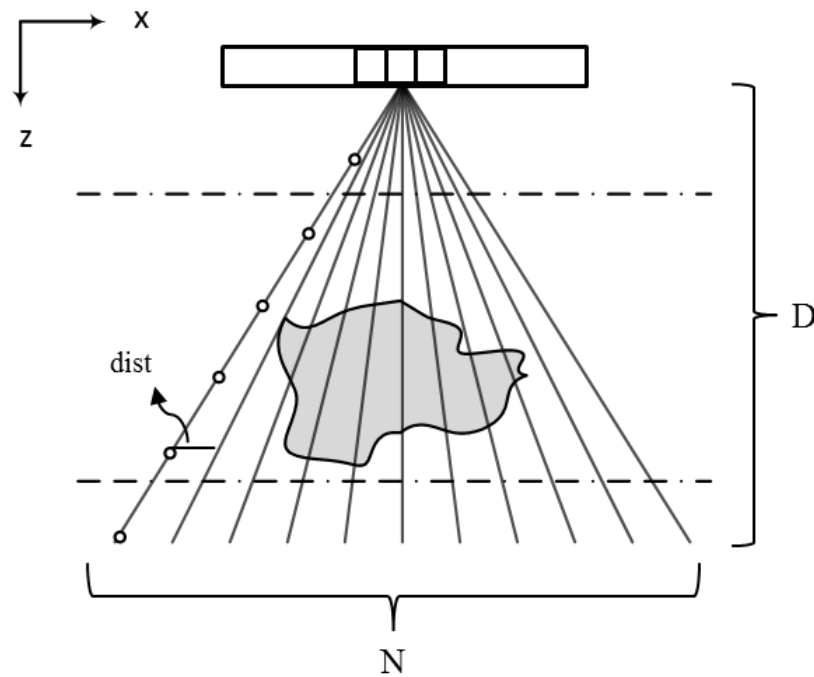
Figure 3-13: Typical sector scanning using 1D phased array transducer

Every time a sound wave (scan line or A − line) is sent towards a predefined direction towards the tissue, the echo needs to be recorded in order to acquire the information in this particular direction. In order to produce the final B−mode image, information from all the scan lines, N in total, is required. Following this reasoning, Frame Ratio or Frame Rate

52

(FR) that declares the number of frames (images) per second can be defined (Equations 3-8 to 3-10).

$$t_A = \frac{2D}{c}$$ (3-8)

$$t_f = N * t_A$$ (3-9)

$$FR = \frac{1}{t_A} = \frac{c}{2 * N * D}$$ (3-10)

In the above, t_A is the time required to record the information of one scan line at a maximum depth D, t_f is the time required to record all the N scan lines or, in other words, one frame (image) and c is the speed of sound inside the biological tissue (usually c = 1540m/s).

Given the case illustrated in Figure 3-13, Lateral Resolution (LR) that was defined in section needs to be redefined. In Equation 3-6 it is shown that the lateral resolution for a single rectangular element is equal to the focal size (dr) of the beam. For a multi-element linear array transducer, the width b can change by the effective width b*, which indicates the width of the active elements of the transducer, and the formula remains the same. Thus, we may rewrite Equation 3-6 for 1D linear array transducer to Equation 3-11. From Figure 3-13, due to the divergence of the scan lines, the actual LR of the system is given in Formula 3-12.

$$d_r = 2\left(\frac{l_f}{b}\right)\lambda$$ (3-11)

$$LR = \max(dr, dist)$$ (3-12)

53

In the above, *dist* is the distance between two consecutive scan lines both at a specific depth. It is obvious that the lateral resolution of the imaging system depends on different parameters such as the focal length (transducers property), number of scan lines (N) and depth that is measured. Another important observation is the fact that for phased array transducers, lateral resolution degrades as the beam propagates deeper inside the tissue.

Now, the process of electrical focusing and steering for a typical 1D phased array transducer will be described. Supposedly that the 1D phased array transducer illustrated in Figure 3-14 is used, and that is composed of 7 elements. In order to focus the beam on a predefined point, part of the total number of elements (or all of them) in the configuration of the transducer are activated, each with a certain delay. Delays are assigned in such a manner that all the sound waves generated from the active elements reach the desired focal point at the same time.
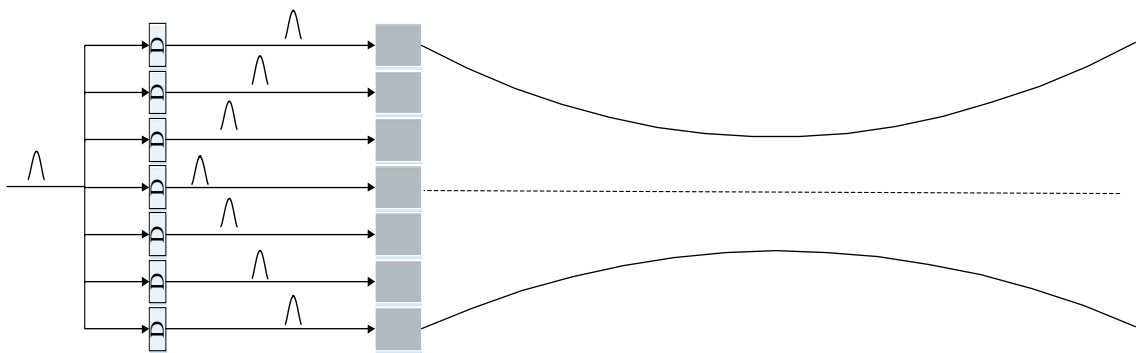
Figure 3-14: Electronic beam focusing during transmission using 1D phased array transducer

The steering of the beam is obtained by assigning different delays in each activated element (Figure 3-15). Combining the electronic delays of Figure 3-14 and Figure 3-15 we can achieve simultaneously, both electronic focusing and steering.

54
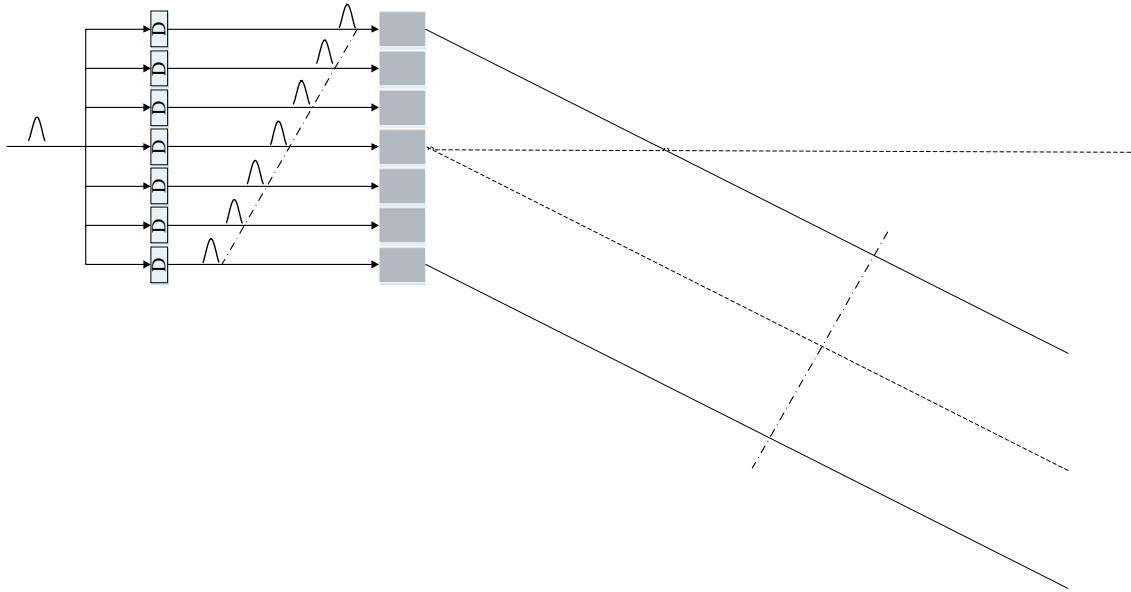
Figure 3-15: Electronic beam steering during transmission using 1D phased array

transducer

During reception the procedure remains almost the same. Figure 3-16 illustrates the case of recording an echo from a particular point (here is point P) during reception. The reflected wave (echo) from this particular point will be measured from all the active elements assigning the corresponding delays. The coherent summation of those signals corresponds to the measurement for that particular point. This whole procedure described above entails the beamforming scheme for the illustrated paradigm for the case of 1D phased array transducer.

55
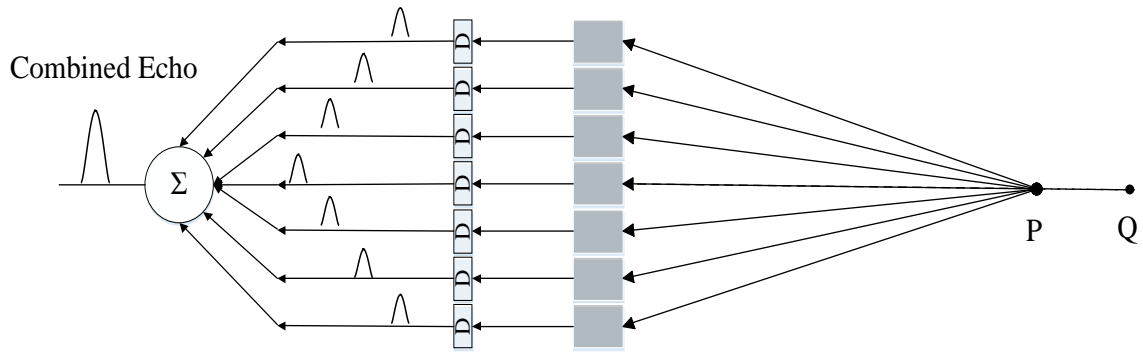
Figure 3-16: Delays assignment during reception.

The interrogation of the region under testing is achieved using the process described above. At this point, it is important to highlight that for each transmitted beam in a particular direction there is only one focal point. On the other hand, during reception we may apply the dynamic receive focusing which is the dynamic adjustment of delays, in order to focus in the echoes coming from different depth zones (Figure 3-16 points P and Q). The number of depth zones per scan line, the number of scan lines and the algorithm that is adopted are critical parameters that characterize the overall performance of the system and the quality of the image to be displayed. Increased number of scan lines will lead to higher lateral resolution (bottom-line is the lateral resolution that can be achieved by the transducer) while at the same time the Frame Ratio (FR) will decline.

Modern volumetric transducers are operating with the same manner. The only difference is that the scanning of ROI is performed in both azimuthal and elevation directions by activating the appropriate row or column of elements each time and assigning the desired delays. Herein, it is important to highlight that all the work described above, is the beamformer's unit responsibility.

56

As mentioned earlier, the front-end processes of the main board of the ultrasound system are responsible for the beamforming scheme. In current systems, front-end can be further divided into the a) analog front-end, that takes care of the analog signal processing of the raw data captured by the system and the b) digital front-end, which contains the beamformer's control unit, the transmit beamformer and the receive beamformer (Figure 3-17). It is obvious from Figure 3-17 that each received signal should go through a number of analog preprocessing steps. Those preprocessing steps require certain hardware components, such as Low-Noise-Amplifier (LNA), Variable-Control Amplifier (VCA) - usually called Time-Gain-Control (TGC) amplifier- and Analog to Digital Converters (ADC). For this reason, the number of channels in the acquisition circuit should be equal to the number of transducer elements or at least equal to the number of the active elements, especially for high quality, real – time imaging. The sophistication and complexity of the system that use more than 128 elements is extraordinary. At this point it is worth recalling that a typical 2D transducer may contain thousands of elements.
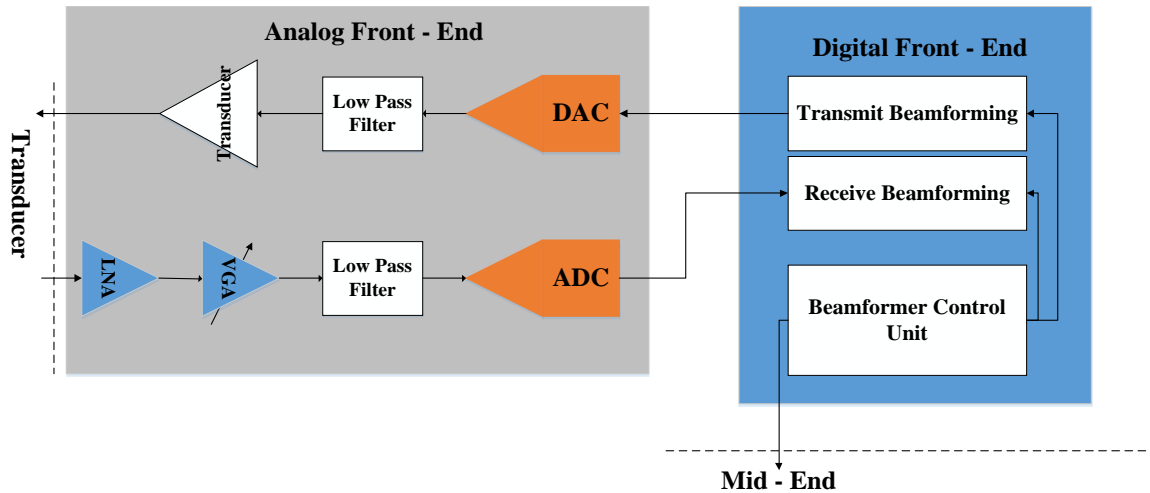
Figure 3-17: Front – end unit of the main board of a typical ultrasound system

3.3.2.2   Signal Processing: Mid – End

The beamformed RF data of each scan line are fed to the mid-end component of the main board. Mid-end is responsible for signal processing techniques, such as filtering, envelop extraction or detection and log compression (Figure 3-18). Signal filtering is used to reduce electronic noise added in the signal through the first stage of processing (analog end). In addition, filtering in this stage may be used in order to select between the fundamental and the harmonic imaging (extraction the second harmonic of the natural frequency of the RF signal). Envelop extraction is usually implemented using Hilbert's Transform. The resulting complex signal is independent of the operating frequency and the magnitude of this signal is the actual detected signal for imaging. Finally, log compression is used to reduce the dynamic range of the original echo signals (about 110dB) in order to fit the dynamic range of a typical grayscale monitor (48dB).

Figure 3-18: Mid – End unit of a typical Ultrasound system

3.3.2.3   Image Processing: Back – End

After the beamformed RF data has been processed and log compressed, it is passed to the back–end part. Back-end is responsible to deliver clinicians a readable image with the best possible quality. The first and most important step is the scan conversion. Scan conversion is used to interpolate the preprocessed data of scan-lines into a rectangular image grid. Finally, after the B-mode image has been created, different image processing techniques may be applied for noise reduction, especially speckle (Figure 3-19). Multiscale, wavelet-based decomposition with soft thresholding as well as anisotropic filtering, are the most commonly filters used.
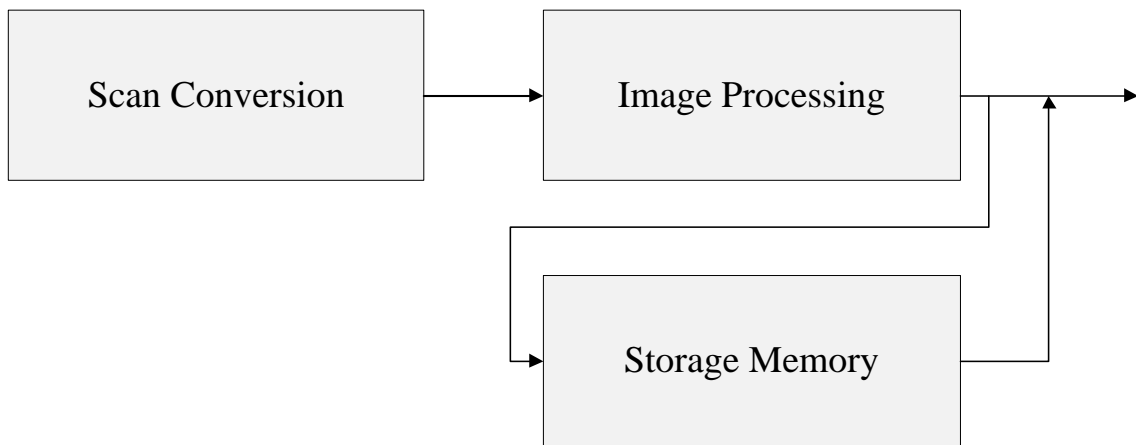
Figure 3-19: Back-end unit of a typical Ultrasound system

59

In particular, for the needs of the current study, it is necessary that the scan conversion component of the back-end unit is a bit further analyzed (Figure 3-20).
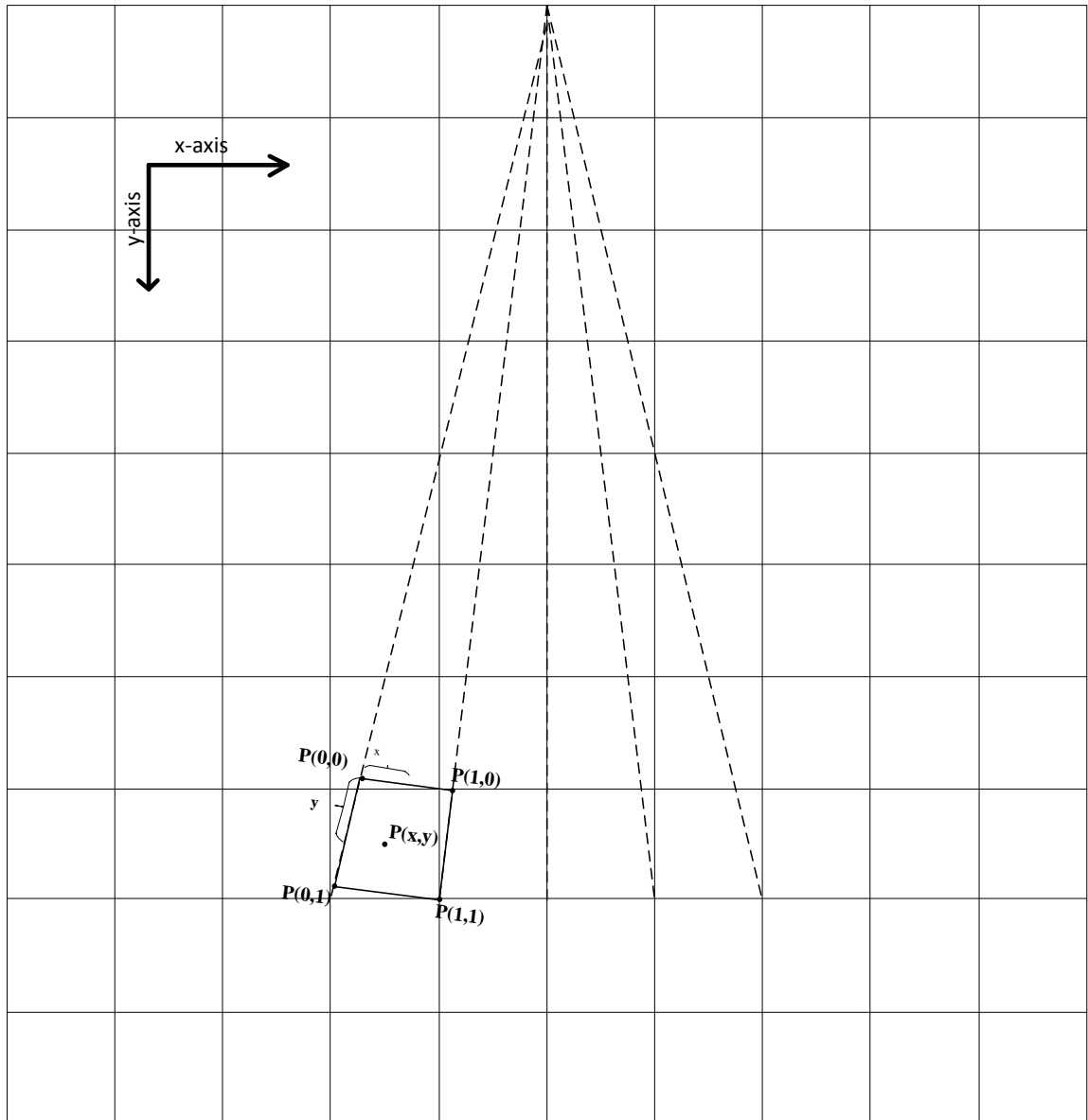
Figure 3-20: 2D scan conversion, mapping the scan lines into a rectangular grid (2D image)

60

2D scan conversion technique is based on interpolation. In Figure 3-21 below, interpolation is illustrated, based on the configuration above (Figure 3-20). The notation mentioned here, is very important in latter chapters of the current dissertation, since it is used extensively. In this, k is the number of scan line $\in xOy$ plane, whereas i is the number of sample that belongs in the scan line k.
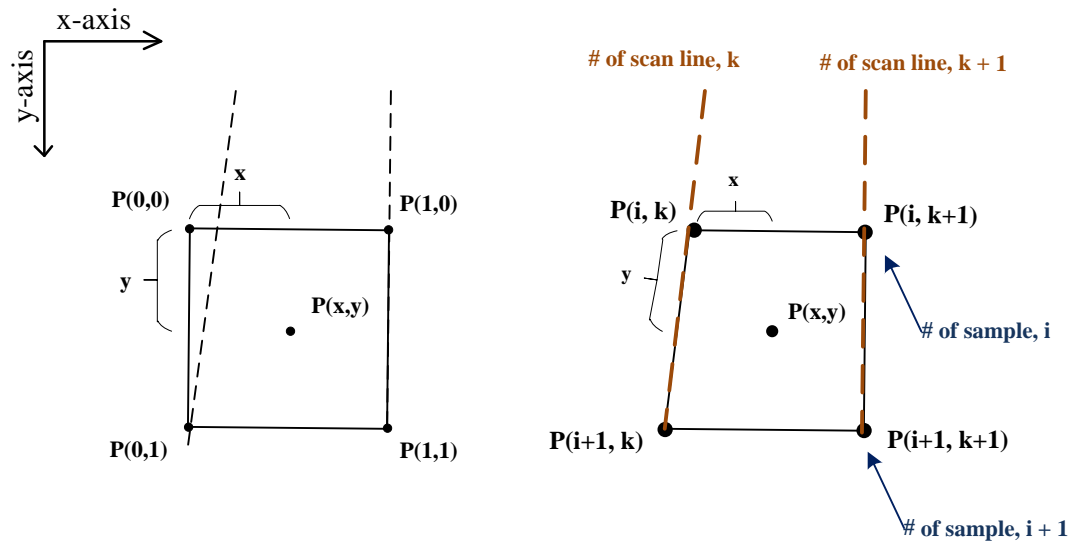
Figure 3-21: Notation of bilinear interpolation approximation, in the case of 2D scan conversion

3.3.3 Monitors

All ultrasound imaging systems used in hospitals or most of the portable ultrasound machines, require a screen in order for the readable image to be displayed. Most of such

61

screens are LCD screens. There are cases though, where the display screen may be the screen of a personal computer or a mobile smartphone.

3.4   Limitations of Ultrasound Systems

In this section, some of the disadvantages of ultrasound machines as well as the challenges that pose to the researchers and designers, are discussed. Throughout the deconstruction of current ultrasound machines many of those challenges were revealed. Trade-offs between focal size and depth of focus that affects the beam profile and the LR, dependence of FR and LR for 1D phased array transducers (and not only), complexity of volumetric transducers are only few of a wide range of key characteristics that researchers should focus on. Herein, we will take a closer look to those.

3.4.1   General Restrictions

3.4.1.1   <u>Dependency on Sonographer's skills</u>

One of the main disadvantages of USI over MRI or CT imaging lies in the fact that the latter two modalities may provide a highly accurate volumetric image of the ROI without the intervention of the clinician (although the presence of the clinician is mandatory the scanning of ROI is performed by the machine). In this case, the body of the subject takes place in a specially arranged chamber while the patient is asked to remain still for few seconds. Depending on the volume of ROI, the location and the type of the abnormality, the whole procedure may endure from a few minutes to more than an hour. The great advantage is that finally clinicians obtain a 3D representation of the whole ROI.

62

On the contrary, ultrasound examination requires the permanent presence and innervation of a sonographer. Sonographer is responsible to manually scan the whole ROI. Using 1D phased array probes (for a typical abdomen examination) real – time images are presented to the monitor. Sonographer is responsible to interrogate the region or organ of interest extremely carefully in order to identify possible pathogens and abnormalities. The whole procedure requires very good anatomy knowledge, stability and 100% attention and still is very vulnerable to human error. Lately, 2D array transducers are able to provide 3D image representation but yet the limited FOV of the sensors along with the current structure of probes requires on the spot examination of trained personnel.

3.4.1.2   Real – Time 3D Ultrasound Imaging

One of the greatest headaches of designers of ultrasound imaging systems is the need for real – time (almost 30 frames per second) volumetric image. In the previous section, the operation of 1D phased array transducer was described and two important observations were derived.

The first observation is that every piezoelectric element of a transducer needs to have its own channel in the analog front – end in order to undergo several preprocessing steps. This may be done in two different ways. The first one is to have an analog front end with as many channels as the number of elements of the transducers in order to increase concurrency. In the case of 2D phased array transducers that are composed of some thousands of elements, this is prohibitive due to the fact that both cost and the complexity of the system are dramatically increased. It is obvious that such a case is not a viable solution for low-cost, portable ultrasound machines. The other way is to use a fixed number

63

of channels and make the elements alternatively use those instead. In this case the FR decreases. Therefore, another critical trade-off that exists in the case of 2D array transducers is identified, among the cost, the complexity and finally the frame ratio.

The second observation is that the triplet LR, number of scan lines and FR constitutes another significant trade-off in the design phase of ultrasound systems. In section 3.3.2.1 was clear how lateral resolution depends on the number of scan lines per image. Additionally, Formula 3-10 indicated the reverse relation between the number of scan lines and the FR. Here lies the main reason why most of the current 3D ultrasound imaging solutions present very poor image quality with reduced resolution. It is extremely difficult to design a real-time machine without sacrificing image's resolution.

Combining both observations above it becomes clear that the whole venturing of portable, low-cost, real-time machine capable of providing high quality volumetric images is an extremely difficult task. In fact, designers and researchers need to take into account numerous restrictions and make several compromises, in order to come up with the appropriate ultrasound machine for the appropriate application.

3.4.2   Image Quality Artifacts

Image quality is indeed one of the weakest's point of USI compared to other medical imaging techniques such as MRI and CT. USI suffers from two characteristics that highly degrade image's quality. The first one is the poor resolution, which is due to either hardware limitations (transducers properties) or to real-time restriction requirements. A typical ultrasound machine may produce images AR between $0.1 - 1$ mm and LR between $1 - 10$ mm. For low-cost systems, these values are closer to the right end of the intervals.

64

The second characteristic is that the quality of the image is affected by numerous artifacts such as speckle noise, high and low attenuation and reverberation to name but few. Herein, the most important ones are described.

3.4.2.1   Speckle Noise

Noise is present in every ultrasound image and is usually known with the term speckle, a multiplicative type of noise formed by the constructive and destructive interference of back scatter signals, from objects (scatterers) much smaller than the system's spatial resolution [63]. Speckle reduction is of great importance, as it can significantly improve human interpretation of ultrasound images and at the same time enhance the overall performance for several image preprocessing and processing tasks (registration, segmentation). Speckle noise and current approaches for reduction of speckle noise are extensively discussed in Chapter 5.

3.4.2.2   High and Low Attenuation Artifact

Most of biological tissues present the same or similar attenuation coefficient with water. This homogeneity has its own merit to the feasibility of ultrasound image creation. Nevertheless, there are certain tissues such as bones that manifest much larger attenuation coefficient compared to soft tissues. The result of beam passing through a bone region is that the most or even whole energy of the beam may be absorbed and everything else beyond this region will appear black in the screen. The opposite effect is encountered when the acoustic beam passes through a region with a very low attenuation coefficient. As a result in this occasion, everything beyond that region may appear very bright making distinguishing of boundaries impossible. In general, in both cases all the information that

65

is hidden beyond these regions cannot be revealed. For current ultrasound systems there is no way to overcome this particular phenomenon but only to partially decrease it during the scanning process, with the radiologist trying to avoid bones or bubbles of air.

3.4.2.3 <u>Side Lobe Artifact</u>

The beam pattern of the transducer and the direction of signal's energy affects a lot the performance of the transducer and the imaging system. In particular, if there is leak of energy towards other directions than the main one, then structures and boundaries that are present at the sidelobes direction, may erroneously appear as a signal from the main lobe. Current solutions are based on adjusting the geometry of transducer elements in order to suppress side lobes or utilizing the second or higher order harmonics.

3.5 Challenges and Ongoing Research on Portable/Wearable POC Ultrasound Systems

In ultrasound medical imaging one can distinguish two major categories of Point-of-Care devices: a) portable ultrasound systems, b) and wearable ultrasound systems. In the former category, many devices have been proposed and are extensively used in hospitals by trained staff. Additionally, PC based systems have been reported. Recent advancements in the field lead to the integration of ultrasonic probes with mobile phones [64]. The latter category proposes the integration of ultrasound sensors with garment in predefined position to interrogate particular regions inside the human body. A representative system in this category was proposed by A. Basak and V. Ranganathan [65] in 2013. This paper described an ultrasonic wearable system of 3 stand-alone CMUT transducers placed in particular

www.manaraa.com

parts of the human body for periodic monitoring. The device was intended to capture the changes of superficial cancer prone organs.

During the last decades, the usability and applicability of ultrasound systems has been significantly improved. Technological advancements in integrated circuits, digital electronics, beamforming techniques and transducer technology [66], [67] have contributed significantly to the development of miniaturized systems with improved computing capabilities, image quality as well as energy performance. These advancements have played an important role in research, regarding low-cost, portable ultrasound systems for POC applications. Such applications include but are not limited to patients been monitored in their bed side, nursing homes or in the Intensive Care Unit (ICU) [9]. These emerging clinical applications have intrigued researchers to propose and develop a wide variety of portable systems each of which has advantages and limitations [65], [68], [69], [70], [71], [72], [73]. Undoubtedly, designing a low-cost ultrasound system able to provide an acceptable and adequate image quality can be a quite challenging task. This venture becomes significantly harder in the case of volumetric ultrasound imaging (3D UI) and this is the main reason why most of the attempts so far, have been mainly focusing on 2D B-mode imaging [68], [69], [70], [71], [72], with a few exemptions [65], [74], [75].

The major obstacle in developing real-time 3D UI for POC systems is their complexity, due to the number of channels required and the low frame ratio, which finally result to questionable image quality that can be achieved. In particular, research studies regarding real-time 3D ultrasound systems, focus on a) transducer design and development, b) array signal processing, beamforming techniques, c) the use of appropriate hardware components

67

and d) image reconstruction methods and visualization. As a result, it becomes really challenging for designers today, to be well-informed and aware of all latest achievements in the above fields, in order to select the best scheme in regards to the application they are dealing with. In the rest of this section the evolvement of those research areas is analyzed.

3D USI systems use 2D phased array transducers [76], [77], [78], [79]. Most of them consist of thousands of piezoelectric elements, in numerous configurations that are wired and integrated to the acquisition circuit. Thus, the main obstacle for the implementation of such systems is the complexity of their architecture that makes the integration of all electronics and their interconnection to the circuit a challenging task. Regarding transducers design, efforts have been mainly focusing on reducing the number of active elements [78], in order to decrease system's cost and complexity while at the same time on improving transducer's spatial response. Most of the studies conducted, target at the optimization of certain parameters, such as lateral resolution, axial resolution, and great lobes reduction, by adjusting the geometrical parameters like the width and height of the elements, pitch between them or the size of the transducers.

Secondly, in order to reduce complexity and the number of channels in the main acquisition board, researchers have turned their interest into applying different beamforming schemes. Beamforming schemes aim at a) reducing the number of active elements, and as a consequence the number of channels in the acquisition board [80], b) reducing the actual time of ROI scanning, as well as c) producing better image quality. This can be achieved by different ways of processing the huge amount of data acquired by the thousands of elements, in order to produce the volumetric image. The gold-standard

that produces the best possible image quality is the conventional phased array (CPA) beamforming scheme. With CPA, all transducer elements are utilized during transmission and reception. However, CPA imaging suffers from high interconnection complexity, system cost and power requirements due to the number of active elements, making its use for low-cost, portable systems prohibited. Another technique that has been proposed, is the Synthetic Aperture (SA) imaging [81] which reduces complexity in the front-end circuit. In SA, a single or small number of elements are selected and exited during transmission and reception, at multiple acquisition steps. The final image is constructed using the superposition principal. Classical SA imaging suffers from low signal–to–noise ratio (SNR) and low contrast resolution. A way to increase SNR is to increase the active number of elements. Moreover, a combination of Phased Array and Synthetic aperture, called Phased Subarray (PSA) has been proposed in order to tackle system's complexity, by reducing the active elements utilized in each firing. Parallel beamforming (PB) imaging has been used in order to meet real – time 3D imaging requirements [82]. In this method, one beam with wide main lobe is produced by a predefined subarray during transmission, while during reception the use of large receive array leads to numerous parallel narrow band receive beams. The described procedure reduces the number of firings by a scale equal to parallel narrow band beams but at the expense of image quality. Other techniques that have been proposed include sparse array processing [83], phased subarray (PSA) [84] imaging, adaptive beamforming [85] to name but few. In [86], an extensive comparative study between SA and PB imaging is conducted and reveals advantages and shortcomings of each method.

69

The third major topic of interest in every ultrasound system is the processes that are required to form the classical B-mode image. The processing chain from the acquisition of beamformed data to image generation, is almost the same for every system. Mid-end and Back-end (Figure 3-22) processes include signal filtering, decimation, envelop detection, log compression, scan conversion and different image processing techniques [52]. However, the hardware components of ultrasound machines that host the aforementioned processes vary, depending on the application. In the case of portable systems, they are mainly based on application specific integrated circuits (ASICs) [70]. Although ASICs are used to achieve miniaturization and cost reduction, systems that use them, lack scalability and functional flexibility. These two properties are of significant importance in a continuous evolving environment of clinical applications for ambulatory and remote monitoring, for both controlled and hostile sites. To effectively tackle lack of scalability and flexibility, and the same time reduce the overall cost, designers turned their interest to digital signal processors (DSPs) and field programmable gate arrays (FPGAs) [68], [72]. Different configurations have been proposed, depending mostly on the requirements of each application. In [69] a system based on an analog board AB – FPGA – DSP – PC was proposed for fast color Doppler imaging . In [71] the integration of the ultrasonic probe directly to a PC was presented. In Figure 3-22, b the common hardware components are shown, along with the processes of ultrasound acquisition chain that are dedicated to each one of them. It is in designer's discretion, biased by systems requirements which module to use and which process to employ in each module.

Last but not least in ultrasound research, ultrasound image processing and ultrasound image enhancement [87], [88] is considered of significant importance. Ultimate goal is to

70

improve the relatively poor ultrasound's image quality. The majority of the efforts so far, have been focusing on alleviating speckle noise; a multiplicative type of noise that obscures image's detail and significantly reduces speed and accuracy of registration and segmentation procedures. In addition to speckle noise, ultrasound images are considered of low resolution, while at the same time they manifest low contrast to noise ratio.

Beamforming and super-resolution (SR) techniques have been adopted to deal with these obstacles. Spatial compounding and adaptive beamforming are techniques widely used in current machines. Regarding SR, although it is closely related to images produced by cameras, satellites etc., [89], [90], [91], the principles it is based on can be applied to ultrasound images as well [92], [93].

71
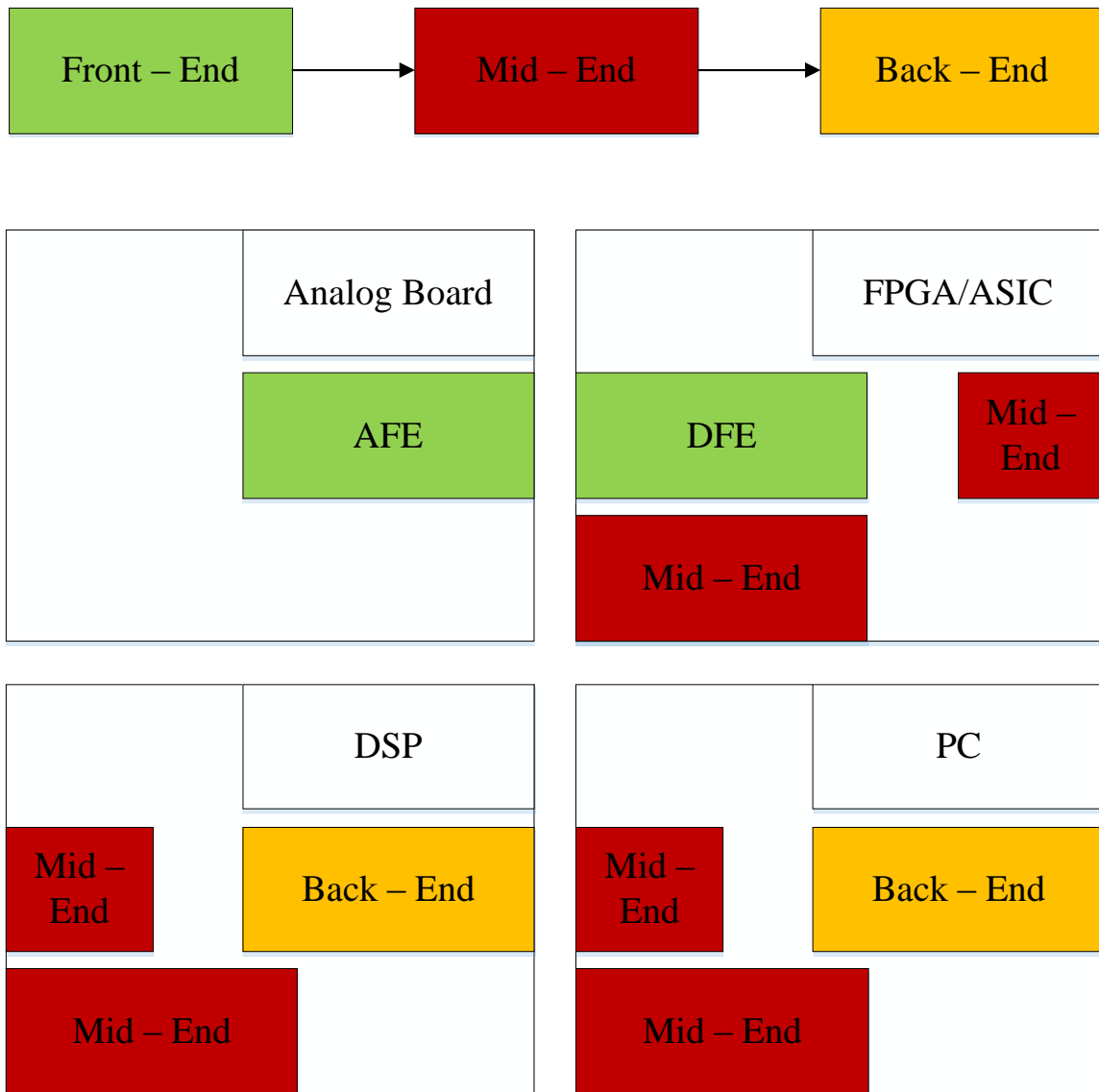
Figure 3-22: a) Typical image processing chain for ultrasound systems; b) Hardware components that might be present in an ultrasound system and which process is dedicated to which component

A more detailed description of speckle noise reduction, super-resolution and image enhancement techniques, is presented in the introductory section of Chapter 5.

3.6   Conclusions

In this chapter the principles and fundamentals regarding medical ultrasonics were presented. All the components of a typical ultrasound system were in depth described whereas limitations and shortcomings were analyzed. In the last section, a brief survey on the ongoing research regarding the portable ultrasound machines was conducted. The current chapter was responsible to provide the reader with the fundamental knowledge regarding ultrasound system architecture and reveal gaps and limitations of portable ultrasound systems, especially for 3D ones.

The main observation is that it is crucial for researchers to collaborate with designers when designing a new ultrasound system and also be able to analyze and apply their findings in order to produce the final product. Depending on the application, designers are responsible to select a set of parameters that are best for their product. Those are the type of transducer, beamforming technique, reconstruction method, processes in ultrasound chain, hardware components, number of channels in main board, number of scan lines and so on. Chapter 3 was one of the most important chapters for the reader to be able to follow the reasoning behind the proposed architecture presented in Chapter 4, as well as the proposed methodology for image de-noising and image enhancement that will be discussed in Chapter 5.

73

4

PROPOSED PORTABLE
3D ULTRASOUND SYSTEM

4.1   Introduction

So far, typical ultrasound machines have been examined and important limitations, restrictions and shortcomings of such systems have been described. In this section, the proposed approach for designing a low- cost, wearable/portable 3D ultrasound system, with extended capabilities, for POC applications, is explained.

The proposal is based on an alternative way of view regarding ultrasound examination. That is, if only structural information is required, clinician's intervention at the scanning/examination phase can be eliminated using volumetric transducers. This can effectively reduce the error incidence frequency during examination (carelessness of clinician). If multiple 2D transducers are placed appropriately and in specific locations, bigger areas can be monitored and clinicians can directly obtain the whole VOI. Only responsibility of the clinician will then be to thoroughly examine the produced 3D image, in a similar way that CT and MRI examination is performed.

74

Although the idea is simple, designing and implementing such a system remains a challenging task. The use of multiple transducers, as will be described in latter chapter, manifest an additional great advantage. This advantage lies in the fact that the redundant information provided by the transducers can be used for image enhancement. In the following sections a more detailed description of the system architecture as well as its operation is given. The way of exploitation of the redundant information will be presented in the next Chapter.

4.2 System Architecture

4.2.1 Motivation and Description

The general architecture of the system has been proposed in [94], [95] and a high level description is given in Figure 4-1. This system is designed to exploit three basic features which actually constitute challenges that modern POC applications need to address. It should be able to a) provide 3D volumetric images of the ROI independently of clinician's skills, b) provide increased FOV capabilities and c) produce 3D B-mode ultrasound images of enhanced quality and resolution, compared to other low-cost portable/wearable solutions. At the same time the complexity of the system should be kept at the lowest possible level.
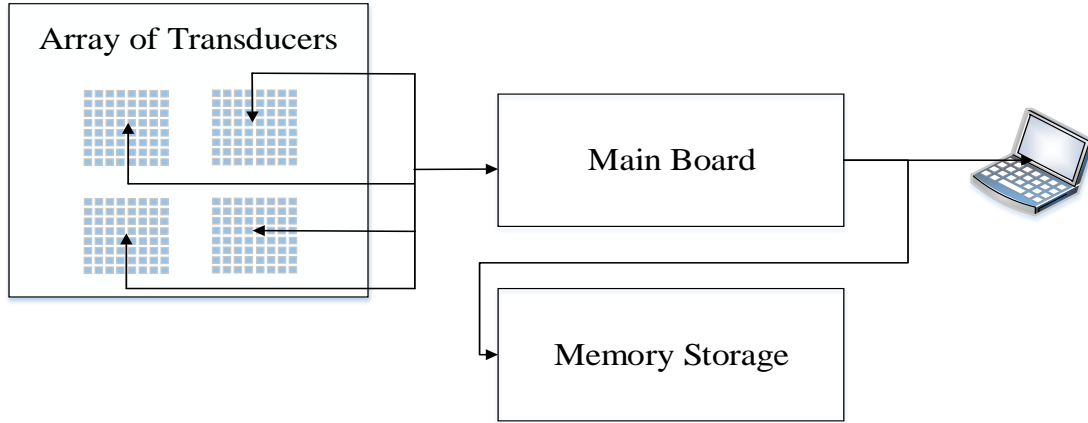
Figure 4-1: High level description of proposed ultrasound system

The approach is based on the observation that by utilizing more than one volumetric transducers in a single system, all three abovementioned features can be incorporated to the system at once. The main advantage though, of using multiple, very simple (smaller number of elements) 2D array transducers, is the reduction of complexity, compared to a system of a single 2D transducer with thousands of elements. Moreover, the deterioration of image quality and resolution of such a system can be compensated by off-processing image fusion and SR techniques as it will be described in later chapters.

This system mainly intends to be used for structural visualization of the human internal body. Thus, at the design phase, several assumptions were made. First and foremost, it was assumed that there is no need for the system to comply with real-time requirements, i.e., 20-30 frames per second. As it is discussed later, this assumption is very critical for the effectiveness of the proposed methodology regarding image enhancement, due to the fact that frequency compounding can be performed, without worrying about time restrictions. Lastly, it was assumed that there are high accuracy 3D motion estimation algorithms that can be used in order to align images, taken from different transducers.

76

4.2.2 System operation

One of the most important steps in designing a system, is to define its purpose. In the current case, the ultimate goal is to provide volumetric B-mode images of the abdomen. Thus, the selected frequency of operation needs to be somewhere between $2-4$ MHz, in order higher penetration depths to be achieved. Secondly, real – time requirement is one of the most challenging tasks for volumetric imaging. Although for the current application there is no need for real – time imaging with the strict meaning of the term (20-30 frames per second), it is important to set an upper limit. An upper limit (at the scale of seconds) was set, in order to capture one image from all the transducers. The formula is given below in (4-1):

$$(\#Transducers) \cdot \left(\frac{\#Scan\_lines}{Frame} \right) \cdot \left(\frac{\#Firings}{Scan\_line} \right) \cdot \left(\frac{2 \cdot Depth}{Speed\_of\_Sound} \right) \leq 10\sec \qquad (4\text{-}1)$$

Knowing the desired maximum depth of the system as well as the number of scan lines and firings for each one of them during the scanning procedure, the total time required to produce an image from each transducer can be computed. In the illustrated example, one firing per scan line was used whereas the focus point was set equal to 90mm. The desired maximum depth was set at 15cm. In each direction, i.e. azimuthal and elevation, 45 scan lines were used. That is, in total 2025 scan lines to produce the image of one sensor. This yields in total time of ~1.5s. As far as the FOV of each transducer is concerned, it was selected to be 45^0 in both directions. The limited FOV was set during the transducer design. Another advantage of the proposed system is that can overcame the limited FOV that is restricted by hardware limitation using multiple transducers. It is worth highlighting that

77

all numbers above have been selected for the example showcased. The system is based on configurable hardware thus it is amenable to changes depending on the applications and its needs and restrictions.

The approach is based on the observation that by utilizing more than one volumetric transducers in a single system, all three abovementioned features can be incorporated to the system at once. The main advantage though, of using multiple, very simple (smaller number of elements) 2D array transducers, is the reduction of complexity, compared to a system of a single 2D transducer with thousands of elements. Moreover, the deterioration of image quality and resolution of such a system can be compensated by off-processing image fusion and SR techniques as it will be described in later chapters.

4.2.3 Transducer's Design

One of the most important features of the system is its sensory unit, i.e., the transducer. As mentioned several times during this dissertation, the system is designed to consist of several volumetric transducers. In particular, for the proposed design, four (4) 2D phased array transducers were selected. 2D phased array transducers are the most commonly used volumetric transducers and their operation is the simplest in regards to volumetric imaging. Moreover, beamforming algorithmic schemes can be straightforward when applied in systems that use 2D phased array transducers. The general design suggests the transducers to be integrated in a belt in an n*m array configuration as shown in Figure 4-2. In particular in our case, we have n=m=2 transducers, as was depicted in Figure 4-3. One transducer will be triggered at a time, in a round robin fashion. In other words, the raw data (log-compressed, envelop-detected scan lines) for the corresponding FOV of each transducer

78

will be produced separately. By doing that, the system complexity is kept at the lowest possible level.
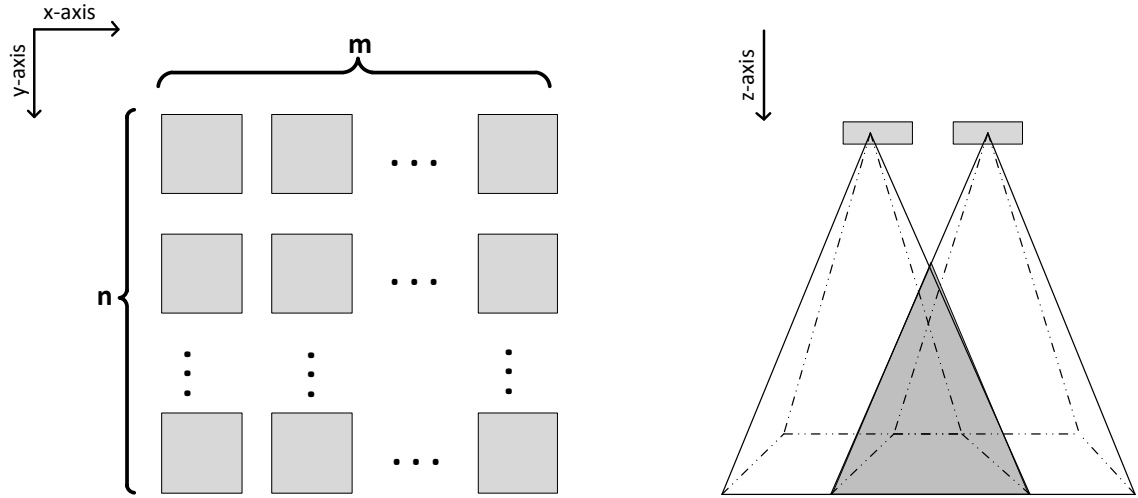
Figure 4-2: General configuration of the transducers (left)-

overlapped region between 2 consecutive transducers (right)

So far, the main difference, between the proposed system and a conventional with a single stand-alone transducer, is the number of transducers being used. The hardware modifications required for the aforementioned transducers configuration will be described later in this chapter.

79
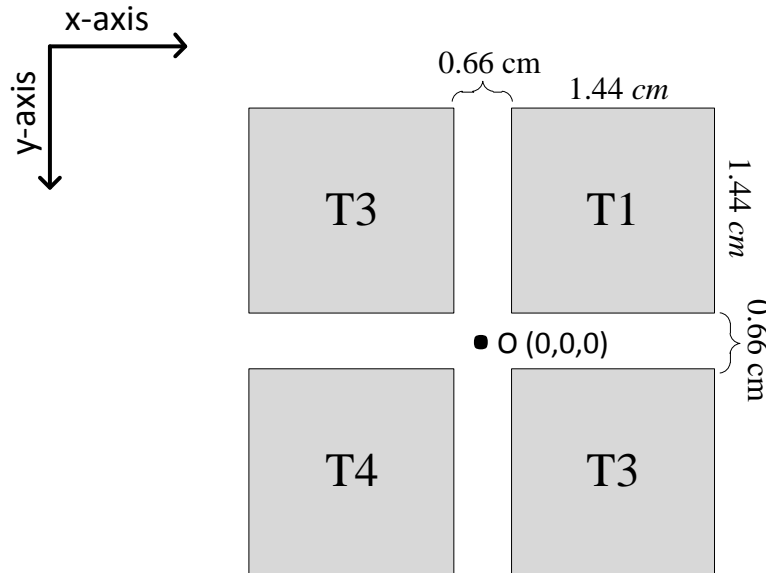
Figure 4-3: Transducers configuration for the proposed system

The design of the transducers was driven by the need to optimize the existing trade-off between a) system complexity and b) depth of penetration. In particular, in order to reduce the complexity, 2D array transducers were used, composed of $16x16 = 256$ elements each. Although 2D array transducers of few elements are not widely used in current systems, their potential and capabilities have been demonstrated. From the other side, in order to increase the depth of penetration, the operating frequency was chosen to be 3 MHz. Besides the previous two requirements, the minimum FOV had to be at least 45º in both azimuthal and elevation directions. Given the number of elements and the operating frequency, a parametric study was performed regarding the dimensions of the transducer. All specifications, i.e., geometrical and functional parameters of the transducer used, are presented in Table 4-1.

80

Table 4-1: Geometrical and functional parameters of the proposed transducer

Parameter	Actual Value
Operating Frequency	3 MHz
Sampling Frequency	100 MHz
Speed of Sound	1540 m/s
Excitation cycles	3 cycles
Total Number of elements	256
Number of elements in the x-direction	16
Number of elements in the y-direction	16
Height of element	0.9 mm
Width of element	0.9 mm
Kerf in the x-direction	50 μm
Kerf in the x-direction	50 μm
Total Width	1.44 *cm*
Total Height	1.44 *cm*

The transducer's design was achieved using FIELD II [40], [41], a publicly available software that runs under the environment of MATLAB. In order to test the performance of the transducer, the beam pattern and the point spread function (PSF) were calculated. The frequency profile of the excitation signal is given in Figure 4-4. In

Table 4-2, certain performance characteristics such as the bandwidth and full width half maximum (FWHM) are presented.

81
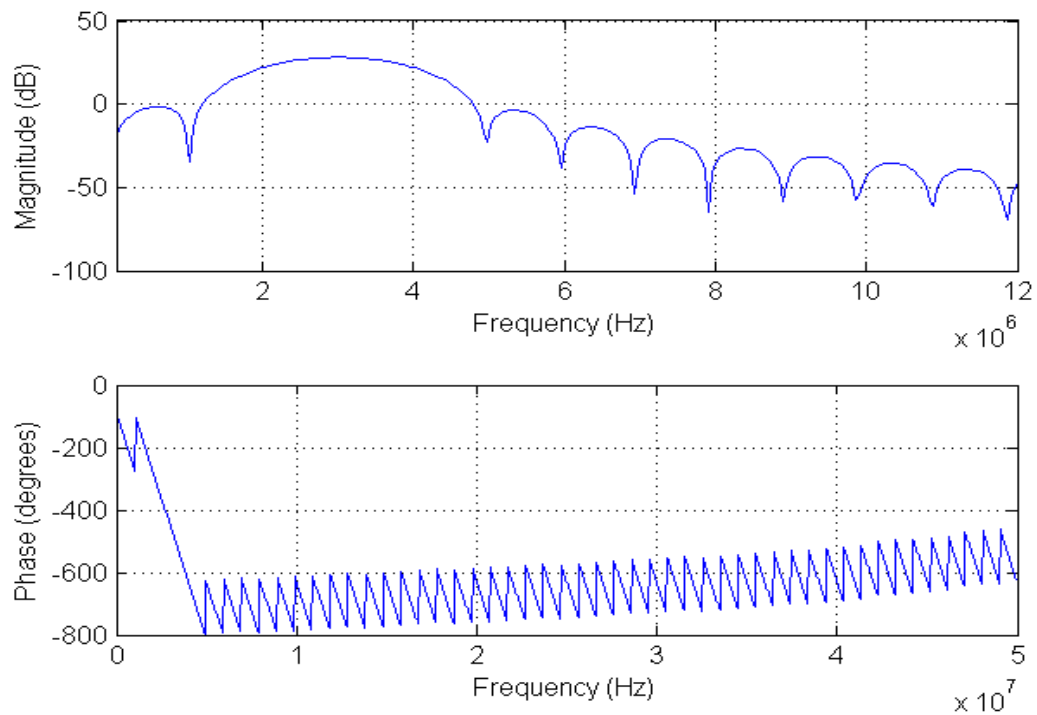
Figure 4-4: Obtained frequency behavior of excitation signal

Table 4-2: Performance characteristics of the proposed transducer

Parameter	Actual Value
Axial Resolution	1.1 mm
Elevation Resolution	8 mm
Azimuthal Resolution	8 mm
FWHM	8 mm
Bandwidth (@ -6db)	2 MHz

Simulations of pulse echo beam pattern show a grating lobe at around 22db lower that the main lobe at $\pm$ 60° (Figure 4-5, a). Thus, the third requirement regarding the desired

82

FOV is met. The PSF for this particular transducer, for different depths is also depicted in Figure 4-5, b.
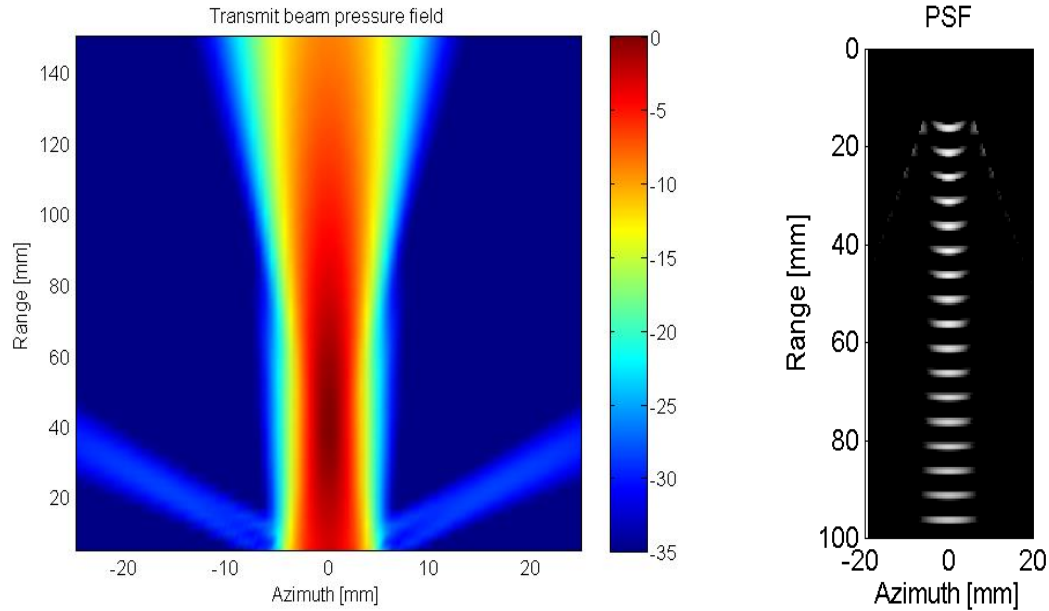
Figure 4-5: a) Beam pattern; b) Point spread function in depth starting from 15mm to 95mm with step 10mm

The calculated results show that the proposed transducer can be successfully used in a real system, especially in the case of low-cost POC applications. The axial resolution of the system depends on the excitation signal and was calculated to be 1.1 mm, while the lateral resolution around 6mm. Although the lateral resolution seems to be quite high, it is considered adequate for general purposes B-mode imaging of the abdomen. Lastly, it is worth explaining the form of PSF. It is obvious that although the focus point was set at 90mm, no focusing is observed. Focusing could have been possible for depths less than 80mm but it would have resulted in a divergent beam for higher depths. By maintaining the focal point at this depth, it is ensured that the beam width will be almost the same for any given depth.

83

4.2.4 Main Board Deconstruction

In this section the architecture of the acquisition board is described. The acquisition board is designed to consist of a single board (main board, MB) and be connected to a personal computer (PC) using appropriate software. The MB is responsible for the analog front-end while at the same time hosts the appropriate devices for digital front-end and signal processing processes. Back-end processes are performed in the PC.

Figure 4-6 illustrates the basic architecture of the system. A number of 16 independent channels for transmission and reception of the waveforms was used. The use of only 16 channels reduces the complexity of the system, the cost and the interconnection requirements while the same time allows for the implementation to be feasible on a single chip. In addition, 16 channels can provide an adequate image quality, as we demonstrated in the previous section, especially for low – cost, portable solutions.

The system is designed to operate as follows. Initially, the transmitter, Tx generates the 16 excitation waveforms that are driven to amplifiers. Then, through two programmable multiplexers the waveforms are mapped to the desired elements of the desired transducer. The back-scattered signals are recorded either by the same group of elements or by a different one, depending on the beamforming scheme to be adopted. We have selected to use 1 MUX of 1024 to 256 (256 Quad channel switches, MAX312L) and 1 MUX of 256 to 16 (64 Quad channel switches, MAX312L) channels. The received signals go through the typical conditioning procedures such as amplification, time-gain compensation and filtering, before the analog to digital conversion. All these procedures (AFE procedures for reception), are performed by 2 fully integrated, 8 channel US AFE (AFE5808AZCF) from

84

Texas Instruments (TI). The ADCs of the US AFE operate at 65 Msps, with the option of 12 or 14 bit resolution, according to the LVDS standard.
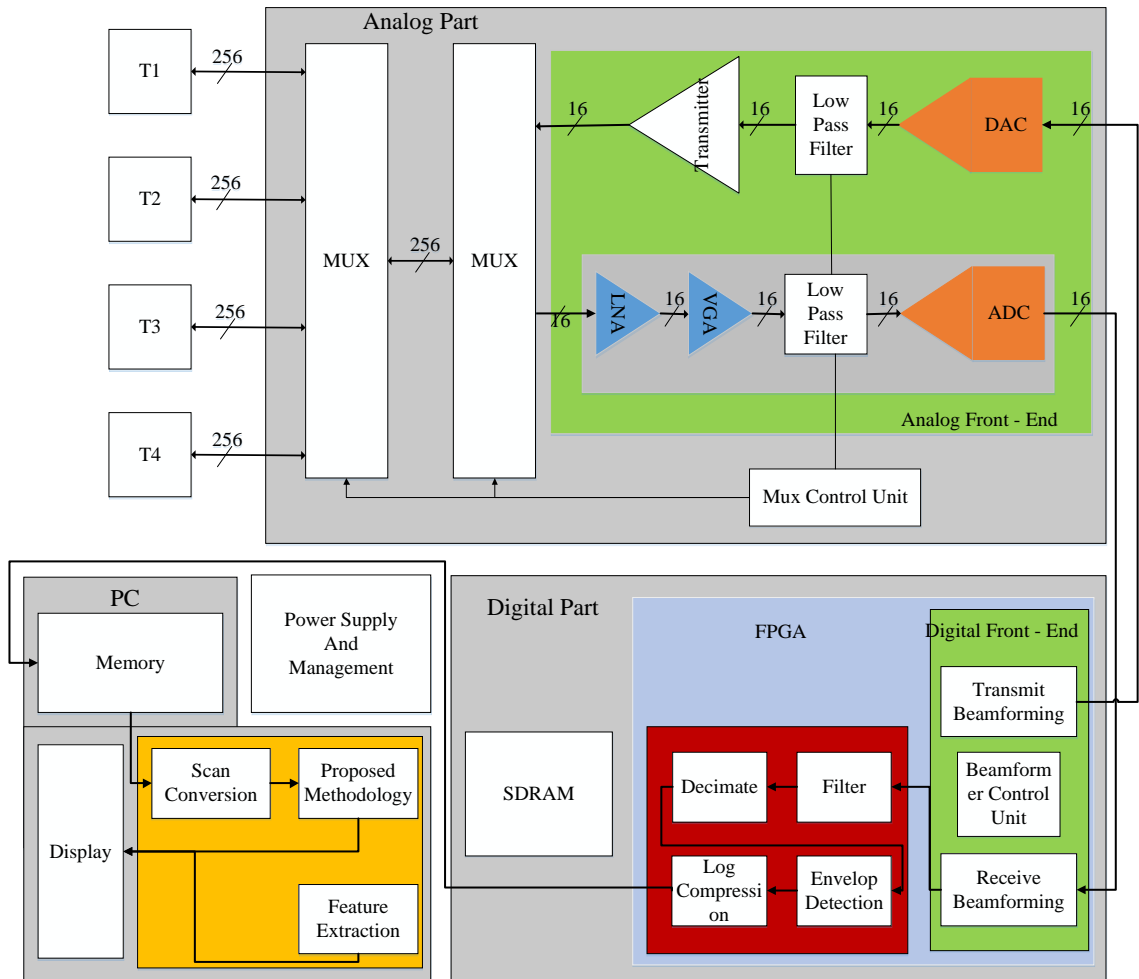
Figure 4-6: Description of proposed ultrasound system

Continuing, the digital signals are fed to the Xilinx Spartan 6 150T FPGA and to the Rx beamformer. Due to the fact that only 16 channels and we are not interested in Doppler imaging at this point, it is reasonable the mid-end processes, such as decimation, envelop detection and log-compression to be performed by the FPGA. This significantly reduces the size, complexity and cost of the system, since there is no need for a new, extra hardware

85

component to be used, such as a DSP to implement the aforementioned steps. Finally, the beamformed log-compressed data are transferred to the PC where are stored for off line processing, or go through the back-end image processing. The described procedure is repeated until the volumetric data of each one of the transducers has been generated.

4.2.4.1 Pulse Generation and Beamforming

As mentioned above, FPGA is responsible for generating the excitation waveforms. The appropriate excitation waveforms are stored in the form of a bitstream in the dedicated SDRAM along with any data possibly required (time delays among channels, number of scan lines, apodization, etc.) from the beamforming scheme currently used. During transmission, the FPGA needs to retrieve the excitation waveform and the corresponding data that are related to each channel and drive the signals to the appropriate LVDS. These signals are fed to the DAC before being amplified in the AFE Tx.

During reception, FPGA is responsible to perform coherent summation of the 16 received signals in order to produce the beamformed data for each scan line. Analogously, the data for the steer, focusing and apodization are stored in the SDRAM.

4.2.4.2 Synchronization and System Interfaces

The synchronization between the FPGA and the analog front-end, especially with the programmable multiplexers is performed through SPI. Therefore, switchers in the AFE are controlled by SPI, to choose the appropriate group of active elements each time. The data exchange between FPGA and the AFE is performed using the high-speed LVDS. The log compressed beamformed data are transferred to the PC through a PCIe standard. In Figure 4-7 the selected interfaces for the proposed ultrasound system are illustrated.

86
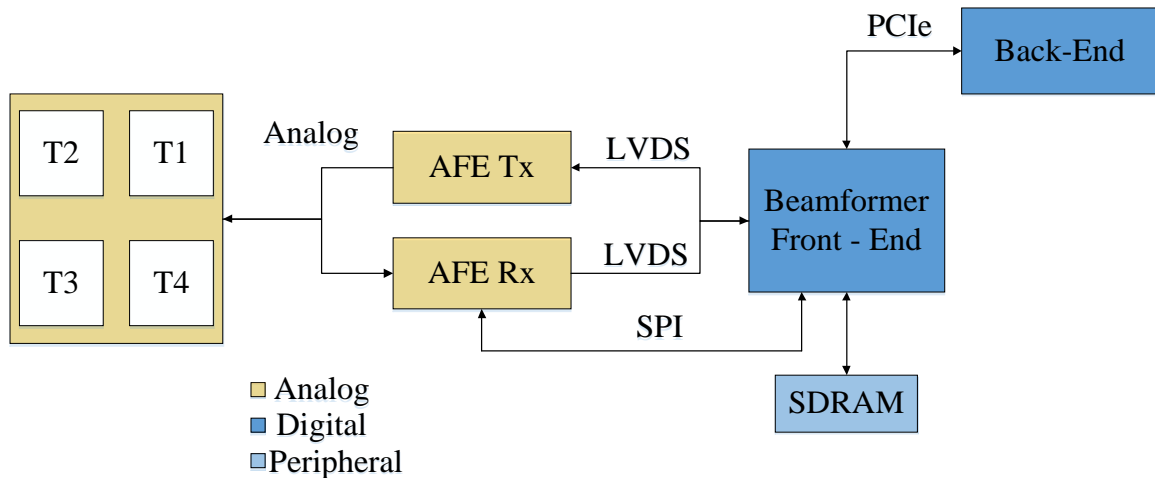
Figure 4-7: Interfaces for the Proposed System

4.2.5 PC: Back-end Processes

As soon as all scan lines from all transducers have been recorded, they are then transferred to a PC where the back-end processes are performed. Typical back-end processes include scan conversion, in order to produce the readable B-mode image and further image processing techniques for image enhancement. In our case, the methodology developed fuses the volumetric images acquired from the four transducers and synthesizes the final outcome. The methodology merges widely used methods, like frequency compounding, spatial compounding and super-resolution techniques, to a single one, in order to produce a speckle-free high resolution image.

The first process of the back-end is the scan conversion. A 3D scan conversion algorithm was implemented, in order to reconstruct the volumetric image from the acquired beamformed log-compressed scan lines of each transducer. The algorithm is an expansion of the 2D scan conversion algorithm developed and provided by Jensen. Continuing, the

87

proposed methodology is an expansion of previous work regarding 2D images given in [39]. Firstly, it exploits the benefits of classical frequency compounding where typical portable 3D ultrasound system is extremely difficult to implement due to time restrictions. As mentioned above, the study focuses on structural B-mode imaging and the real-time requirement can be omitted for now, assuming that there are quite accurate algorithms for motion estimation for breathing and motion cancellation. Having this in mind, the system can be configured to produce different images form each sensor using different excitation frequencies. The second part of the proposed methodology widely exploits the benefits of super-resolution technique. A 3D SR algorithm that receives as an input the compounded images from the four transducers and produces the final wide view image was developed. The maximum gain of the proposed methodology can be achieved in places where the overlap of the FOV of the transducers in maximized. This is achieved for deeper regions. The success of this methodology is that the loss of lateral resolution for deeper regions can be compensated by the gain achieved from overlapped regions.

4.3 Conclusions

One disadvantage of such a system is that it appears to be time consuming. Given the previous description the actual time required to monitor the whole region of interest is 4 times the time required to capture the 3D representation of a single one transducer. But, given its purpose and the fact that such a system can be used for typical B-Mode imaging this is not considered as a serious problem that affects scanning effectiveness. At this point we would like to mention that such an approach is applicable for typical B – Mode imaging where there are no organs that present rapid changes such as heart. One of the main

88

advantages with this configuration is that the sonographer is not responsible for scanning the region. The 3D region will be automatically created after few seconds. Thus, the requirement of real-time (30 frames per second), which is one of the main restrictions for the 3D ultrasound imaging, may be omitted in this case. The second great advantage is the image quality improvement that can be achieved when using the information from multiple sensors. In the next chapter a general image processing methodology for image enhancement is presented based on the proposed configuration of multiple transducers. The methodology is firstly developed and tested for the case of 2D images in order to verify its effectiveness and also guide the selections to be made for the final 3D image processing methodology presented in Chapter 7.

5

PROPOSED IMAGE ENHANCEMNET METHODOLOGY

5.1 Introduction

In the current chapter, some of the most effective techniques that are widely adopted for ultrasound image enhancement are discussed. Different methodologies that are applied in current systems will be described, along with various fidelity criteria that are used in order to measure and estimate the performance of the image processing techniques.

Finally, a new methodology for image enhancement based on the proposed ultrasound system presented in the previous chapter, will be presented and explained in details. This methodology combines signal and image processing techniques with the ultimate objective to improve the quality of ultrasound images. The methodology is proposed having in mind the following two objectives; a) to perform image de-speckling/de-noising and b) to result in resolution improvement.

5.2 Background in Ultrasound Image Processing

Ultrasound image processing embraces methods such as filtering for image de-noising, image registration and image segmentation for wide variety of applications (malignant region extraction). The current study focuses on different filtering techniques that are widely used in ultrasound applications in order to get rid of the speckle noise, described later in this chapter. Image registration and segmentation techniques as well as the notion of Super-Resolution (SR) technique are being discussed.

SR algorithms that are used in camera technology is a technique where multiple Low Resolution (LR) images are combined to produce a High Resolution (HR) image [96] of the same scene. There are also references of SR techniques used in ultrasound images. SR, is considered of significant importance for our case due to the fact that the proposed system is capable of capturing multiple images from different sensors. Thus, for the overlapped regions the low resolution images can be combined and create a higher resolution images. The proposed algorithm is based – on a new ultrasound de – speckling scheme, combined with a SR method in order to produce a de-noised higher resolution image. Herein, the required background in order for the steps and reasoning behind the proposed methodology to be followed, are presented.

5.2.1. Speckle Noise Reduction

In Chapter 3, speckle noise which is the primary type of noise in ultrasound images was mentioned several times. In this chapter, deeper insights regarding noise in images and in particular, speckle noise for ultrasound images are discussed. Firstly the definition of

91

speckle noise is given, then the way it affects ultrasound images is discussed and finally the way it has been fronted so far is analyzed.

Noise in any signal in general, is considered to be an unwanted artifact that degrades the quality of that signal. In images, noise can be manifested as random fluctuations of the actual image's intensity. Most of the times, noise is passed into images during signal acquisition procedure. Thus, the electronic circuit of the imagery system under consideration is the number-one factor responsible for noise artifacts. Errors may also occur during image transmission. One very interesting thing about noise is that these unwanted fluctuations in image's intensity, usually present a specific pattern. Different imagery systems create different artifacts (that is different patterns). Due to those patterns we may have different types of noise. The most common ones are: Gaussian noise, salt and pepper noise (impulse noise), Rayleigh noise, Poisson noise and so on.

Moreover, noise may degrade the quality of an image in different ways. These ways may follow a specific noise model. Two are the most commonly used models that have attracted the attention of the researchers throughout the years: The additive noise model (Equation 5-1) in which noise of a specific type (specific pdf) is added in the desired noise-free image and the multiplicative noise model (Equation 5-2) where the image has been produced as the outcome of a multiplication between the noise and the original image.

$$g(x, y) = f(x, y) + n(x, y) \tag{5-1}$$

$$g(x, y) = f(x, y) * n(x, y) \tag{5-2}$$

One very interesting argument is that knowing the model noise and the type of it that is present in an image we can select or design an appropriate filter in order to be effectively

applied for this particular application. It is true that different filters, either in the spatial or in the frequency domain can deal with a specific types of noise. For instance, a median filter can effectively remove salt and pepper noise from an image but on the other hand, does not present similar behavior when applied for a Gaussian type of noise removal. In this case, noise can be easier removed using an average filtering.

Herein, we study how speckle noise in ultrasound images can be modelled and removed using different filtering methods. Speckle noise is a random granular pattern that is created due to elementary scatterers inside a resolution cell. The resolution cell is defined by the transducer properties. Depending on the number and the topology of scatterers inside the resolution cell, the incident sound wave is reflected towards multiple directions with different amplitudes and phases. The backscattered coherent echoes that are captured from the transducer undergo a destructive or constructive interference randomly. This random pattern defines the speckle noise, which is created during the acquisition of ultrasound images and depends on the operating frequency used by the system (operating frequency changes the relative topology of scatterers inside the resolution cell). Speckle noise can be modelled as multiplicative type of noise. In [97], Arsenault and April showed that the logarithmic transform of noisy image that suffers from speckle noise results in an approximation of Gaussian additive noise.

$$\log(g(x, y)) = \log(f(x, y)) + \log(n(x, y)) \tag{5-3}$$

$$l(x, y) = k(x, y) + e(x, y) \tag{5-4}$$

Thus, any common filter can be used to remove the undesired part of the signal. Still, common filters may manage to remove the noise but have the tendency to blur the image and loose particular critical information of the image such as edges.

Distribution models such as Rayleigh (if number of scatterers per resolution cell is large), Rician and K – distribution (if number of scatterers per resolution cell is large) are extensively used in order to describe speckle noise [98]. Different approaches that effectively deal with speckle noise have been proposed in the literature [99], [100], [101] and are usually categorized in compounding methods and in post processing methods. Compounding methods either in the spatial [102], [103] or in the frequency domain are based on averaging the information retrieved from multiple images or on applying split spectrum techniques [100] to the original signal. Post processing methods usually apply different types of filtering on the final ultrasound image. Lee, Frost, Kaun, and Weiner filters are the most common ones. Beside those filters, wavelet, curvelet and contourlet based filters have been implemented with great success [104], [105], [106]. Compounding techniques may be more effective but result in reduced frame ratio and usually require hardware modification and very fast and accurate registration schemes.

5.2.2. Fidelity Criteria

In order to assess the performance and the effectiveness of a de-noising algorithm and to be able to compare them with other algorithms in the literature various performance measures have been used. The most commonly used measures are presented here. Signal to noise ratio (SNR) is defined as the power ratio between the signal and the unwanted noise and for images is given with Equation 5-5. In order to compare the original image

94

with the filtered image mean square error (MSE) is defined as the average of the squares of the errors and depicted in Equation 5-6. Peak signal to noise ratio (PSNR) [107] like is SNR is the ratio between the maximum possible power of signal and the power of noise. In our case maximum power of signal is 255 (for grayscale image) and the noise is the error introduced by the filtering (MSE). Another important measure is the structural similarity measure (SSIM). SSMI measure most of the times is more consistent with human perception about the quality of the image than PSNR or MSE. The signal-to-mean square error (SMSE) given in [108], is used instead of signal to noise ratio (SNR) for multiplicative type of noise. Two other measures are used as an attempt to incorporate edge preservation after the filtering. That is the coefficient correlation (ρ) and the edge preservation coefficient (β) that are given in [109]. Apart from the performance measure it is critical to visually evaluate the outcome of every method.

The formulas for all these measures are presented below:

- Signal to Noise Ratio

$$SNR(I(x, y)) = \frac{\mu(I(x, y))}{s(I(x, y))} \tag{5-5}$$

- Mean Square Error

$$MSE(I(x, y), I_{comp}(x, y)) = \frac{1}{mn} \sum_{x=1}^{x=m} \sum_{y=1}^{y=n} (I(x, y) - I_{comp}(x, y))^2 \tag{5-6}$$

- Structural Similarity Measure

$$SSIM(I(x, y) - I_{comp}(x, y)) = \frac{(2\mu_I \mu_{I_{comp}} + c_1)(2\sigma_{I, I_{comp}} + c_2)}{(\mu_I^2 + \mu_{I_{comp}} + c_1)(\sigma_I^2 + \sigma_{I_{comp}}^2 + c_2)} \tag{5-7}$$

95

- Signal to mean square error (SMSE) [108]

$$SMSE = 10\log_{10}\left(\frac{\sum_{i=1}^{K} F_i^2}{\sum_{i=1}^{K}\left(\hat{F}_i - F_i\right)^2}\right) \tag{5-8}$$

- Coefficient of correlation (ρ) [109]

$$\rho = \frac{\Gamma\left(f - \bar{f}, \hat{f} - \bar{\hat{f}}\right)}{\sqrt{\Gamma\left(f - \bar{f}, f - \bar{f}\right) * \Gamma\left(\hat{f} - \bar{\hat{f}}, \hat{f} - \bar{\hat{f}}\right)}} \tag{5-9a}$$

where $\bar{f}$, is the mean value of original, $\bar{\hat{f}}$ is the mean value of the de-noised image and Γ is:

$$\Gamma(f_1, f_2) = \sum_{i,j \in ROI} f_1(i,j) * f_2(i,j) \tag{5-9b}$$

- Edge preservation measure (β) [109]

$$\beta = \frac{\Gamma(\Delta f - \overline{\Delta f}, \widehat{\Delta f} - \overline{\widehat{\Delta f}})}{\sqrt{\Gamma(\Delta f - \overline{\Delta f}, \Delta f - \overline{\Delta f}) * \Gamma(\widehat{\Delta f} - \overline{\widehat{\Delta f}}, \widehat{\Delta f} - \overline{\widehat{\Delta f}})}} \tag{5-10}$$

In the above, Δf is a high pass version of f obtained by 3x3-pixel standard approximation of Laplacian of Gaussian (LoG).

5.3 Super-Resolution (SR) Imaging in Ultrasound

The inherent problem of general purpose probes that are composed of phased array transducers is that image resolution is degrading as beam propagates in deeper tissues. That is either due to conical like region scanning or due to beam profile of transducer utilized.

96

A simple way to improve lateral resolution is to increase the number of scan lines inside the scanning region, resulting in decreasing frame ratio. In addition image resolution depends on the acoustic frequency utilized. The higher the frequency the better the resolution but on the other hand, the higher the frequency the less the penetration depth. Thus, arbitrary increase the frequency can result in the undesired effect of small penetration depth.

In this section, the potentials of applying a highly promising and relatively new post processing technique in order to improve ultrasound image resolution are examined. SR is a very interesting technique recently used in camera technology, in order to extract more information about a specific scene recorded by multiple cameras [96]. With SR, high resolution (HR) images can be produced by drilling information from numerous low resolution (LR) images. Super-resolution technique seems to be very promising for low quality ultrasound images [110], [111], [112] especially taking into account the numerous overlapped regions created using the proposed ultrasound architectural scheme. As mentioned earlier the lateral resolution worsens in respect to penetration depth. That is due to a) phased array transducers where the distance between two consecutive scan lines increases for higher penetration depths and b) the divergent form of the beam profile from the focal point and after.

One very interesting observation based on the proposed architectural scheme and the utilization of multiple phased array transducers, is illustrated in Figure 5-1. The configuration of the transducers creates regions of overlaps. These regions are monitored by more than one transducers. As a consequence, more than one image can be generated

97

for the same scenes (the basis of SR technique). For higher penetration depths, the overlapped regions get bigger while there is possibility that more sensors/transducers monitor the same region providing even more images for that particular scene. Thus, there is a point after which certain regions are monitored from all the transducers of the system. In these regions the maximum gain from SR technique can be exploited. Thus, the intention of the proposed architecture and the proposed image processing methodology is to try to compensate the loss of resolution for deeper tissues using the redundant information of those overlapped regions. Herein lies the basis of the methodology developed for the 2D presented in Chapter 6, case, for 3D images in Chapter 7.
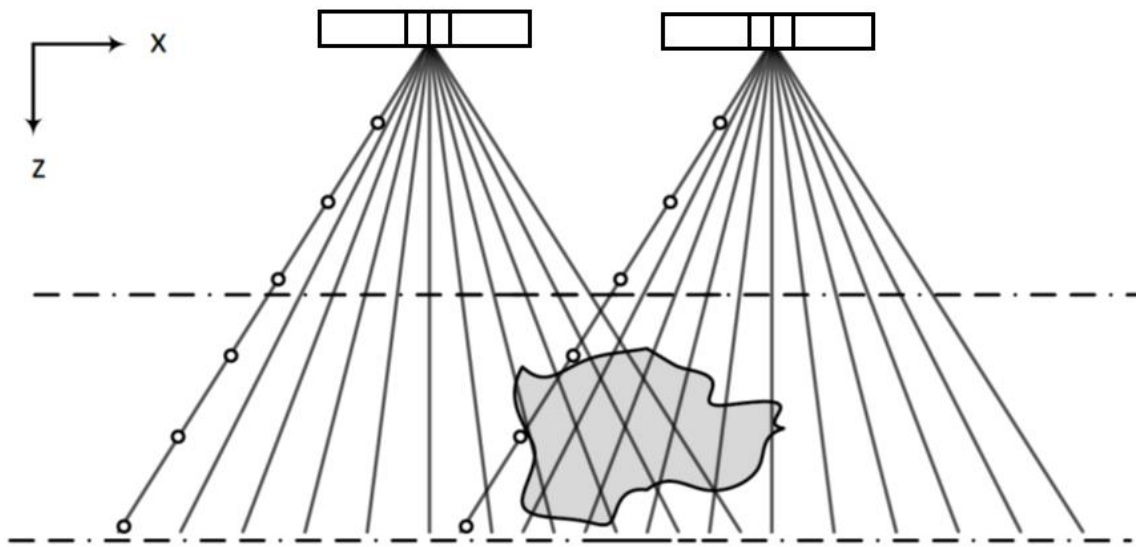
Figure 5-1: Overlapping region of two adjacent transducers

Another observation derived from Figure 5-1, is that inside the overlapped regions the density of measurements per unit area is increased. As a consequence a better estimation of the missing value during the interpolation of scan conversion can be achieved.

The first and most important step of super-resolution algorithm, after having the LR images, is the registration process. A very accurate registration algorithm is the key in order to maximize the beneficial information that can be extracted from multiple images. A sub-pixel image registration algorithm is actually required in order to exploit the SR technique. The next step is the reconstruction of the High Resolution (mapping on the HR grid) image or the interpolation process. Finally, the last step take cares of any blurring or noise problems encountered by applying a deconvolution method.

5.4 New Ultrasound Image Enhancement Methodology

In this section, a new methodology for ultrasound image enhancement is proposed and explained in details. This methodology is driven and highly dependent on the architectural scheme described in the previous chapter, thus it requires multiple images of the same scene. This can be achieved either by a stand-alone hand-held system that is manually forced to monitor the same scene from different angles, or by using multiple transducers at predefined locations to monitor the same scene (like the proposed system). The methodology is considered to be a general purpose methodology in the essence that can be applied for both 2D and 3D ultrasound images regardless the number and the configuration of the transducers. In this section the basic steps of the methodology are described and the reason why these steps can be effectively utilized for the proposed case is justified. The results, when applied in both 2D and 3D ultrasound data are presented in Chapters 6 and 7 respectively. The methodology is developed and applied for the case of 2D images in order to test its effectiveness and at the same time to guide our choices of certain parameters for the final 3D methodology designed especially for the 3D system presented in Chapter 4.

The methodology deals with two of the most important limitations of current systems, enlisted earlier; a) speckle noise and b) low resolution images. Firstly, to deal with speckle noise a combination of frequency and spatial compounding is performed. As it was described earlier in this chapter frequency and spatial compounding are very effective techniques but are extremely time consuming. Both of them are based on the averaging of multiple images of the same scene. Given the advancements on power capabilities of computer and in the field of digital electronics both techniques are widely applied for real-time 2D image applications. For real-time 3D applications this is almost impossible, especially in the case of low-cost devices. Due to the fact that real-time monitoring is not required for the proposed system, both spatial and frequency compounding seem extremely attractive. Secondly, to deal with the low image resolution problem, a Super-resolution algorithm was performed. The suitability and applicability of a super-resolution algorithm the proposed architecture or for any architecture that uses multiple transducers was explained in the previous section.

At this point it's worth highlighting the fact that problems such as grating lobe's signal or low and high attenuation artifacts are not taken under consideration. Although we firmly believe that can be effectively alleviated with the proposed architecture if certain modifications in the methodology. The general block diagram of the methodology is illustrated in Figure 5-2 and all the steps are described below.

100
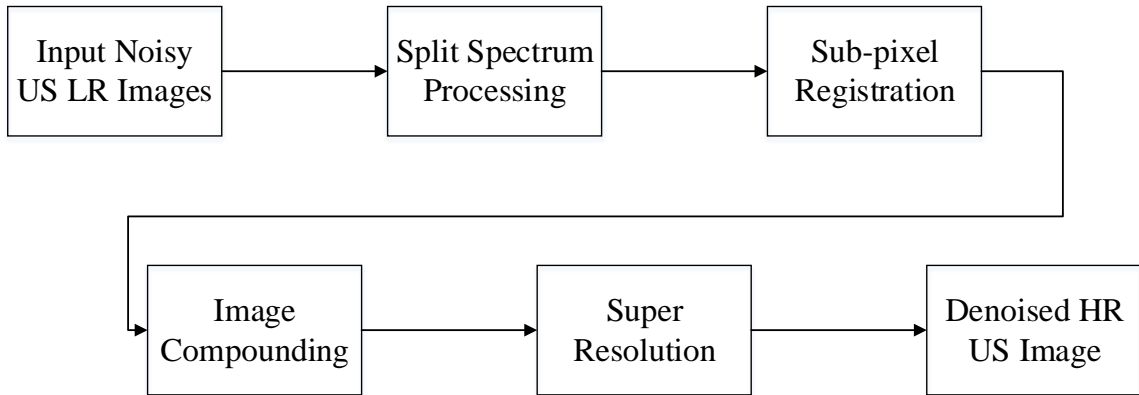
Figure 5-2: Proposed methodology for high quality high resolution ultrasound images

The generic methodology to be implemented (Figure 5-2) is described here and all the steps are explained one by one:

- Input LR Images: Assuming that n is the number of transducers of the system and assuming that each one of them can produce k images acquired with different frequencies around the central frequency. Thus, every sensor will record a certain area and will acquire k images of this area. In total, $T = n*m$ images will be produced. The key characteristic here is that there will be a significant amount of overlap especially from images captured by adjacent transducers.

- Split Spectrum Processing: One image from the set of k images (n in total) produced from each transducer will go through a mild split spectrum processing. This is not the actual de – speckling method to be used. As it was mentioned in this chapter ultrasound images suffer from speckle noise that degrades a lot the performance of image processing techniques such as image registration and image segmentation. The degradation in the performance can be considered either in terms of

101

computational complexity or in terms of accuracy and effectiveness of the algorithm. Thus, this step is performed as a quick preprocessing step before the image registration take place. It is obvious that this step is quite crucial, due to the fact that spatial compounding and especially super-resolution algorithms require very accurate image registration processes in order to produce the desired outcome. Otherwise, there is the possibility, the opposite effect to be produced.

- Sub-pixel image registration: It is obvious that image registration is one of the most important steps of the methodology. A very accurate and highly effective image registration algorithm would be extremely helpful at this stage. Image registration is needed in order the images captured from different transducers to be mapped into the same coordinate system and be able to be combined. For both compounding methods and SR techniques, image registration is extremely essential. Especially for the case of SR, sub-pixel image registration is required. For the reason explained above the SSP technique was applied first one n images (one from each senor) Thus, image registration is performed using only these n images that have been de-noised through the SSP.

- Image Compounding: In this step spatial or frequency averaging can be performed. Knowing the transformation parameters among the sensor from the previous step, all the images can be forced to lie in the same coordinate system. Then image averaging in the images captured from the same sensor (m images) with different frequencies is applied (frequency compounding).

102

- Super-resolution: In the final step, image super-resolution technique is applied in the LR compounded images obtained in the previous step (in the obtained n de-noised images). SR is applied for the overlapped regions only and one single HR de-noised image can be obtained. The steps of a classical SR algorithm were mentioned in section 5.3. Due to the fact that image registration has been performed in step 3 of the proposed methodology, only the remaining steps for the SR method (interpolation and de-blurring) are performed here.

Herein a generic form of the methodology was described. It is applicable for both 2D ultrasound images as well as for 3D ones.

5.5 Conclusions

In Chapter 5, a brief introduction to ultrasound imaging was presented. Terms such as noise, speckle noise, de-specking, frequency and spatial compounding were discussed. In addition, techniques such as image registration, image segmentation and super-resolution that are used in ultrasound image processing were presented. The ultimate goal was to link these notions and techniques with the generic proposed methodology for ultrasound image enhancement presented above. In Chapter 6 a case study for 2D images is conducted and the methodology is developed for 2D images. The findings of the case study performed for 2D images are used to guide certain selections (form of SSP, which SR algorithm, etc.) for the final 3D image enhancement methodology.

6

PROPOSED METHODOLOGY FOR 2D ULTRASOUND IMAGES

6.1 Introduction

In this chapter, the proposed methodology that was previously introduced (section 5.4), is implemented in the case of 2D simulated ultrasound images. This step is very critical for the current dissertation, since the validity and effectiveness of the proposed image enhancement scheme for a typical B-mode ultrasound image, has to be first tested before it gets implemented for 3D images. Therefore, instead of using 3D volumetric representations directly, 2D images were first created using 1D phased array transducers. The obtained results are also presented in this chapter together with a comparative study that was conducted between the proposed algorithm for image enhancement and other de-noising and super-resolution techniques. The obtained results are very promising for the next step and the implementation for 3D images, showing that the proposed scheme outperforms classical image de-noising algorithms, with respect to various performance

104

measures. In fact, the final de-noised HR image appears to have significantly increased CNR and SNR compared to a single image obtained with a single transducer. For the purposes of this chapter, the publicly available Field II toolbox [113],[114] under MATLAB 2012Rb environment was extensively used. Field II use was critical, in order to create the simulated data required in order to apply our methodology.

6.2 Experimental Set Up

As mentioned earlier, the Field II simulation toolbox was used, mainly due to the fact that it is publicly available and widely used by the research community for ultrasound transducer design and simulations. In particular, Field II and MATLAB give researchers the capability to a) design completely new ultrasonic transducers, b) produce artificial phantoms of different geometries that represent specific parts of the human body, and finally c) process the raw A-lines (or backscattered echoes) in their preference, in order to produce the B-mode image. Moreover, raw A-line data give researchers the flexibility and freedom to apply new beamforming schemes, as well as signal processing algorithms for image enhancement.

Below the experimental set up that was used in order to apply and test the proposed methodology is unwrapped. The analysis focuses on the description of the following three components:

    a) The transducers used in this paradigm (type and number) (section 6.2.1),

    b) The reference phantom that was used to represent possible cysts inside the human body (section 6.2.2)

105

c) The procedure followed while applying the generic methodology for 2D images (section 6.2.3).

Finally, the implementation results are discussed in section 6.2.4.

6.2.1 Transducers Configuration

Given the objective of this chapter which is not to design a totally new transducer that provides advanced characteristics over existing ones, but to test and validate the performance of a newly proposed image enhancement algorithm, typical 1D phased array transducers were used. The transducers were designed by the Field II team and are given in one of the examples in their official webpage. The use of 1D array transducers was adopted in order to produce 2D ultrasound image data instead of 3D and speed up the process. Below, the configuration and the number of the ultrasound transducers that were used for the current experiment are presented.

Three 1D phased arrays transducers were used with identical geometrical characteristics. For the needs of the current paradigm the transducers were placed in a row (Figure 6-1), perfectly aligned in order to produce the desired overlapped regions. The transducers were excited with different frequencies around the resonant frequency, with the intention to apply the frequency compounding method on the produced B-mode images.
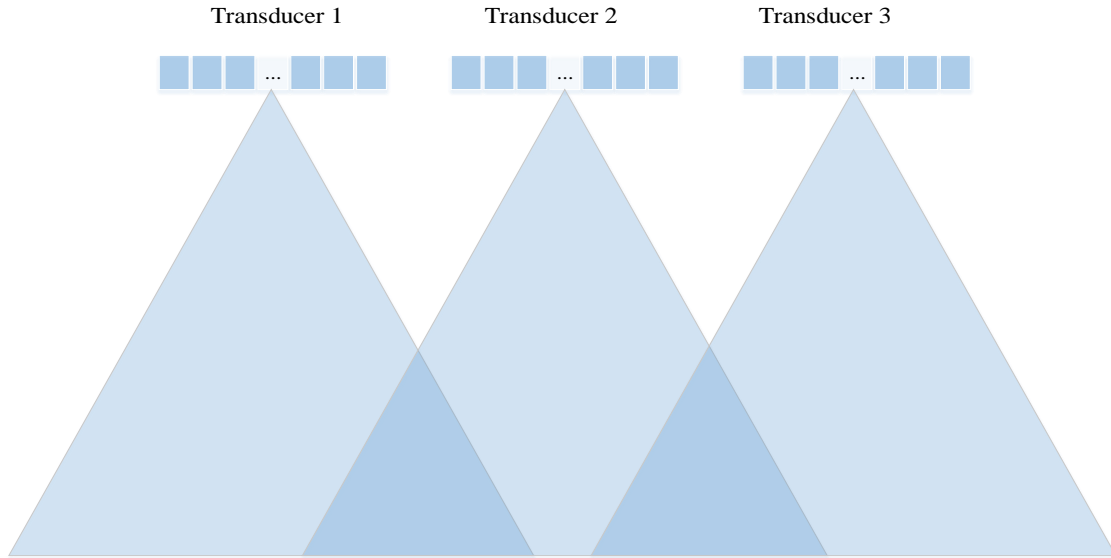
Figure 6-1: 1D phased array transducer's configuration for the experimental set up

The geometrical characteristics for all transducers were identical and are summarized in the Table 6-1.

Table 6-1: Characteristics of the utilized transducers

	Transducers 1-2-3
Type	1D phased array
fo (MHz)	5
f (MHz)	4.5, 4.75,5,5.25,5.5
Number of elements	128
Width of elements(mm)	0.154
Kerf (mm)	0.0308

6.2.2 Cyst Phantom

After selecting the number and configuration of the transducers to be used, the next step is to define the structure of the artificial phantom. The simple cyst phantom that was finally used, is illustrated in Figure 6-2. As shown, the phantom consists of 10 blob-like

107

structures, nine of which represent cysts and the other one a high reflectance circular structure. The position of each cyst and their dimensions were predefined and carefully selected in such a way so that the respective cysts lie inside the FOV of all three transducers, while some of them manifest diameter not larger than the lateral resolution of the system. After selecting the aforementioned transducers configuration and cyst phantom, the proposed methodology was implemented in MATLAB for 2D images, using the simulation capabilities of FIELD II. Just to mention here, that knowing the exact structure and position of the cysts, the CNR can be easily calculated. CNR is considered one of the most significant measures in order to quantify the improvement in the image quality.
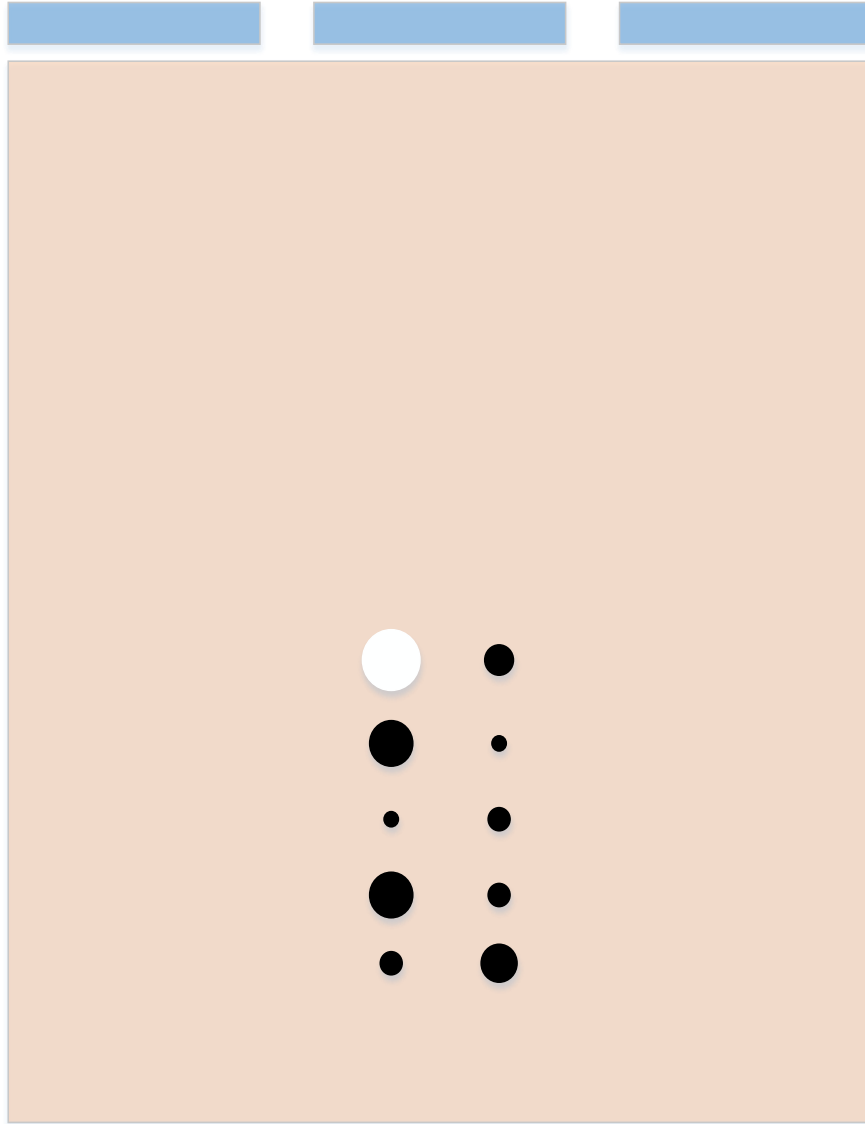
Figure 6-2: Artificial phantom utilized

6.2.3 Procedure

FIELD II produced the raw A-line backscattered signals which were in turn used to create the B-mode ultrasound images. In order to perform the SSP technique, which is part of the proposed methodology, existing code -signal processing algorithms (envelop

109

detection, log compression and 2D scan conversion) provided and already implemented in MATLAB by the FIELD II team - was modified accordingly.

The procedure that was followed for this experimental set up was similar to the one presented in section 5.4 with the appropriate modifications, and can be described in the following steps:

1. Each transducer provides 5 images of the same scene. In total 3x5=15 images.

2. Light SSP on one of the 5 images produced by each sensor.

3. Perform sub-pixel image registration to find the transformation (known in the simulation) using the SSP processed images.

4. Perform frequency compounding using the 5 original images of each sensor. Result: three compounded images.

5. In the fifth step, one of the following techniques are implemented and tested, in order to study their effect on the final image:

    a) Perform spatial compounding and monitor and compare the result of only image de-noising.

    b) Align the images and perform spatial compounding to the compounded images form transducer 1 and 2 and then to transducer 2 and 3. Then apply super-resolution technique to the two compounded images of the previous stage. Result: Final HR de-noised image.

    c) Align the images and perform super-resolution technique to the three compounded images of the previous stage. Result: Final HR de-noised image.

110

In this section the results of the applied algorithm are presented and discussed. The section is divided in two parts. The first part (6.2.4.1) presents the results of applying image compounding methods only (steps 1 to 5.a mentioned above), whereas the second (6.2.4.2) shows the results of adding super-resolution techniques to the compounding methods (steps 1 to 4 and 5.b, 5.c mentioned above). Acting in this fashion, the effect that different steps have on the final image can be identified and analyzed.

6.2.4.1 <u>Results of De-speckled Image</u>

In Chapter 5, various compounding methodology schemes were discussed that are widely applicable nowadays. Moreover, the fact that simple averaging techniques seem to perform better than image processing schemes or signal processing like SSP (although may require hardware modification) was highlighted. Due to the fact that the proposed methodology is entirely based on a novel multi-transducer scheme, such methods appear to be very appealing. Here the results of the first version of the procedure are presented and analyzed.

As mentioned earlier, in step 4 of the procedure, frequency compounding (averaging) to all 5 images of different frequencies produced by each transducer, was performed. To the three newly generated images, named fr_comp1, fr_comp2 and fr_comp3, spatial compounding was performed. Then, knowing the registration parameter from step 3, the final de-noised image **FrComp/SpComp** was produced. A visual representation of the above, is given in Figure 6-3.

111
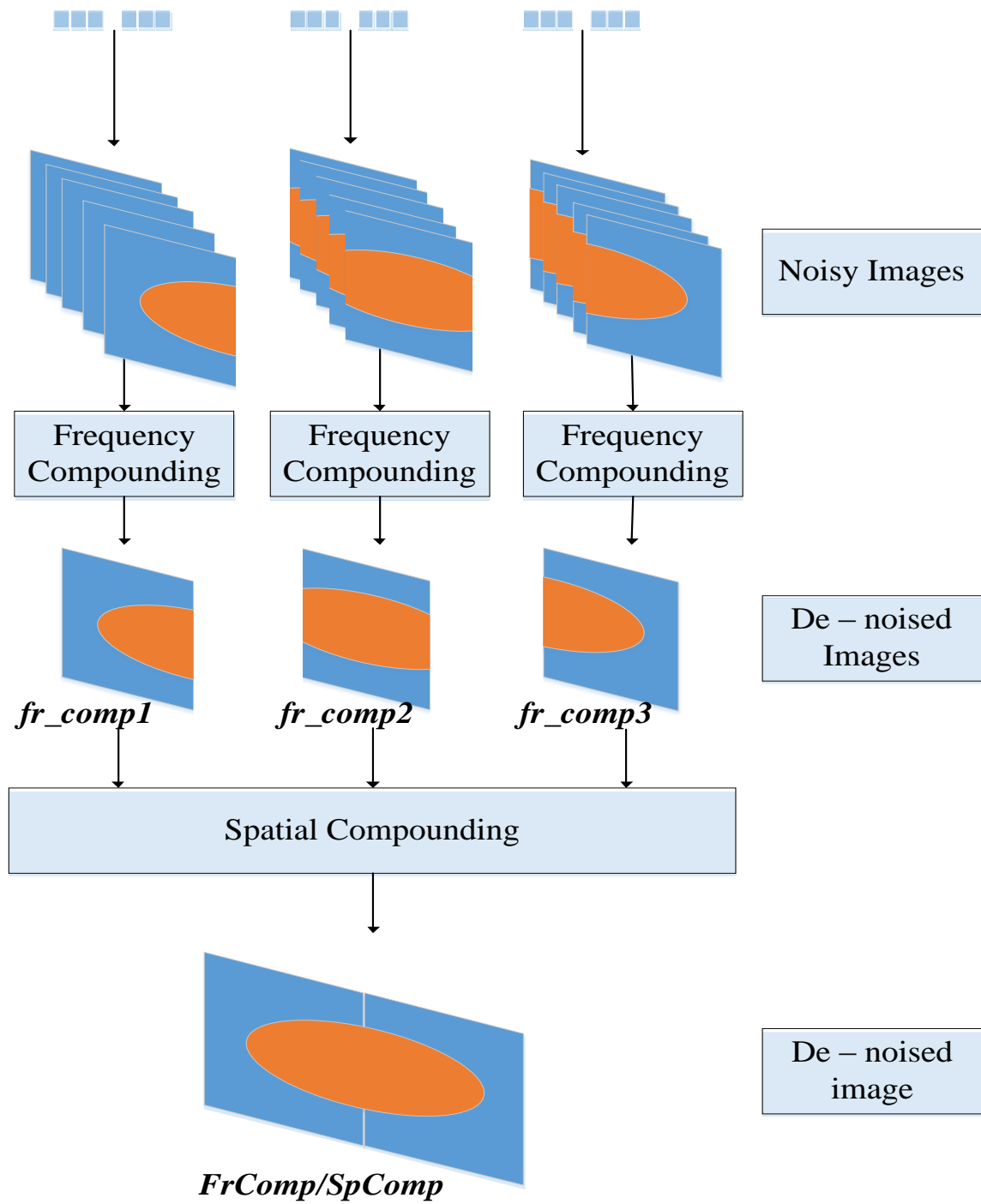
Figure 6-3: Version 1a) Image de-noising using frequency and spatial compounding

After performing the procedure mentioned shown in Figure 6-3, we went one step further and reversed steps 5.a and 4 (

Figure 6-4). That is, firstly spatial compounding was performed, registering all the images produced by different transducers. The five resulted images were named sp_comp1, sp_comp2, sp_comp3, sp_comp4 and sp_comp5, where the index from 1 to 5 represents the different frequencies applied from 4.5 to 5.5 MHz with step 0.25 MHz, as is also shown in Table 6-1. Then frequency compounding to those 5 images was applied. The final de-noised image was named **SpComp/ FrComp**.

The assessment of the performance of the described procedure was done by calculating all the fidelity criteria presented in section 5.2.2. That is, CNR, MSE, RMSE, SMSE, SNR, PSNR, CCRO, BITA, SSIM. Besides this, 5 additional software-based de-speckling schemes were implemented and their values of the performance measures were compared to the ones produced by the proposed algorithm. The implemented filters were the median filter, Wiener filter, Kaun filter, Frost Filter and the anisotropic diffusion filter. The comparative Table 6-2 with all the implemented schemes and the corresponding values is given below.
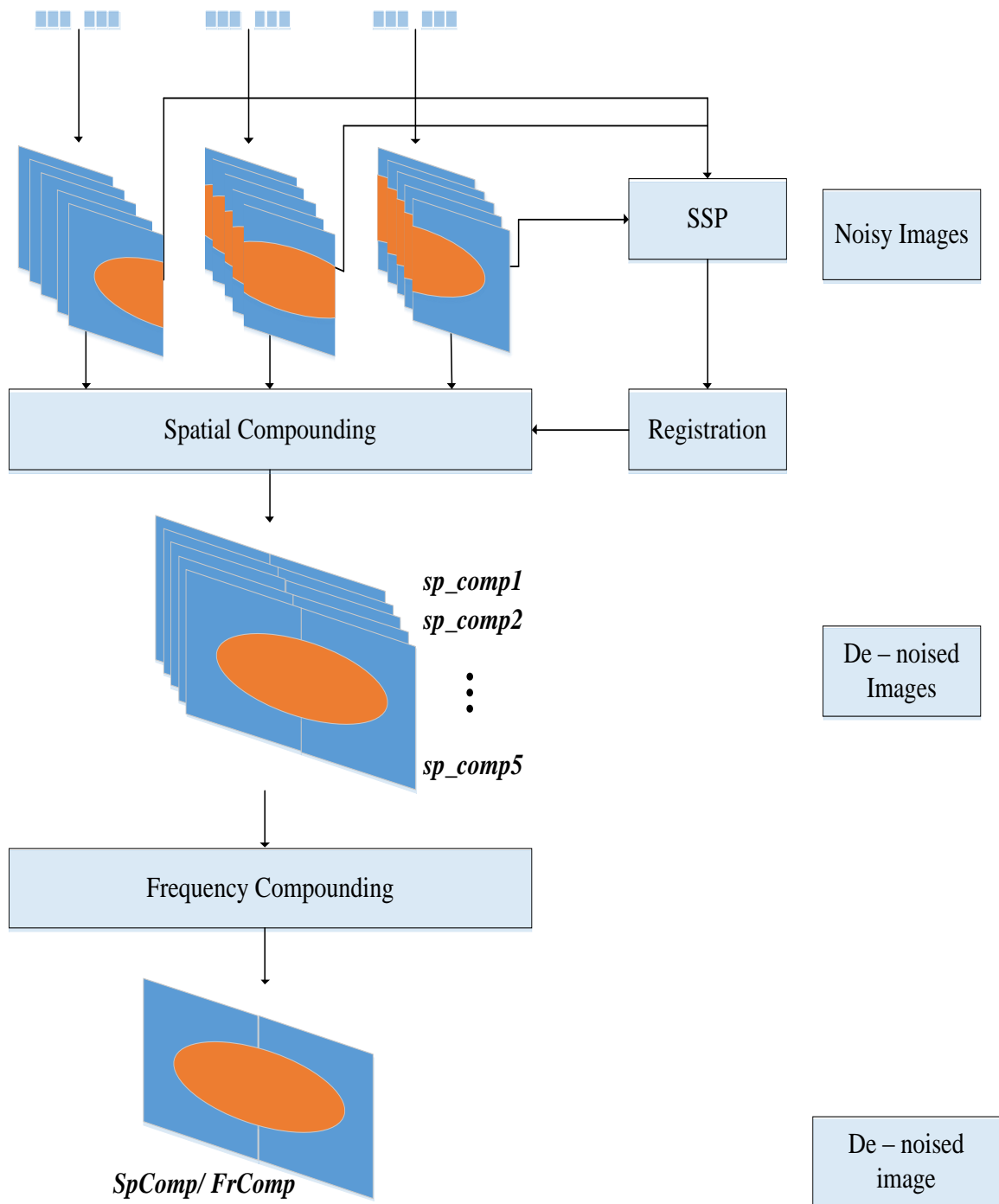
Figure 6-4: Version 1b) Image de-noising using spatial and frequency compounding

Table 6-2: Performance measures for different image de-noising methodologies

Scheme/Filter	CNR	MSE	RMSE	SMSE	SNR	PSNR	CCRO	BITA	SSIM
Original	0.1472	n/a	n/a	n/a	12.815	n/a	n/a	n/a	n/a
FrComp/SpComp	**0.2298**	0.0093	0.096	10.358	**19.079**	68.434	0.7709	0.5301	0.9996
SpComp / FrComp	**0.2202**	0.0094	0.097	10.311	**19.384**	68.373	0.7705	0.5216	0.9996
Median	0.1309	0.0100	0.100	9.5865	17.882	68.128	0.7772	0.2226	0.9998
Wiener	0.0992	0.0070	0.084	10.969	18.292	69.626	0.8333	0.6054	0.9998
Kaun Filter	0.1227	0.0069	0.083	11.262	17.041	69.714	0.8352	0.3150	0.9998
Frost Filter	0.1147	0.0086	0.093	10.152	17.249	68.757	0.8247	0.0449	0.9998
Anisotropic Filter	0.0741	0.0092	0.096	9.6499	19.526	68.447	0.7969	0.3681	0.9997

From Table 6-2, three very important observations can be derived. The first one is that both proposed schemes, i.e., **FrComp/SpComp** and **SpComp/FrComp**, present almost the same values for all the validated fidelity criteria. Thus, this provides us with the flexibility to choose either scheme at our convenience. For instance, it is better, in terms of speed, to first perform the averaging (for the frequency compounding) and then one registration to the 3 compounded images (fr_comp1, fr_comp2 and fr_comp3). The second observation is that only the proposed methodology presents increased contrast ratio compared to the others. That is of great importance considering that one inherent problem of ultrasound imaging is the low contrast ratio. Finally, we may observe the highly increased signal to noise ratio. In fact, the SNR of the proposed methodology is one of highest among all tested schemes.

The above analysis and testing safely concludes to the general statement that *the compounding schemes perform the expected way*.

In Figure 6-5 below, a summary of the results is given.
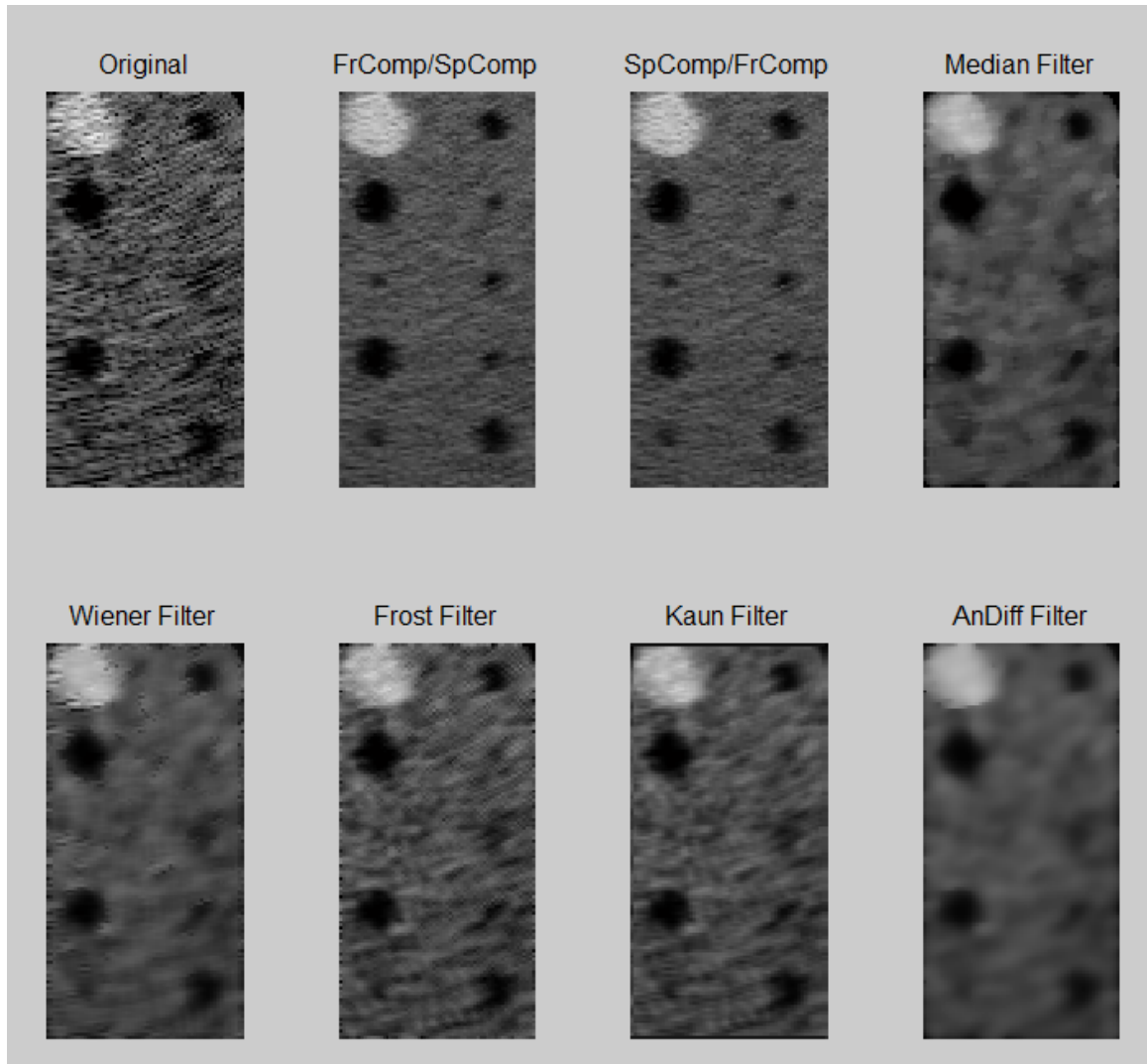
Figure 6-5: Comparison of images produced, given the described phantom, after implementation of different de-noising schemes

In Figure 6-6, the images produced after implementation of **FrComp/SpComp** and **SpComp/FrComp** schemes are only depicted together with the original one. As shown, in the original B-mode image someone is unable to distinguish small structures that have dimensions near the lateral resolution of the transducer. Furthermore, these structures are

116

not very well delineated. Finally, speckle noise in the original B-mode image is apparent. Regarding the de-speckled images using common filters, it is obvious that the speckle noise is reduced, which is also why all of them present high SNR compared to the original, but is clear that some of the structures have been completely vanished. In some cases, like the anisotropic diffusion filter, over-smoothing (related to the highest SNR on the table) can be observed. Over-smoothing is most of the times undesired, especially in medical images and ultrasound imaging that speckle is also related to biological tissue properties.
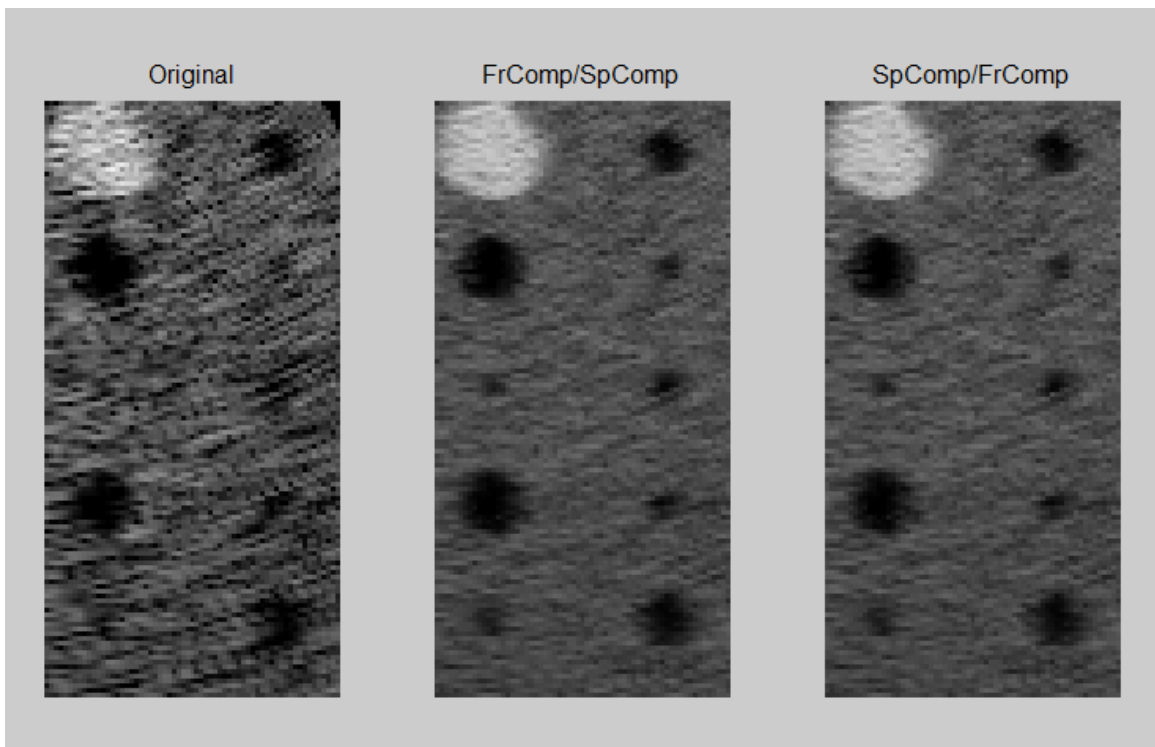
Figure 6-6: Obtained results using a stand-alone transducer VS the proposed methodologies FrComp/SpComp & SpComp/FrComp

Clearly, the most desirable results have been produced by the proposed de-specking scheme. Relatively speaking, although the scheme presents very high SNR no blurring is observed. More importantly, hidden structures have now revealed and in addition most of

the cysts are correctly delineated as perfect circles. In Figure 6-7, a graphical representation of the cysts that have been revealed using the compounding schemes, is illustrated. Someone may claim that the resolution has already been improved. Those first results are very promising, if we consider the fact that, to this point, only the results of half of the proposed methodology have been presented. The results of the whole methodology and the incorporation of the SR scheme are presented in the next section.
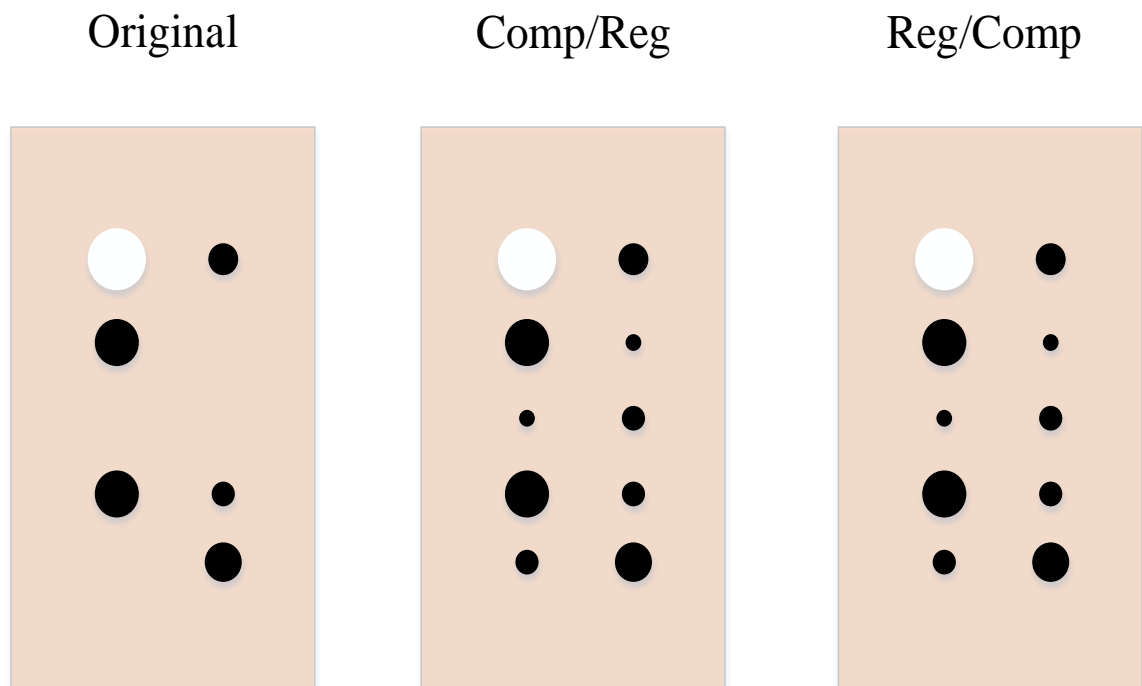
Figure 6-7: Graphical representation of obtained results using a stand-alone transducer VS the proposed methodologies FrComp/SpComp & SpComp/FrComp

6.2.4.2   Results of High-Resolution De-speckled Image

Although there has been few attempts in the literature to incorporate super-resolution schemes to an ultrasound machine, most of those attempts target to the exploitation of

118

super-resolution during the beamforming procedure [93]. This is related to the increased computational time and hardware complexity required to form the final SR image.

The current work intends to take advantage of the multiple sensors of the system and perform super-resolution on the multiple low-resolution B-mode images, already produced by the sensors. In that way it avoids to deteriorate the hardware complexity of the system, whereas the SR technique can be applied as a post-processing method. In section 6.2.3, it was mentioned that 2 different schemes were to be implemented.

Firstly, we implemented step 5.b and performed spatial compounding to the fr_comp1 and fr_comp2 as well as to fr_comp3 and fr_comp3, producing the images fr_comp_sp12 and fr_comp_sp23, respectively. Then super-resolution was applied to images fr_comp_sp12 and fr_comp_sp23. The final image was labeled SR2.

In the second scheme described in step 5.c, the super-resolution algorithm was implemented to the three compounded images fr_comp1, fr_comp2 and fr_comp3. This case is illustrated in Figure 6-8. The final image developed was labeled SR3. The CNR and the SNR for both schemes are presented in Table 6-3 and both B-mode images are given in Figure 6-9 along with the original one (in the case of a single transducer).

119

Noisy Images

Frequency Compounding   **Frequency Compounding**   **Frequency Compounding**

De – noised Images

fr_comp1   *fr_comp2*   *fr_comp3*

Super Resolution

HR De-noised Image

SR3
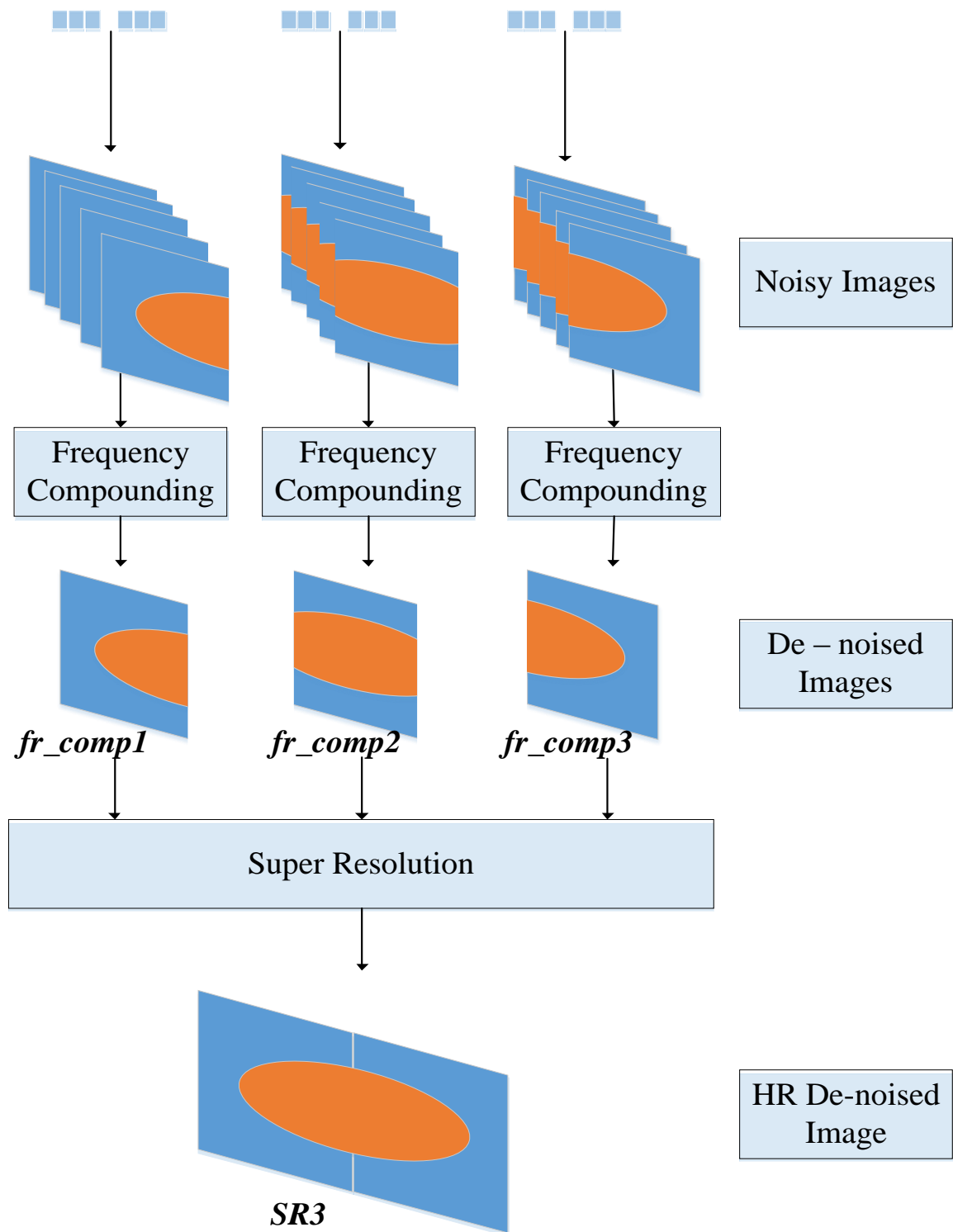
Figure 6-8: Super resolution image HR de-noising scheme

Table 6-3: CNR and SNR for the utilized SR schemes

	CNR	SNR
Original	0.1472	12.8157
SR2	0.3050	17.8178
SR3	0.2885	18.3070
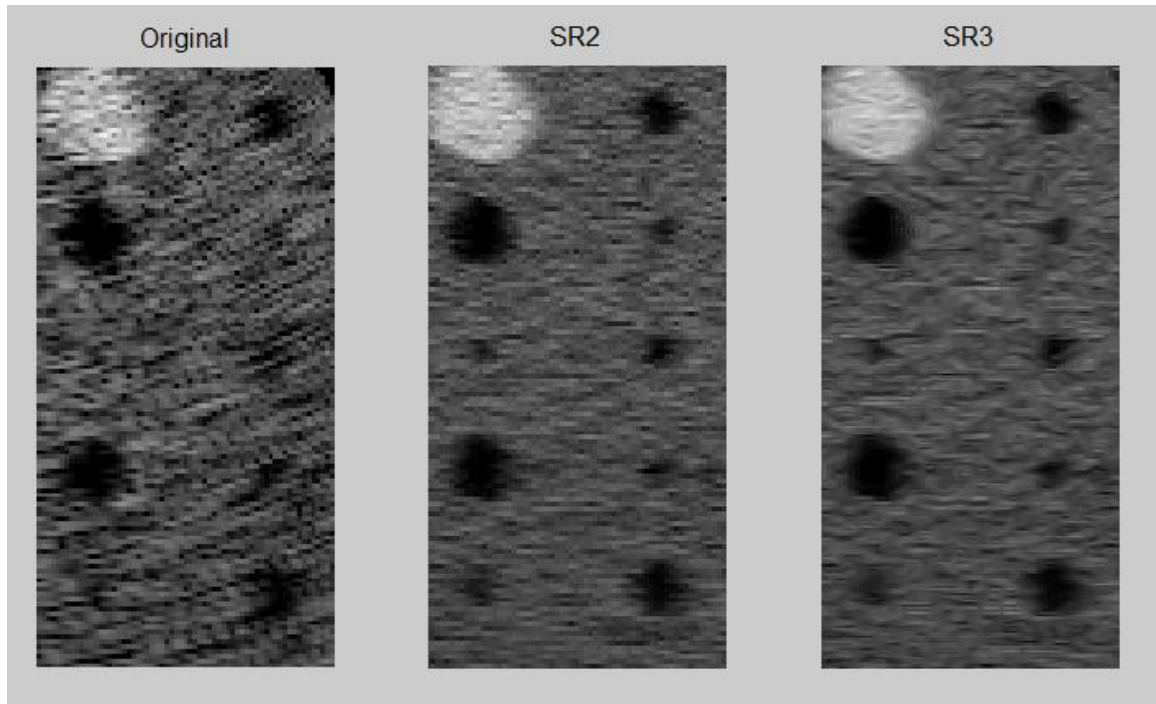
Figure 6-9: Obtained results using a stand-alone transducer VS the proposed

methodologies SR2 & SR3

Both Table 6-3 and Figure 6-9 indicate the significant improvement in the final image. The SNR is significantly higher compared to the original case, while the CNR for both SR schemes is higher than all previously examined de-speckling images.

In Figure 6-10, the two SR schemes are depicted, along with the two compounding schemes discussed in the previous section.

121
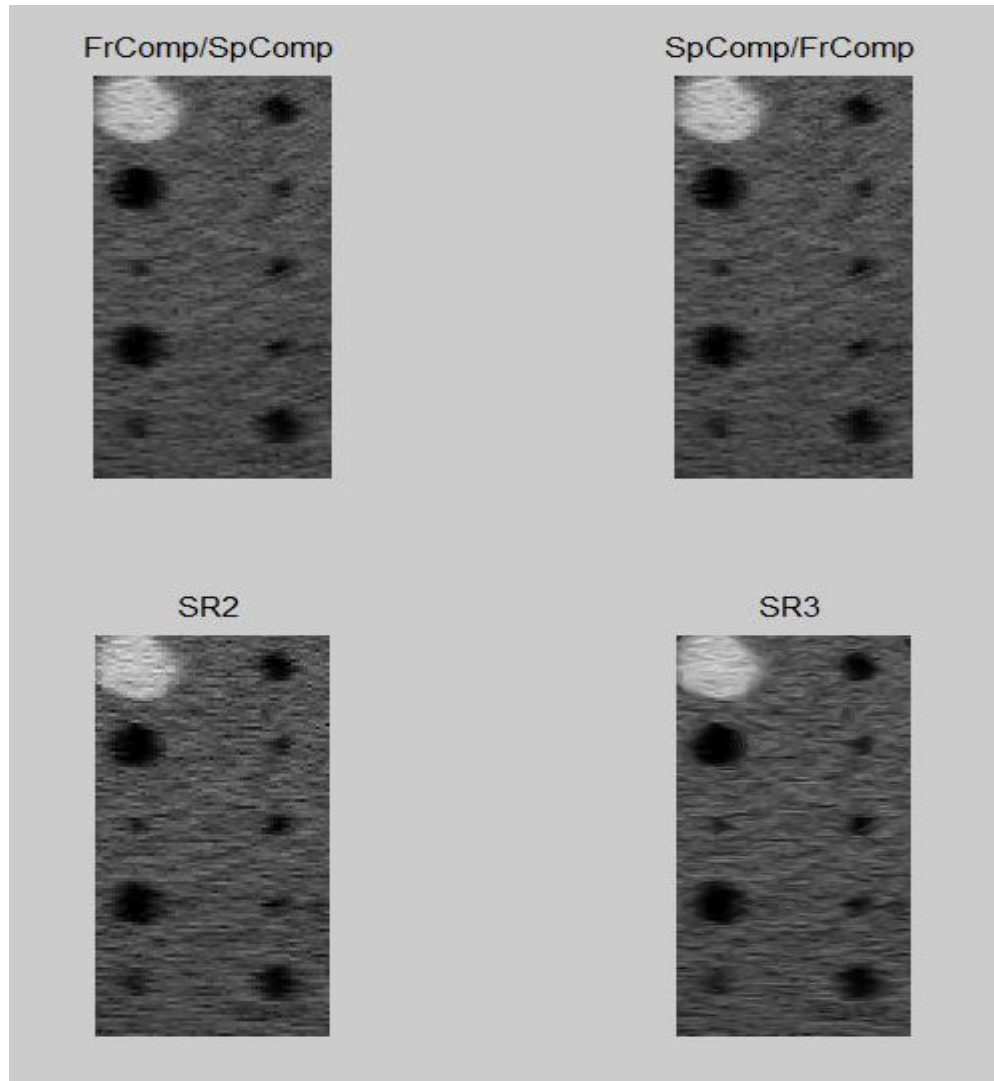
Figure 6-10: De-speckling VS SR methodologies results

At this point it is important to highlight that an SR scheme can produce even better results if it includes more than two or three images of the same scheme.

6.3 Supplementary Material

In the previous section the effectiveness of the proposed image enhancement methodology was established. In fact, all the formerly implemented proposed schemes presented an increase in the image quality. The betterment of image quality was not only

122

evident in the performance measures calculated but also obvious by simple visual inspection of the produced images. During the development of the proposed methodology different schemes and techniques were tested. In this section the results of two different studies are briefly discussed; the first in regards to the technique of split spectrum processing (SSP) and the other in regards to the super-resolution algorithms. Both studies were conducted in order to select the parameters and techniques for the final 3D methodology that will be presented in the following chapter.

6.3.1 Split Spectrum Processing (SSP)

The well-known technique of split spectrum processing was performed using different values of width and separation among the Gaussian-like band pass filters. The total number of filters used each time was defined by the effective bandwidth (3 MHz), the width of the Gaussian filter and the separations between two consecutive filters. Certain performance measures have been calculated and presented in Table 6-4 for all configurations under consideration. The resulted compounded images are given in Figure 6-11.

Table 6-4: Split Spectrum Processing

	Original	**(w =0.5, s =0.4)**	**(w =0.75, s= 0.5)**	**(w =1, s=0.75)**
SNR	16.3952	26.5950	24.8419	23.6703
MSE	n/a	0.0305	0.0211	0.0156
PSNR	n/a	63.2851	64.8913	66.1988
SSIM	n/a	0.9963	0.9976	0.9983

123
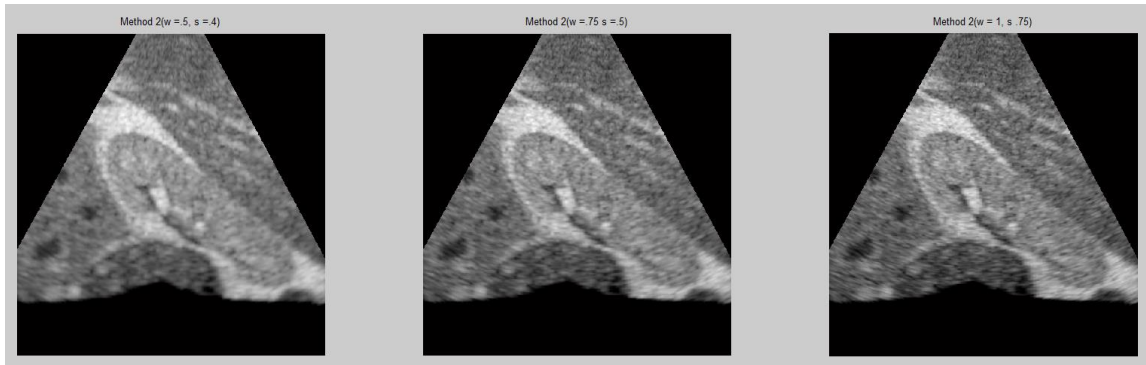
Figure 6-11: Obtained results for compounded images, left (w =0.5, s =0.4), middle (w =0.75, s= 0.5) and right (w =1, s=0.75)

Due to the fact the SSP technique is a preprocessing step, used to alleviate the problem of noise before applying image registration, it is desired to be quite fast. From Table 6-4 can be observed that all schemes present significant improvement in SNR with small differences among them. This is the main reason why the third scheme was preferred. In fact, the third scheme uses the least number of filters and is faster than the other two, while at the same time presents significant increase in the SNR compared to the original image.

6.3.2 Super-resolution Schemes

A new super-resolution algorithm was implemented based on the shift among the transducers, in the sub-pixel scale. The implemented algorithm was compared with the most commonly used super-resolution algorithms in the literature. The comparison was made by visual inspection. The obtained results show that the designed algorithm present similar behavior with the Projection onto Projects Sets, (POCS) algorithm. The fact that the proposed SR algorithm is a non-iterative one (fast), and that the obtained results are similar to the POCS algorithm, demonstrates its correctness and justify its use as the basic SR algorithm in the proposed methodology. A detailed description of the proposed

124

algorithm is given in Chapter 7, exclusively for 3D volumetric images. Below are the results of the following SR algorithms; a) proposed, b) Papoulis and Gerchberg [115], c) Projection onto Convex Sets d) Iterative Back Projection [116], e) Robust Super Resolution [117], f) Normalized Convolution [118]. The presented images for the 5 super resolution algorithms were produced using the publicly available GUI superresolution_v_2.0 developed by the Laboratory of Audiovisual Communications (LCAV), Ecole Polytechnique Federale de Lausanne (EPFL).

| a) Proposed SR | b) PG | c) POCS |
| d) BP | e) RS | f) NC |
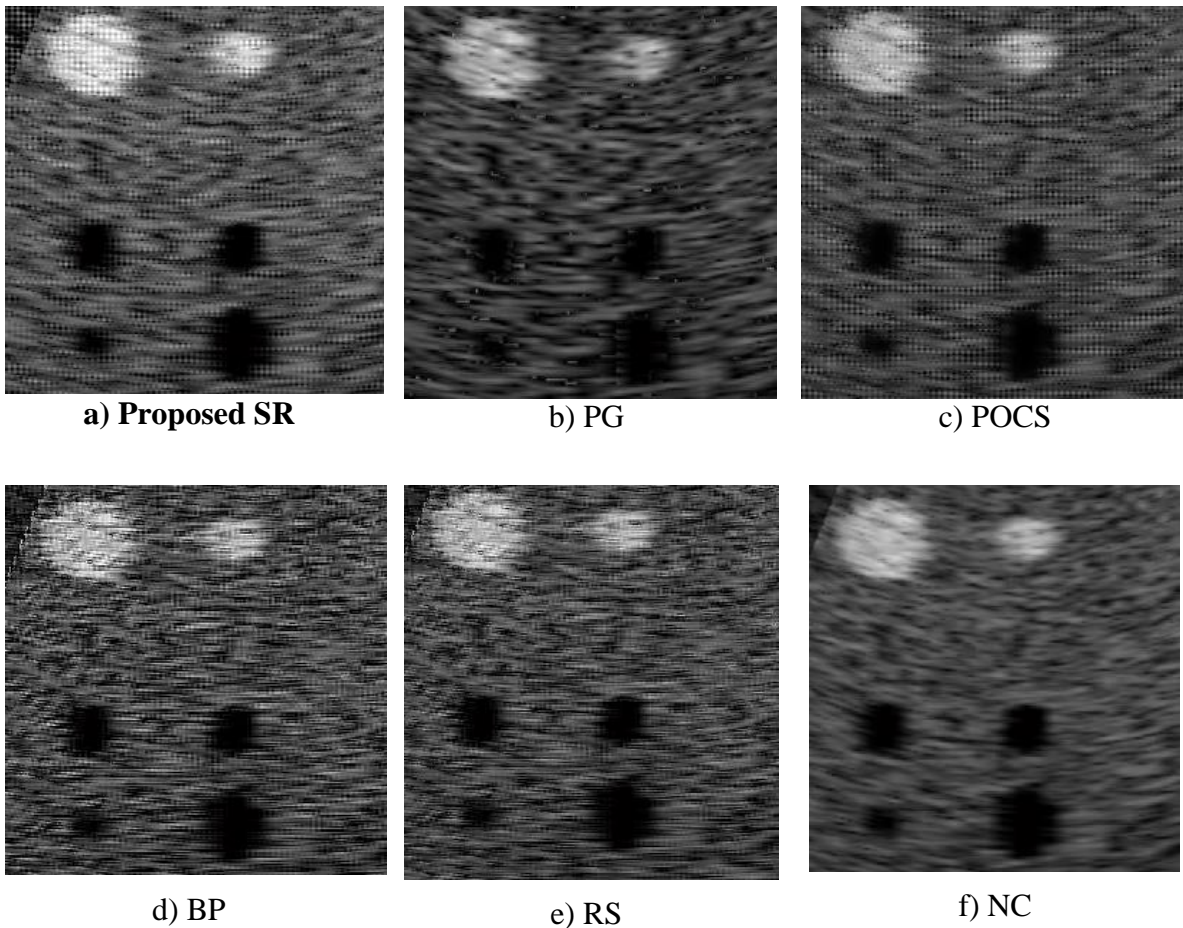
Figure 6-12: Obtained results from different super-resolution schemes

6.4 Conclusions

In this chapter, different versions of the methodology presented in Chapter 5 were applied in 2D images and the obtained results were evaluated. In addition, a visual comparison between the proposed SR algorithm and existing well-known was performed. The main findings of the 2D case study can by summarized below:

1. Regarding the compounding schemes compare to original images

   - Both Proposed schemes present similar values for all the PM

   - CNR and SNR are significantly improved

   - SNR is better compared to other methodologies and without over-smoothing

   - Much better visual results

     - Better delineation of boundaries

     - New structures were revealed

2. Regarding Super resolution schemes compared to original images

   - Higher image resolution

   - CNR and SNR are significantly improved for both schemes.

   - SNR is similar compared to other methodologies but without over-smoothing

   - Much better visual results

     - Better delineation of boundaries

126

> ➢ New structures were revealed

3. Regarding Super resolution compared to compounding schemes

- Higher image resolution

- CNR was slightly improved while SNR appears to be slightly degraded for both schemes.

- Both SR schemes appear to present a slightly better boundary delineation

4. Regarding SSP study

- Increasing the number of filters by decreasing the width and the separation parameters

5. SR algorithms compared to well-known SR algorithms

- Similar visual results with POCS

- Chessboard effect

Overall, the proposed SR methodology presented the most promising results. As both schemes manifested the higher CNR which is one of the most important parameter for performance evaluation of ultrasound images, as well as both schemes manifested the most pleasant visual results. SNR was calculated to be less than the one calculated using only compounding schemes, but due to this fact, SR schemes avoid over-smoothing (not desired effect) the image. Additionally, the analysis conducted regarding SSP techniques lead to the selection of an SSP scheme that uses few filters. Finally, the comparison among the SR schemes verify that the proposed SR algorithm behaves similar with well-known ones.

127

Thus, given the fact that is non-iterative and can be expanded for the case of 3D was selected to be the main SR algorithm of the 3D methodology.

The main drawback of a POCS-based algorithm (like the proposed one) is the chessboard effect. The chessboard effect can be minimized by increasing the number of input images. In the next chapter, the final 3D image enhancement methodology is constructed based on the findings in this chapter.

7

PROPOSED METHODOLOGY FOR 3D ULTRASOUND IMAGES

7.1 Introduction

This chapter is the last step, for the objectives of the current dissertation to be met. The outline of the generic image enhancement methodology was mentioned in Chapter 5, while in this chapter its actual implementation in the case of 3D images is ventured. Here, the final 3D image enhancement methodology is described in details. As already mentioned several times throughout this dissertation, the ultimate goal of the methodology developed in Chapter 5, is to compensate for the loss of image quality of the proposed 3D USI system presented in Chapter 4. Thus, this methodology was actually designed with respect to the limitations (image quality degradation) that the proposed 3D ultrasound system presents. Although the system uses 2D phased array transducers that produce volumetric images (3D), the analysis conducted in Chapter 6 for 2D images (using 1D phased array transducers) was critical for the development of the final 3D image enhancement

129

methodology. Indeed, the results from the 2D images case study confirm the adequacy and effectiveness of the proposed methodology.

7.2 Experimental Set Up

7.2.1 Transducers Configuration

The configuration of the transducers is the same with the topology presented in section 4.2.3 and illustrated in Figure 4-3. The transducers were excited with different frequencies around the resonant frequency as an intention to apply the frequency compounding method on the produced B-mode images. The geometrical characteristics for all the transducers were identical and can be summarized in Table 7-1. More details on the characteristics were given in section 4.2.3.

Table 7-1: Geometrical characteristics of all transducers, in the case of 3D image enhancement methodology

	Transducers 1-2-3-4
Type	2D phased array
f_0 (MHz)	3
f (MHz)	3, 3.5
Number of elements	256
Length of elements(mm)	0.9
Width of elements(mm)	0.9
Kerf in the x-direction (μm)	50
Kerf in the y-direction (μm)	50

7.2.2 Cyst Phantom

Following the same reasoning with the one discussed in section 6.2.2, the simple cyst phantom illustrated in Figure 7-1, was used. The phantom consists of 7 blob-like structures and all of them represent cysts.
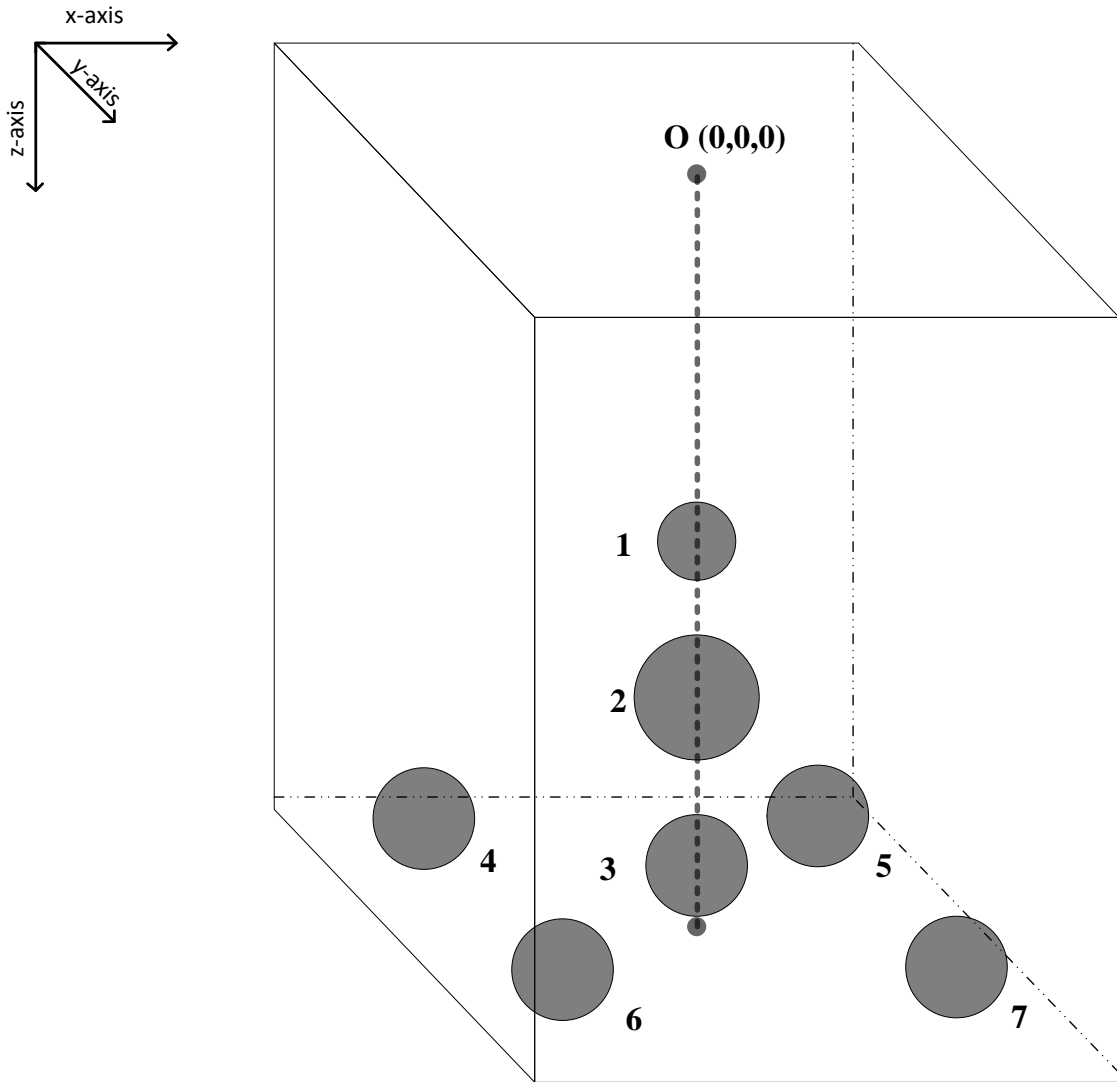
Figure 7-1: Selected phantom in the case of the 3D image enhancement methodology

The position of each cyst and their dimensions were carefully selected in such a manner that some of them lie inside the FOV of all three transducers, whereas others manifest

131

diameter similar to the lateral resolution of the system. The phantom was implemented in MATLAB. The cysts dimensions and coordinates are given in Table 7-2, below:

Table 7-2: Cysts dimensions and their coordinates, in the case of the phantom used for the 3D image enhancement methodology

Structures	Center Coordinates (mm)	Radius (mm)
Cyst 1	0, 0, 45	5
Cyst 2	0, 0, 60	8
Cyst 3	0, 0, 80	7
Cyst 4	-20, -20, 80	7
Cyst 5	20, -20, 80	7
Cyst 6	-20, 20, 80	7
Cyst 7	20, 20, 80	7

The volume of the cyst phantom, illustrated in Figure 7-1, is $V = 80 \cdot 80 \cdot 100 = 640,000 mm^3$. As far as the total number of scatterers is concerned, it was selected to be 130,000. Thus, the number of scatterers that are included inside $1mm^3$ is $n_s = {130,000}/{640,000} = 0.2$. Given the axial and lateral resolution of the transducer described in 4.2.3, the volume of one resolution cell can be calculated, $V_c = 8 \cdot 8 \cdot 1.1 = 70.4 mm^3$. This suggest that inside a single resolution cell the number of scatterers are $n_{c_s} = 0.2 \cdot 70.4 = 14$. From the theory, when n_{c_s} is larger than 5, the fully developed speckle model can be applied. That is that the echo signal produced by the simulation software can be considered as a band-pass random process.

132

7.3 New 3D Image Enhancement Methodology

In this section we describe in details the implemented algorithm for the case of 3D images, as well as the procedure followed for the 3D case.

The procedure followed for this experimental set up and for the case of volumetric images is similar to the one presented in section 5.3 for 2D images, with the appropriate modifications. It is described below in details.

1. Each transducer provides 2 images of the same scene. In total $4 \cdot 2 = 8$ images

2. Light SSP in one of the 2 images produced by each sensor

3. Perform sub-pixel image registration to find the transformation (known in simulation) using the SSP processed images

4. Perform frequency compounding using the two original images of each sensor. Result: Four compounded images

5. Perform super resolution technique to the four compounded images of the previous stage. Result: Final HR de − noised image

6. 3D Image enhancement

In this case, due to high computational time restrictions, fewer images were selected to be produced by each transducer, compared to the 2D case. Although steps 2 and 3 are part of the procedure, they were not actually performed since the sub-pixel shifts among the transducers (among the images) were already known. Below each one the aforementioned steps are explained in details.

133

7.3.1 Raw Data Generation (Raw A-lines, RF signal)

After simulating the designed 2D phased array transducers in FIELD II and MATLAB, the volumetric phantom presented in 7.2.2 was constructed. Then, the above transducer configuration was adopted and the transducers were placed at the appropriate location in the surface of the volumetric phantom. Field II was used to produce the raw signals (A-lines) recorded from each transducer. The scanning of the region was performed following the procedure presented in section 6.2. Thus, from a single recording of each transducer $45 \cdot 45 = 2025$ items of A-lines were produced. In other words, for a single volumetric image to be produced, 2025 A-lines were required. In order to capture those A-lines, Classical Phased Aperture (CPA) beamforming technique was implemented.

7.3.2 Volumetric Image Generation – Developed 3D scan conversion

Firstly, the beamformed A-lines are enveloped detected using Hilbert's transform and then the enveloped detected data are log-compressed, in order for the signals to have the appropriate dynamic range. The resulted log-compressed, envelop detected signals are now in the appropriate form to undergo the scan conversion technique.

On the contrary to the 2D case, in order to produce the volumetric images a new image reconstruction algorithm, for 3D scan conversion had to be developed. The notion of scan conversion for the 2D case was introduced in section 3.3.2.3. For this case, the missing data (voxels instead of pixels) of the 3D grid can be estimated by interpolation. The developed algorithm was based on the concept of trilinear interpolation, shown in Figure 7-2, below.

134
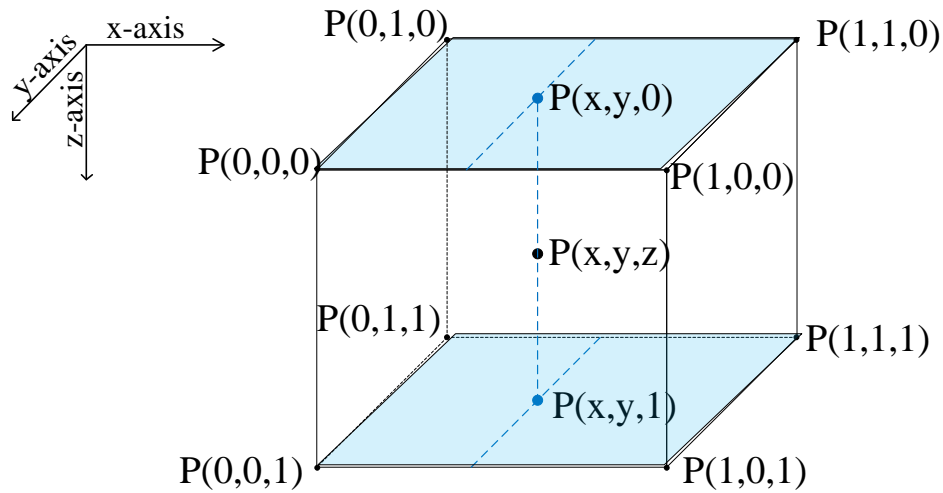
Figure 7-2: Trilinear interpolation of missing voxels

Trilinear interpolation can be performed in the following three steps, consisting of two bilinear interpolations followed by one linear. With respect to Figure 7-2, these steps are:

1. Computation of $P(x, y, 0)$, as a bilinear interpolation at the xOy plane, at $z = 0$

2. Computation of $P(x, y, 1)$, as bilinear interpolation at the xOy plane, at $z = 1$

3. Computation of $P(x, y, z)$, using linear interpolation for $P(x, y, 0)$, and $P(x, y, 1)$.

Due to the fact that trilinear interpolation is performed in the way described above, 10 weights are needed to be calculated (four for each of the bilinear steps 1 and 2, and two for the linear step 3).

In order for the missing data of the 3D grid to be interpolated, the nearest values of log compressed, envelop detected signals are required (Figure 7-3).

135
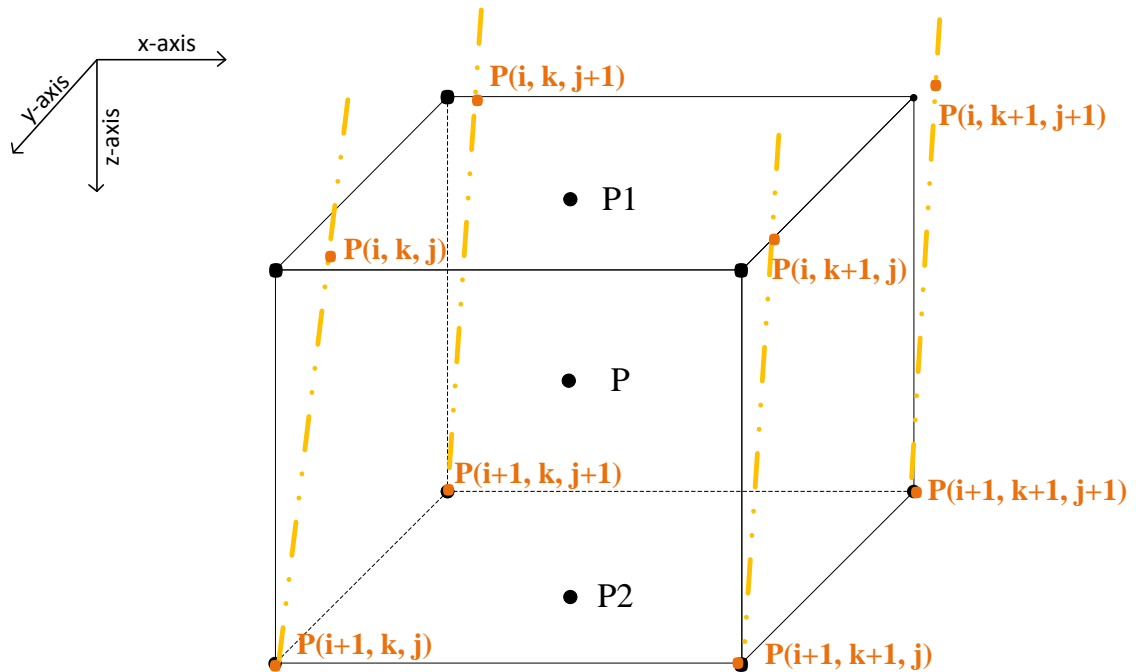
Figure 7-3: Notation of the trilinear interpolation approximation, in the case of 3D

scan conversion

The 3D scan conversion algorithm can be summarized in the following steps:

1. Initialization of the 3D image matrix (zero values)

2. Matrix scanning and identification for each pixel of the following:

    a) closest scan lines (4), as shown in Figure 7-3

    b) closest samples (2), as shown in Figure 7-3

3. Calculation of the weights $w_1, w_2 \cdots w_{10}$

4. Perform the actual interpolation, consisting of:

136

a) Bilinear interpolation of P_1 using weights w_1, w_2, w_3, w_4, as follows:

$$P_1 = w_1 \cdot P(i,k,j) + w_2 \cdot P(i,k,j+1,) + w_3 \cdot P(i,k+1,j+1) + w_4 \cdot P(i,k+1,j) \qquad (7\text{-}1)$$

b) Bilinear interpolation of P_2 using weights w_5, w_6, w_7, w_8, as follows:

$$P_2 = w_5 \cdot P(i+1,k,j) + w_6 \cdot P(i+1,k,j+1,) + w_7 \cdot P(i+1,k+1,j+1) + w_8 \cdot P(i+1,k+1,j)$$

$$(7\text{-}2)$$

c) Linear interpolation of P using P_1 and P_2 with respective weights w_9 and w_{10}, as follows:

$$P = w_9 \cdot P_1 + w_{10} \cdot P_2 \qquad (7\text{-}3)$$

Above, $P(i,k,j)$, is the actual recorded value of the ith sample that belongs in the scan line k, at plane j.

7.3.3 Frequency compounding

Following the procedure described above, 8 volumetric images (2 per transducer) were generated. Frequency compounding was performed to each pair of images produced by the same transducer, resulting in 4 compounded images. At this point it is worth highlighting that the steps of SSP and sub-pixel registration were omitted, due to the fact that the positions of the transducers were already known (they had been carefully selected in advance) and as a result the shifts of the transducers were known as well. That resulted to speed-up the whole process, excluding a step that was not one of the current work objectives, i.e., 3D motion estimation. On the contrary, implementation of an SR algorithm is one of the most important objective of this dissertation, since it is a prerequisite for the

137

successful implementation and effectiveness of the proposed ultrasound system. That is why for the next step a new super resolution algorithm was developed and implemented.

7.3.4 New 3D Super Resolution Algorithm

The 3D super resolution algorithm implemented in this section, is a generic one. That is, it can be applied in an arbitrary number of LR volumetric input images. Although 2D super resolution has attracted the interest of a numerous researchers from different fields, SR for 3Dimensional data has not yet been studied extensively. This is why very few references of 3D applications of the SR can be found in the literature. Consequently, there is a difficulty to assess the proposed SR algorithm and the proposed methodology in general. The algorithm to be presented here is based on super resolution via image wrapping, but differs from similar algorithms in the essence that drills information of the topology of the presented system.

The algorithmic steps of the implemented algorithm are the following ones:

1. Choose a reference 3D image from the pool of 3D LR input images

2. Find the motion field from the rest LR images with respect to the reference image (known for the case presented)

3. Construct the HR cubic grid, scale-up the LR images (cubic interpolation) and wrap them to it

4. Assign weights to each voxel of each image (w_t), depending on:

   - the distance between the position of image's voxel and the center of the transducer

138

- the distance between the position of image's voxel and the actual voxel on the HR grid

5. Perform image fusion given the weights assigned before. The resulting image is the compounded HR volumetric image (I_{CHR})

At this point it is worth highlighting the way the fusion was achieved. As described in step 4, for each voxel of all interpolated images, a weight was assigned. This introduces two new types of information to the proposed algorithm; a) global information and b) local information. The term global information refers to information in regards to the topology of the system. In the described topology, the system consists of four transducers. For each voxel, the idea is to weight more information coming from the closest transducer. From the other side, the local information term refers to the information that can be introduced to the algorithm in regards to the neighbors of the voxel on the HR grid.

Thus, the weight of each voxel of each interpolated image is a function of the following form:

$$w_t(x, y, z) = a * g_t(x, y, z) + (1 - a) * l_t(x, y, z) \qquad (7\text{-}4)$$

In equation (7-4) above, t can take values from 1 to 4, depending on by which transducer the image was captured. Moreover, w_t is the weight of the voxel $P(x, y, z)$ of the interpolated image produced by the transducer t. In addition, g_t and l_t are the global and local information functions respectively, of the voxel $P(x, y, z)$. Finally, values a and $(1-a)$ ($a \in [0,1]$) indicate to what extend global and local information respectively, affect the weights.

139

The final HR image (step 5) is calculated using the following formula:

$$I_{CHR}(x, y, z) = \frac{\sum_{t=1}^{4}(I_{CINTt}(x, y, z) * w_t(x, y, z))}{\sum_{t=1}^{4} w_t(x, y, z)} \tag{7-5}$$

In equation (7-5) above, I_{CHR} is the compounded HR image, whereas I_{CINTt} each one of the interpolated compounded images that had been previously obtained.

7.3.5 3D Image Enhancement

In the 3D case, there is one more step in order to achieve further enhancement of the final result. In particular, the type of enhancement performed aims at image contrast enhancement.

In this step classical image processing techniques were applied. The algorithmic steps for this part can be summarized as follows.

1. Given the input of the previous step (I_{CHR}), image multiplication was applied

2. Perform a controlled histogram equalization

The outcome of the first step is the multiplied image given by the following relationship:

$$I_{MCHR}(x, y, z) = I_{CHR}(x, y, z) * I_{CHR}(x, y, z) \tag{7-6}$$

In equation (7-6) above, I_{MCHR} is the multiplied, compounded HR image obtained from an element-wise multiplication.

140

The outcome then undergoes a controlled histogram equalization. That is, the mapping function is introduced by the user. It was found that applying the sigmoid function given in equation (7-7), the maximum CNR was achieved:

$$I_{EHR}(x, y, z) = b * \left(\frac{1}{1 + \exp(c * (-I_{MCHR}(x, y, z) + c))} \right) \tag{7-7}$$

Where I_{EHR} is the final enhanced HR volumetric image, b and c are constants, selected to have values 0.95 and 0.35 respectively, after histogram inspection.

In the above equation, the final enhanced HR volumetric image, is the outcome of sigmoid transformation to the intensity of each voxel of the multiplied compounded HR volumetric image.

7.4 Results

In this section the results obtained after applying the proposed methodology for 3D ultrasound images are presented. The section is divided into three subsections; the first one deals with the presentation of the input images (generated images using a single transducer). The second, presents the results obtained after applying the methodology for the compounded HR image (I_{CHR}), while the third one presents the results obtained for the enhanced HR image (I_{EHR}).

In both latter cases, all results were visually compared with a scaled up (cubic interpolation) version of original images. Interpolated images are usually used as benchmarks for testing SR algorithms. Then, the most important performance measures, i.e., signal to noise ratio (SNR) and contrast to noise ratio (CNR) were calculated in order

141

to quantify the improvement in the image quality. The results obtained for those two measures showed significant improvement in both cases. In addition, the results were visually assessed and got compared to the original images. In order to visualize the 3D space, the orthogonal slices of the obtained images are presented.

7.4.1 Original Images

One slice of the volumetric input images is given in Figure 7-4 and Figure 7-5 below. In all images, the region with the 3 cysts has been extracted. In Figure 7-4, the images obtained from transducers 1-4, with operating frequency 3MHz are given, while in Figure 7-5 the respective images with operating frequency 3.5MHz.

All of the images present poor quality. This is mainly due to the low lateral resolution of the transducers, as well as the fact that during the scanning process only 45 scan lines were used in the azimuthal direction (x). That resulted in numerous missing values which need to be estimated during the scan conversion algorithm.

In the original images shown both Figure 7-4 and Figure 7-5, only one cyst is visible, whereas another can be only hardly distinguished and the third can be identified. In none of the images though, the actual shape and size of the cysts has been correctly depicted.

142

Transducer T3

Transducer T1

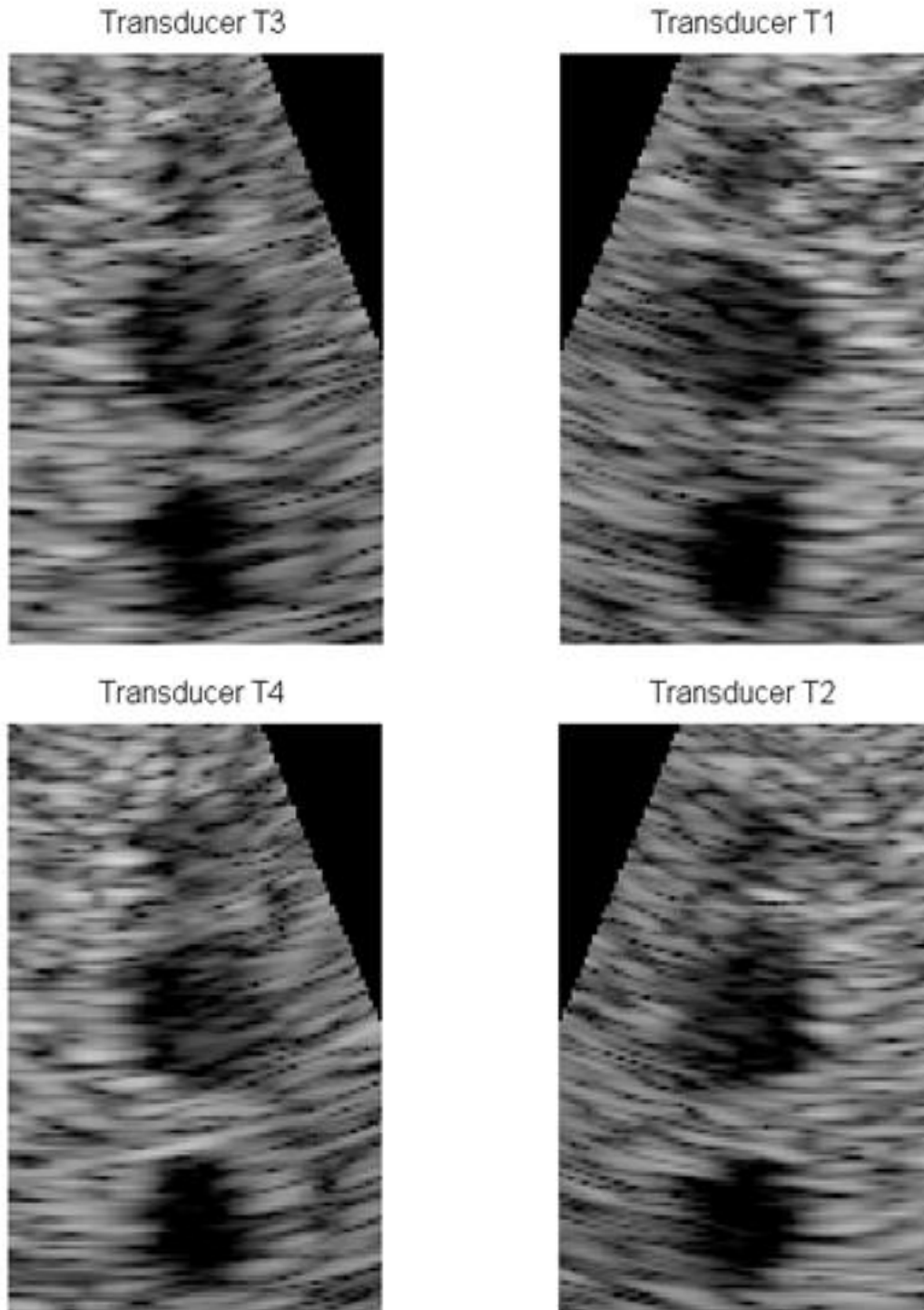Transducer T4

Transducer T2

Figure 7-4: One slice of the volumetric input images produced by stand-alone

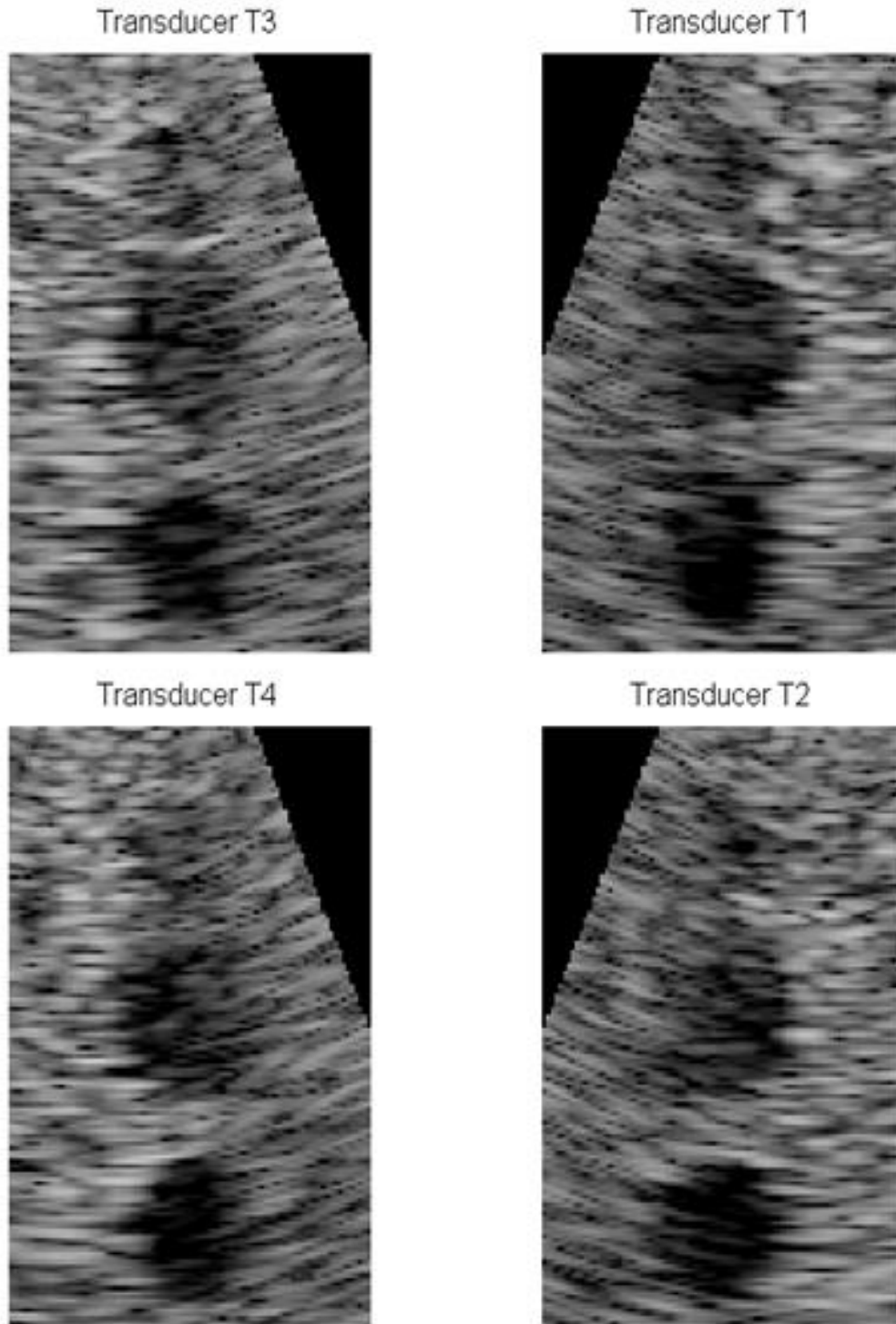*transducers with operating frequency 3MHz*

Figure 7-5: One slice of the volumetric input images produced by stand-alone transducers with operating frequency 3.5MHz

As mentioned above, interpolation schemes are used in order to assess the performance of SR algorithm. Scale up of the input images by factor was applied, using cubic interpolation in order for the input images to match the resolution of the outcome of the methodology.

The scaled up images are illustrated in Figure 7-6 and Figure 7-7. All of them appear to be the same with the original ones. In order to quantify the quality of the produced images of CNR and SNR were calculated and are presented in Table 7-3 below. The CNR was computed for the 3 cysts illustrated in the obtained image. Those are the cysts 1, 2, 3 depicted in Figure 7-1.

Table 7-3: Calculation of CNR and SNR of the interpolated volumetric images

	CNRCyst1	CNRCyst2	CNRCyst3	SNR
Interpolated Image1	0.1443	0.1867	0.3496	16.6836
Interpolated Image2	0.1292	0.1398	0.3700	16.1310
Interpolated Image3	0.1670	0.1811	0.3469	16.9079
Interpolated Image4	0.1422	0.1565	0.3425	16.1588
Interpolated Image5	0.1637	0.1593	0.3499	16.7861
Interpolated Image6	0.1399	0.1314	0.3250	16.8639
Interpolated Image7	0.1389	0.1525	0.3105	17.4317
Interpolated Image8	0.1028	0.1743	0.3223	16.6918

145

Figure 7-6: One slice of the volumetric interpolated input images produced by stand-alone transducers with operating frequency 3MHz

Interpolated Image: Transducer T3
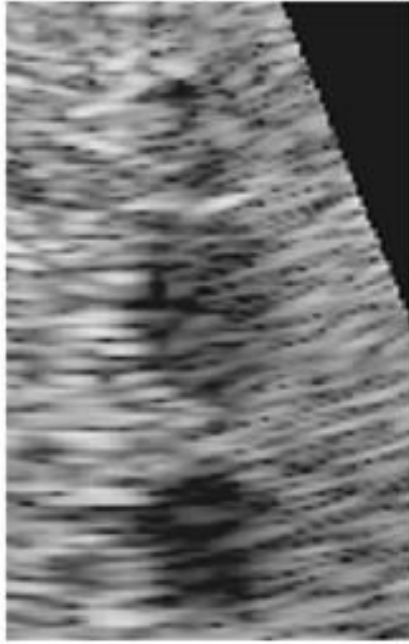
Interpolated Image: Transducer T1
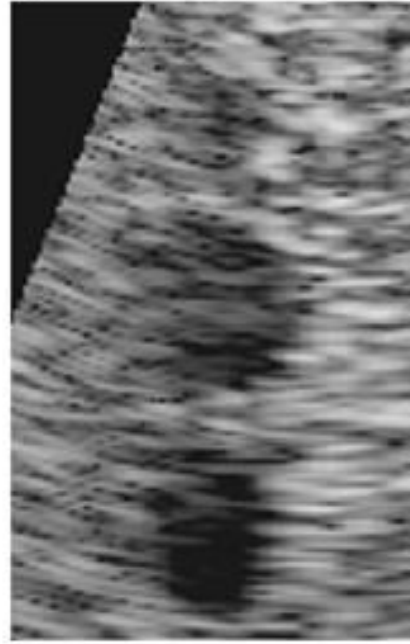
Interpolated Image: Transducer T4
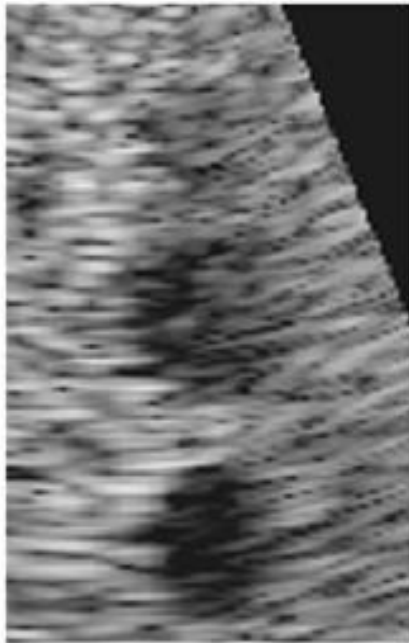
Interpolated Image: Transducer T2
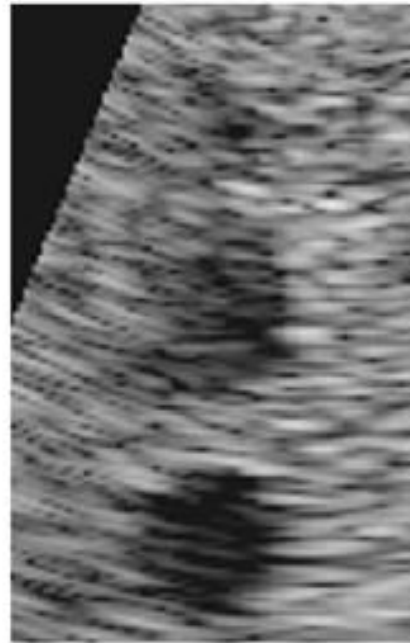
Figure 7-7: One slice of the volumetric interpolated input images produced by stand-

alone transducers with operating frequency 3.5MHz
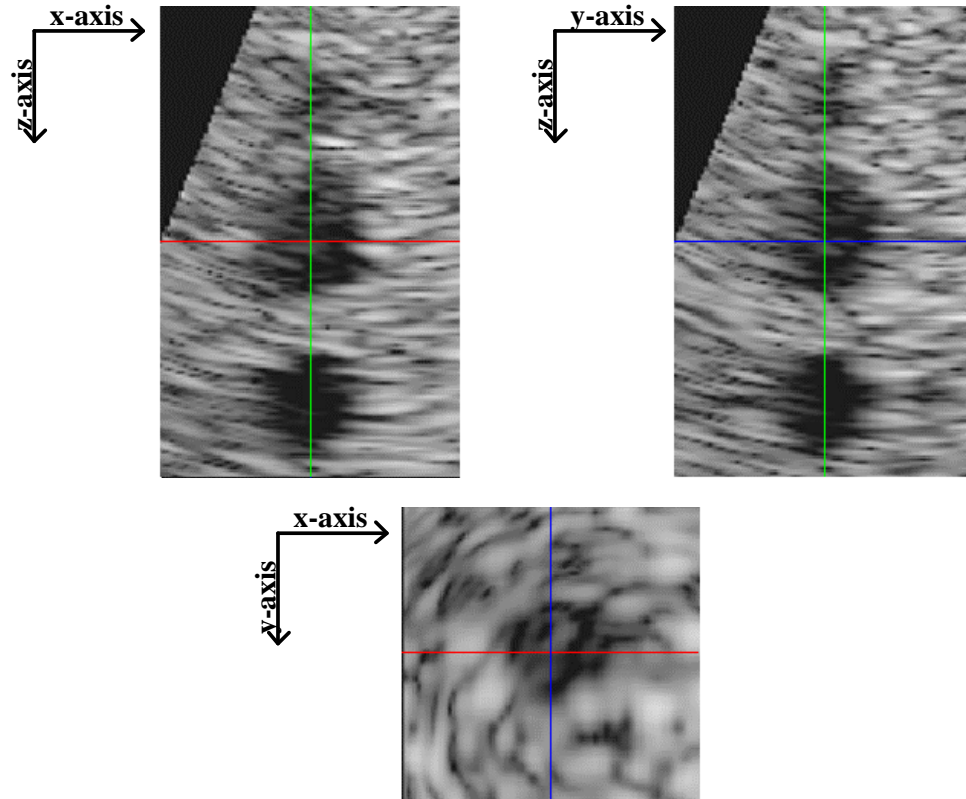
Figure 7-8: Orthogonal slices of the interpolated volumetric image, produced by transducer 1, with operating frequency 3MHz

The limitation of the transducers used for the proposed configuration is apparent. In Figure 7-8 and especially for the xy plane, the low resolution of the image produced, which in particular of the lateral one is very severe.

7.4.2 *Compounded HR Image* I_{CHR}

Having the scaled up version of the original images, the performance of the algorithm can be evaluated. The obtained results from the compounded HR image are given in Figure 7-9 and Table 7-4.

148
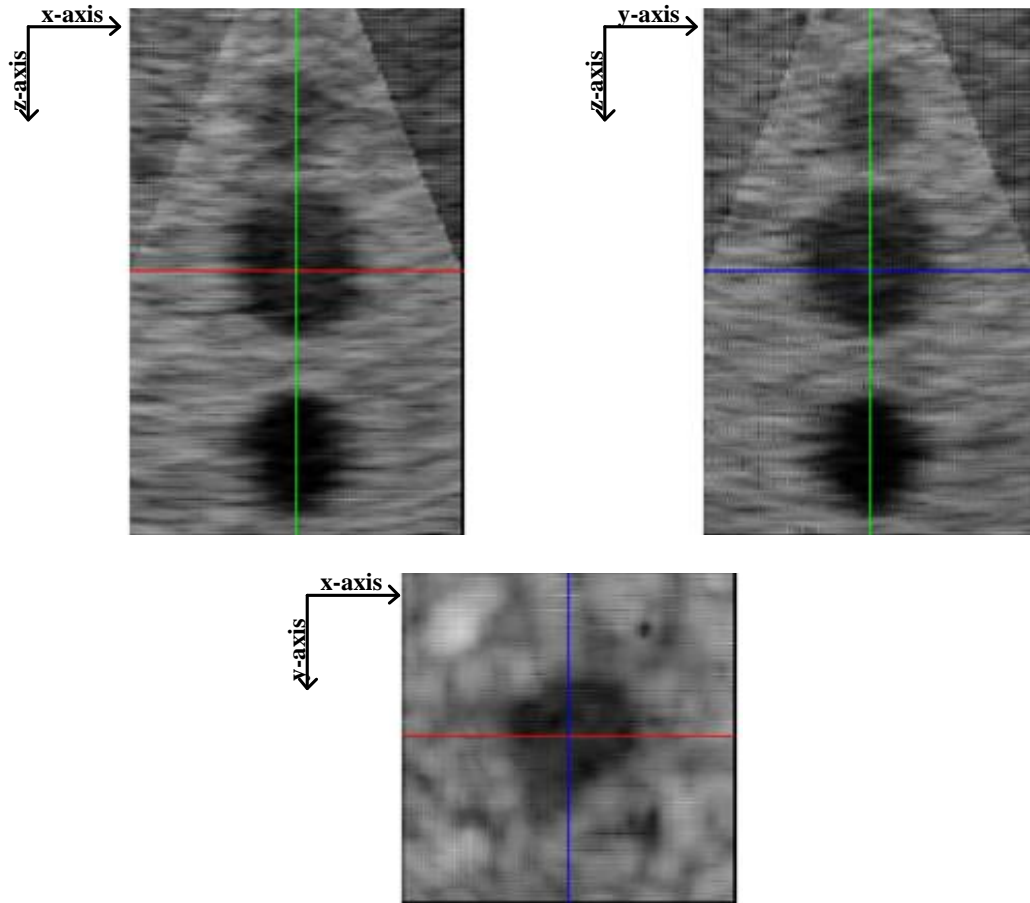
Figure 7-9: Orthogonal slices of the compounded HR volumetric image

It is obvious from all the slices presented in Figure 7-9 that the improvement observed for the case of compounded HR image is significant. All the cysts have been identified and all of them are better delineated. Lateral resolutions seems to have been improved. The corresponding performance measures for this case are depicted in Table 7-4. While in Figure 7-10 one interpolated image is compared with the obtained compounded HR image.

149

Table 7-4: Calculation of CNR and SNR of the compounded HR volumetric image

	CNRCyst1	CNRCyst2	CNRCyst3	SNR
Compounded HR Image	0.1979	0.2179	0.4786	32.7740

Interpolated Image   Compounded HR Image
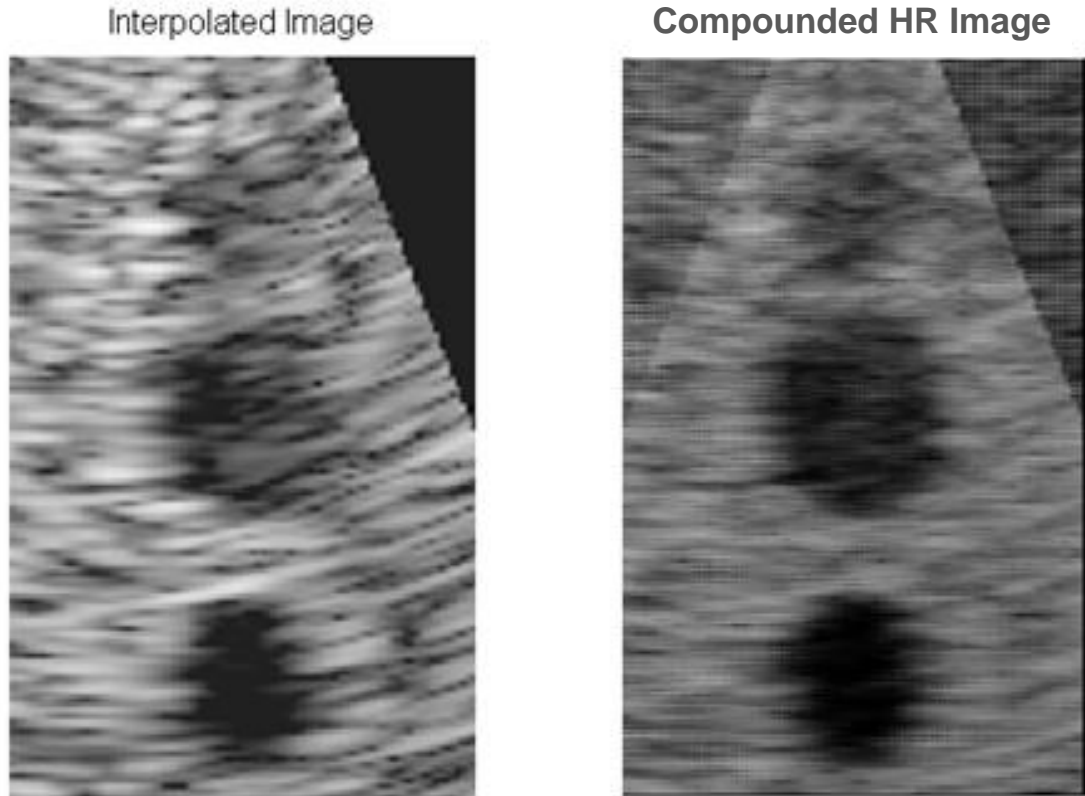
Figure 7-10: Comparison between the interpolated volumetric image and the

compounded HR image

Both the table and the figure illustrate the significance of improvement. One drawback of the implemented SR algorithm is that manifest the chessboard effect and that the images appeared to be a little over-smoothed.

7.4.3 Enhanced Super Resolution

In the enhanced super resolution image that was produced after image multiplication and a histogram equalization with sigmoid as a mapping function, those two artifacts appears to be significantly reduced. The orthogonal slices presented in Figure 7-11, manifest the achieved betterment on the quality for the final image. All the cysts are perfectly delineated. The improvement is obvious in all orthogonal planes. The undesired noise seems to have been completely removed, while the image maintains the speckle characteristics
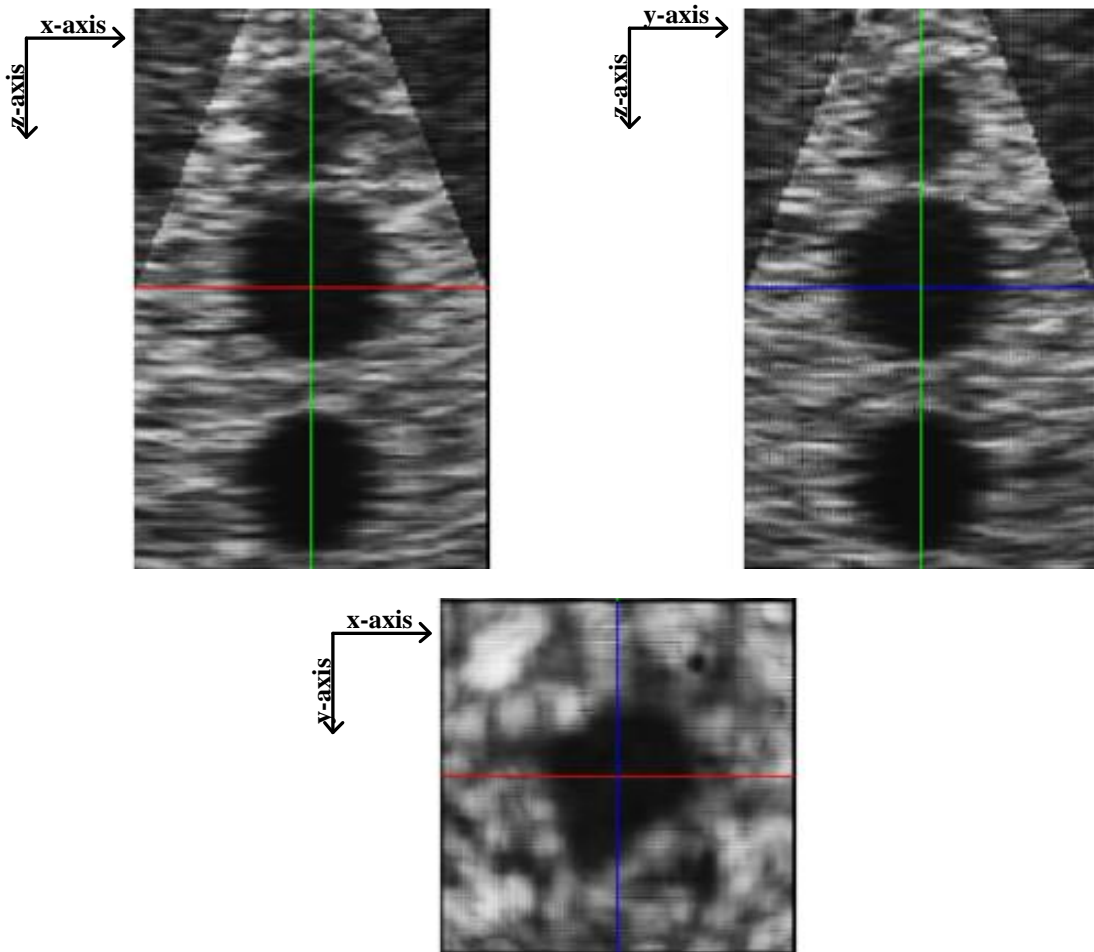
Figure 7-11: Orthogonal slices of the enhanced HR volumetric image

151

In Table 7-5, the performance measures for the case of the final enhanced HR image are given, while in Figure 7-12 the final obtained image is compared with the one of the original interpolated images.

Table 7-5: Calculation of CNR and SNR of the enhanced HR volumetric image

	CNRCyst1	**CNRCyst2**	**CNRCyst3**	**SNR**
Enhanced SR Image	0.4154	0.3263	0.5471	19.4425
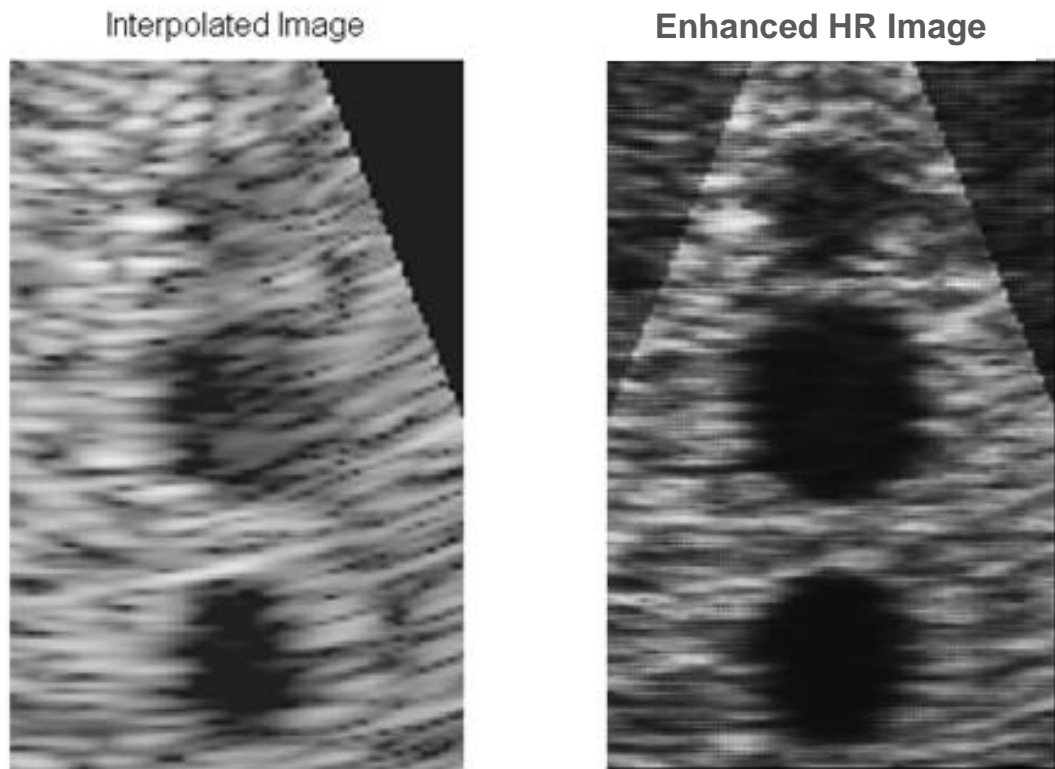
Figure 7-12: Comparison between the interpolated volumetric image and the enhanced

HR image

152

In the following table (Table 7-6) the cumulative results are presented, while in Table 7-7 and Table 7-8 the percentage improvement for all CNR and the SNR has been calculated for the case of Compounded HR image and the enhanced HR image.

Table 7-6: Comparative table with CNR and SNR for all abovementioned imaging techniques

Techniques	CNRCyst1	CNRCyst2	CNRCyst3	SNR
Enhanced SR	**0.4154**	**0.3263**	**0.5471**	**19.4425**
Comp SR	**0.1979**	**0.2179**	**0.4786**	**32.7740**
Interpolated Image1	0.1443	0.1867	0.3496	16.6836
Interpolated Image2	0.1292	0.1398	0.3700	16.1310
Interpolated Image3	0.1670	0.1811	0.3469	16.9079
Interpolated Image4	0.1422	0.1565	0.3425	16.1588
Interpolated Image5	0.1637	0.1593	0.3499	16.7861
Interpolated Image6	0.1399	0.1314	0.3250	16.8639
Interpolated Image7	0.1389	0.1525	0.3105	17.4317
Interpolated Image8	0.1028	0.1743	0.3223	16.6918

Table 7-7: Percentage improvement in CNR and SNR between Compounded SR and interpolated images

Compounded SR				
Techniques	CNRCyst1	CNRCyst2	CNRCyst3	SNR
Interpolated Image1	37.1%	16.7%	36.9%	96.4%
Interpolated Image2	53.2%	55.9%	29.4%	103.2%
Interpolated Image3	18.5%	20.3%	38.0%	93.8%
Interpolated Image4	39.2%	39.2%	39.7%	102.8%
Interpolated Image5	20.9%	36.8%	36.8%	95.2%
Interpolated Image6	41.5%	65.8%	47.3%	94.3%
Interpolated Image7	42.5%	42.9%	54.1%	88.0%
Interpolated Image8	92.5%	25.0%	48.5%	96.3%

153

Enhanced SR

Techniques	CNRCyst1	CNRCyst2	CNRCyst3	SNR
Interpolated Image1	187.9%	74.8%	56.5%	16.5%
Interpolated Image2	221.5%	133.4%	47.9%	20.5%
Interpolated Image3	148.7%	80.2%	57.7%	15.0%
Interpolated Image4	192.1%	108.5%	59.7%	20.3%
Interpolated Image5	153.8%	104.8%	56.4%	15.8%
Interpolated Image6	196.9%	148.3%	68.3%	15.3%
Interpolated Image7	199.1%	114.0%	76.2%	11.5%
Interpolated Image8	304.1%	87.2%	69.7%	16.5%

As it is observed in Table 7-8 the improvement of CNR varies from 47.9% to 304.1% while for the SNR form 11.5% to 20.5%. The results seems to be quite satisfying. At this point, is worth highlighting that although the improvement in the SNR doesn't seem to be that high, this doesn't mean that the de-noising wasn't that effective. On the contrary, it is obvious form Figure 7-12 that most of the noisy voxels that lie inside the cysts have been disappeared. This is has been achieved without oversmoothing the rest of the image. For all the above the algorithm seem to be quite effective in undesired noise reduction, while at the same time maintains the images inherent characteristics.

7.4.4   Image Segmentation

In order to evaluate the achieved improvement in image quality, a 3D image segmentation algorithm using simple threslholding was implemented applied to the interpolated images, as well as to the final enhanced HR image. Assuming that cysts represent dark areas with values close to 0 in the grayscale level and knowing their dimensions and exact location inside the cyst phantom, it was a detrimental task to calculate

154

the percentage of correctly identified voxels (voxels that were correctly identified to be part of the cyst) in the two cases (before and after the methodology). In the following figures, the results of the segmentation for the 3 first cyst before and after applying the image enhancement methodology are presented.
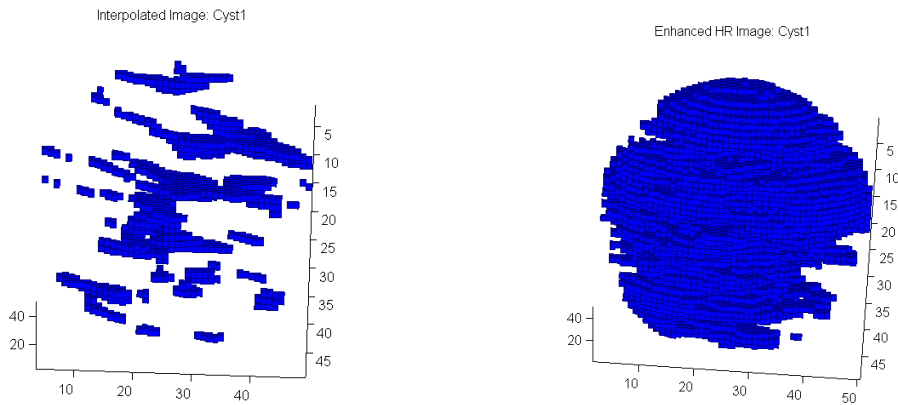
Figure 7-13: Obtained results after applying segmentation on cyst 1 left) Interpolated image 1 and right) Enhanced HR image
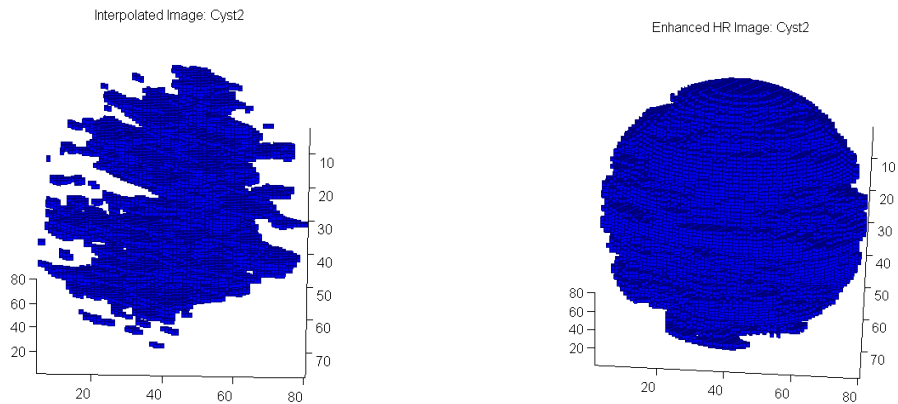
Figure 7-14: Obtained results after applying segmentation on cyst 2 left) Interpolated image 1 and right) Enhanced HR image

155
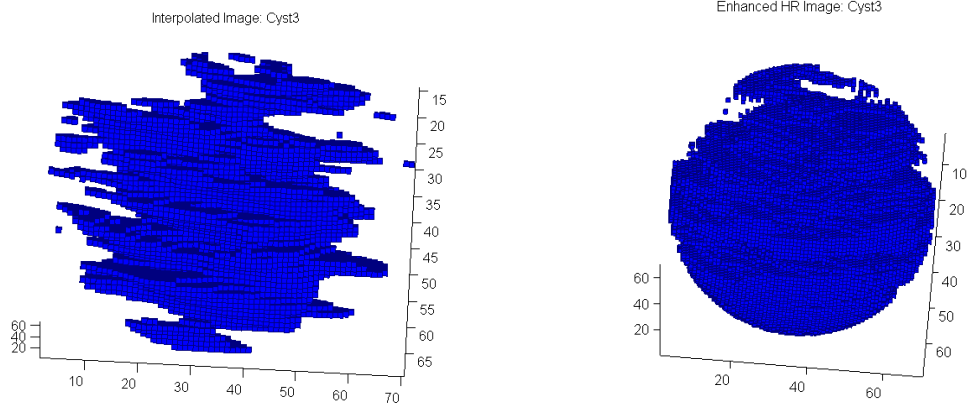
Figure 7-15: Obtained results after applying segmentation on cyst 3 left) Interpolated image 1 and right) Enhanced HR image

From Figure 7-13 and Figure 7-15, the improvement in outcome of the segmentation is apparent. In order to quantify those results, the ratio of the correctly identified voxels to the total volume of the cysts was calculated and given in Table 7-9 and Table 7-10 for the original interpolated image 1 and the final enhanced HR image respectively.

Table 7-9: Image 1: Percentage of correctly identified voxels for three cysts

	CNRCyst1	CNRCyst2	CNRCyst3
Correct (voxels)	2134	44738	44900
Total (voxels)	65267	267761	179579
Percentage (%)	3.27	16.71	25.00

Table 7-10 Enhanced HR Image: Percentage of correctly identified voxels for the three cysts

	CNRCyst1	CNRCyst2	CNRCyst3
Correct (voxels)	37250	212898	130942
Total (voxels)	65267	267761	179579
Percentage (%)	57.07	79.51	72.92

156

Comparing Figure 7-13 to Figure 15, useful conclusions can be conducted. It is obvious that after applying the methodology, even a simple image segmentation algorithm can produce quite accurate results. All the identified cysts in the case of the Enhanced HR image, appear to be quite dense and to have the correct shape (spherical). Finally, comparing Table 7-9 with Table 7-10, the increase in percentage of correctly characterized voxels is more than obvious. The aforementioned results increase our confidence that a more complex 3D image segmentation algorithms can be applied directly to the enhanced image and automatically extract the ROIs and provide these regions to the doctors.

7.5 Conclusions

The obtained results of the enhanced HR image revealed a significant improvement in the CNR up to 304.1% depending on the size and the location of the cysts inside the phantom. The corresponding improvement for the SNR was recorded to be up to 20.5%. The methodology manages to reduce speckle noise without oversmoothing the image. Visually, a significant improvement is observed comparing the obtained image after applying the methodology and the interpolated one capture by a single transducer. The improvement can be assessed by the revealing new structures as well as the much better boundary delineation. Overall, it can be safely stated that the proposed 3D image enhancement methodology is more than suitable to exploit the potentials of the proposed 3D multi transducer system.

8
CONCLUSIONS

8.1 Recapitulation

One of the objectives of the current work was to investigate possible shortcomings, challenges and areas that are amenable for further improvement, in the field of POC monitoring and especially for POC imaging systems in order to come up with a novel system in field. In the second chapter, a survey on different types of POC sensor – based systems for monitoring applications was presented as an intention to reveal scientific fields that require further attention from researchers and designers. A metric to assess the maturity level of each examined device and another one to weight the contribution of various scientific areas responsible for the final outcome was developed. In that way, we identified of certain systems that require efforts to achieve an acceptable maturity score was possible, in order to focus on those systems.

Throughout this dissertation research, it was obvious that imaging point-of-care systems are not as widely spread as the systems for physiological signal monitoring. For

this particular reason, the focus of the current study was the very promising ultrasound systems. In Chapter 3, the background of ultrasound imaging systems was presented and the limitations, artifacts and challenges of such systems were revealed. Under these circumstances a novel ultrasound system for low – power POC applications with extended capabilities with respect to the current ones was proposed in Chapter 4. In Chapter 5, the ultrasound imaging techniques applied in current systems were discussed, and a new methodology based on the novel architecture for ultrasound image enhancement was proposed. The results of the aforementioned methodology applied for 2D ultrasound images were presented in Chapter 6. Finally, in Chapter 7, the methodology presented in Chapter 5, was applied for 3D simulated ultrasound images. The proposed 3D image enhancement methodology was based on the transducers configuration presented in Chapter 4. Below we state the major findings and conclusions of our study, as well as future work needed for further extension of our task, which entails the study and design of novel low-cost, low-power ultrasound machine, for POC abdominal region monitoring.

8.2 Conclusions

Herein the most important conclusions drawn throughout this study, are pointed out:

- First of all, the performed survey in Chapter 2 highlighted several technological advancements during the last decades that have been the driving forces for the production of numerous wearable or even implantable medical devices, for a wide variety of medical applications. Although the heterogeneity of those devices and the prominent role they may play in the betterment of the current healthcare system

159

is significant, it was clear that there is still room for improvements in order for POC devices to be fully functional and incorporated in today's healthcare system. Moreover, there are major trade-offs for both wearable and implantable devices which further drove this study to focus on designing and developing a novel ultrasound machine with enhanced capabilities.

- Due to the basic principle of the proposed portable ultrasound design to reduce the required time for region scanning (and increase the FR), the resolution of the image that could be obtained was degraded. The loss in the resolution was compensated by taking advantage of the multiple transducers and the overlapped areas created. In particular, the phased $-$ sub $-$ array (PSA) technique during the beamforming procedure contributed significantly to the reduction of the system complexity and the number of hardware components required.

- A clear improvement on the final 2D image produced by applying the proposed image enhancement methodology was observed. The betterment of the resolution was obvious even by visual inspection and several hidden structures in the original images were revealed of hidden structures whereas clear delineation of certain boundaries was achieved.

- As it was anticipated the results of the 3D version of the methodology present similar and even better behavior. For the 3D case, a new super resolution algorithm was developed, based on the well-known POCS SR algorithm. The difference is that each voxel in the HR grid is calculated based on global and local information introduced by the configuration of the transducers. The obtained results of the enhanced HR image revealed a significant improvement in the CNR up to 304.1%,

160

depending on the size and the location of the cysts inside the phantom. The corresponding improvement for the SNR was recorded to be up to 20.5%. The methodology manages to reduce speckle noise without over smoothing the image. Visually, a significant improvement was observed comparing the obtained image after applying the methodology and the interpolated one capture by a single transducer. The improvement can be assessed by the revealing new structures as well as the much better boundary delineation.

- Overall, it can be safely stated that the proposed 3D image enhancement methodology is more than suitable to exploit the potentials of the proposed 3D multi transducer system.

8.3 Future Work

The current dissertation research study can be the starting point towards more exhaustive work in the field of medical ultrasonics. The potential of ultrasound imaging systems, given the currently conducted research in the field of digital electronics, image enhancement and in particular in image reconstruction and super resolution techniques is limitless. For all those reasons, the current work could be further extended. Potential additions that can be applied are the following:

- Further improvement in the design of the 2D phased array transducer could be investigated.

- A better beamforming scheme may be applied in order to produce either faster of better results. The possibility of use parallel or adaptive beamforming could be examined.

161

- Other 3D super resolution techniques could be tested and evaluated. In particular, an SR technique for the overlapped regions, during image reconstruction seem quite attractive for the proposed configuration.

- We anticipate that the current study will be the driving force for the actual development of a prototype of the aforementioned system in order to test its capabilities in practice.

162

REFERENCES

[1]   Kost, G. J. (1995). Guidelines for point-of-care testing. Improving patient outcomes. American journal of clinical pathology, 104(4 Suppl 1), S111-27.

[2]   Gatzoulis, L., & Iakovidis, I. (2007). Wearable and portable eHealth systems.*Engineering in Medicine and Biology Magazine, IEEE*, *26*(5), 51-56.

[3]   Husten, C. G., Lewin, L. S., Marks, J. S., Fielding, J. E., & Sanchez, E. J. (2009). *The economic argument for disease prevention: distinguishing between value and savings*. Partnership for Prevention.

[4]   Ward, S. A., Parikh, S., & Workman, B. (2011). Health perspectives: international epidemiology of ageing. *Best Practice & Research Clinical Anaesthesiology*, *25*(3), 305-317.

[5]   Harvey, A., Brand, A., Holgate, S. T., Kristiansen, L. V., Lehrach, H., Palotie, A., & Prainsack, B. (2012). The future of technologies for personalised medicine.*New biotechnology*, *29*(6), 625-633.

[6]   Onuki, Y., Bhardwaj, U., Papadimitrakopoulos, F., & Burgess, D. J. (2008). A review of the biocompatibility of implantable devices: current challenges to overcome foreign body response. *Journal of diabetes science and technology*,*2*(6), 1003-1015.

[7]   Ziegler, A., Koch, A., Krockenberger, K., & Großhennig, A. (2012). Personalized
        medicine using DNA biomarkers: a review. *Human genetics*, *131*(10), 1627-1638.

[8]   Mascini, M., & Tombelli, S. (2008). Biosensors for biomarkers in medical
        diagnostics. *Biomarkers*, *13*(7-8), 637-657.

[9]   Moore, C. L., & Copel, J. A. (2011). Point-of-care ultrasonography. *New England
        Journal of Medicine*, *364*(8), 749-757.

[10]   Morris, T. J., Pajak, J., Havlik, F., Kenyon, J., & Calcagni, D. (2006). Battlefield
        medical information system–tactical (BMIST): the application of mobile computing
        technologies   to   support   health   surveillance   in   the   Department   of
        Defense. *Telemedicine Journal & e-Health*, *12*(4), 409-416.

[11]   Wise, K. D. (2007). Integrated sensors, MEMS, and microsystems: Reflections on a
        fantastic voyage. *Sensors and Actuators A: Physical*, *136*(1), 39-50.

[12]   Fox, A., Griffith, R., Joseph, A., Katz, R., Konwinski, A., Lee, G., & Stoica, I.
        (2009). Above the clouds: A Berkeley view of cloud computing. *Dept. Electrical
        Eng.   and   Comput.   Sciences,   University   of   California,   Berkeley,   Rep.
        UCB/EECS*, *28*, 13.

[13]   Weiland, J. D., & Humayun, M. S. (2008). Visual prosthesis. *Proceedings of the
        IEEE*, *96*(7), 1076-1084.

[14]   Fayad, J. N., Otto, S. R., Shannon, R. V., & Brackmann, D. E. (2008). Cochlear and
        Brainstem Auditory Prostheses``Neural Interface for Hearing Restoration: Cochlear
        and Brain Stem Implants". *Proceedings of the IEEE*, *96*(7), 1085.

164

[15] Turner, J. A., Loeser, J. D., Deyo, R. A., & Sanders, S. B. (2004). Spinal cord stimulation for patients with failed back surgery syndrome or complex regional pain syndrome: a systematic review of effectiveness and complications. *Pain*,*108*(1), 137-147.

[16] Coffey, R. J. (2009). Deep brain stimulation devices: a brief technical history and review. *Artificial organs*, *33*(3), 208-220.

[17] Staples, M. (2010). Microchips and controlled-release drug reservoirs. *Wiley Interdisciplinary Reviews: Nanomedicine and Nanobiotechnology*, *2*(4), 400-417.

[18] Oresko, J. J., Jin, Z., Cheng, J., Huang, S., Sun, Y., Duschl, H., & Cheng, A. C. (2010). A wearable smartphone-based platform for real-time cardiovascular disease detection via electrocardiogram processing. *IEEE Transactions on Information Technology in Biomedicine*, *14*(3), 734-740.

[19] Jaw, F. S., Tseng, Y. L., & Jang, J. K. (2010). Modular design of a long-term portable recorder for physiological signals. *Measurement*, *43*(10), 1363-1368.

[20] Brown, L., Van de Molengraft, J., Yazicioglu, R. F., Torfs, T., Penders, J., & Van Hoof, C. (2010, August). A low-power, wireless, 8-channel EEG monitoring headset. In *Engineering in Medicine and Biology Society (EMBC), 2010 Annual International Conference of the IEEE* (pp. 4197-4200). IEEE.

[21] Patel, S., Lorincz, K., Hughes, R., Huggins, N., Growdon, J., Standaert, D. & Bonato, P. (2009). Monitoring motor fluctuations in patients with Parkinson's disease using wearable sensors. *, IEEE Transactions on Information Technology in Biomedicine,13* (6), 864-873.

165

[22] Poh, M. Z., Swenson, N. C., & Picard, R. W. (2010). A wearable sensor for unobtrusive, long-term assessment of electrodermal activity. *IEEE Transactions on Biomedical Engineering*, *57*(5), 1243-1252.

[23] Rickard, J., Ahmed, S., Baruch, M., Klocman, B., Martin, D. O., & Menon, V. (2011). Utility of a novel watch-based pulse detection system to detect pulselessness in human subjects. *Heart Rhythm*, *8*(12), 1895-1899.

[24] Kim, G. D., Yoon, C., Kye, S. B., Lee, Y., Kang, J., Yoo, Y., & Song, T. K. (2012). A single FPGA-based portable ultrasound imaging system for point-of-care applications. *IEEE Transactions on Ultrasonics, Ferroelectrics, and Frequency Control, 59*(7), 1386-1394.

[25] Cheong, J. H., Ng, S. S. Y., Liu, X., Xue, R. F., Lim, H. J., Khannur, P. B.& Je, M. (2012). An inductively powered implantable blood flow sensor microsystem for vascular grafts. *IEEE Transactions on Biomedical Engineering, 59*(9), 2466-2475.

[26] Valdastri, P., Menciassi, A., Arena, A., Caccamo, C., & Dario, P. (2004). An implantable telemetry platform system for in vivo monitoring of physiological parameters. *IEEE Transactions on Information Technology in Biomedicine, 8*(3), 271-278.

[27] Troughton, R. W., Ritzema, J., Eigler, N. L., Melton, I. C., Krum, H., Adamson, P. B. & Homeostasis Investigators. (2011). Direct left atrial pressure monitoring in severe heart failure: long-term sensor performance. *Journal of cardiovascular translational research*, *4*(1), 3-13.

166

[28] Cong, P., Ko, W. H., & Young, D. J. (2010). Wireless batteryless implantable blood pressure monitoring microsystem for small laboratory animals. *Sensors Journal, IEEE*, *10*(2), 243-254.

[29] Leonardi, M., Pitchon, E. M., Bertsch, A., Renaud, P., & Mermoud, A. (2009). Wireless contact lens sensor for intraocular pressure monitoring: assessment on enucleated pig eyes. *Acta ophthalmologica*, *87*(4), 433-437.

[30] Meng, X., Kawoos, U., Huang, S. M., Tofighi, M. R., & Rosen, A. (2012, June). Implantable wireless devices for the monitoring of intracranial pressure. *16th International Symposium on Consumer Electronics (ISCE), 2012 IEEE* (pp. 1-2).

[31] Kawoos, U., Warty, R., Tofighi, M. R., Kralick, F. A., Yoo, D., Neal, T., & Rosen, A. (2009, January). Embedded microwave system for monitoring of intracranial pressure. In *Radio and Wireless Symposium, 2009. RWS'09. IEEE* (pp. 119-122).

[32] Fletter, P. C., Majerus, S., Cong, P., Damaser, M. S., Ko, W. H., Young, D. J., & Garverick, S. L. (2009, June). Wireless micromanometer system for chronic bladder pressure monitoring. *2009 Sixth International IEEE Conference* in *Networked Sensing Systems (INSS)* (pp. 1-4).

[33] Karargyris, A., & Bourbakis, N. (2010). Wireless capsule endoscopy and endoscopic imaging: A survey on various methodologies presented. *Engineering in Medicine and Biology Magazine, IEEE*, *29*(1), 72-83.

[34] Mohammed, M. I., & Desmulliez, M. P. (2011). Lab-on-a-chip based immunosensor principles and technologies for the detection of cardiac biomarkers: a review. *Lab on a Chip*, *11*(4), 569-595.

167

[35] Mastrototaro, J. J. (2000). The MiniMed continuous glucose monitoring system.*Diabetes technology & therapeutics*, *2*(1, Supplement 1), 13-18.

[36] Pantelopoulos, A., & Bourbakis, N. G. (2010). A survey on wearable sensor-based systems for health monitoring and prognosis. *Systems, Man, and Cybernetics, Part C: Applications and Reviews, IEEE Transactions on*, *40*(1), 1-12.

[37] Tsakalakis, M., & Bourbakis, N. G. (2014, August). Health care sensor—Based systems for point of care monitoring and diagnostic applications: A brief survey. In *Engineering in Medicine and Biology Society (EMBC), 2014 36th Annual International Conference of the IEEE* (pp. 6266-6269).

[38] Yang, J., DeRidder, N., Ume, C., & Jarzynski, J. (1993). Non-contact optical fibre phased array generation of ultrasound for non-destructive evaluation of materials and processes. *Ultrasonics*, *31*(6), 387-394.

[39] Holmes, C., Drinkwater, B. W., & Wilcox, P. D. (2005). Post-processing of the full matrix of ultrasonic transmit–receive array data for non-destructive evaluation. *NDT & E International*, *38*(8), 701-711.

[40] Borenstein, J., & Koren, Y. (1988). Obstacle avoidance with ultrasonic sensors. *IEEE Journal of Robotics and Automation, 4*(2), 213-218.

[41] Ward, A., Jones, A., & Hopper, A. (1997). A new location technique for the active office. *Personal Communications, IEEE*, *4*(5), 42-47.

[42] Pedersen, J. F. (1980). Ultrasound evidence of sexual difference in fetal size in first trimester. *British medical journal*, *281*(6250), 1253.

[43] Badea, R., & Ioanitescu, S. (2012). *Ultrasound Imaging of Liver Tumors-Current Clinical Applications*. INTECH Open Access Publisher.

[44] Reuwer, P. J. H. M., Rietman, G. W., Sijmons, E. A., Van Tiel, M. W. M., & Bruinse, H. W. (1987). Intrauterine growth retardation: prediction of perinatal distress by Doppler ultrasound. *The Lancet*, *330*(8556), 415-418.

[45] Malizos, K. N., Hantes, M. E., Protopappas, V., & Papachristos, A. (2006). Low-intensity pulsed ultrasound for bone healing: an overview. *Injury*, *37*(1), S56-S62.

[46] Siegel, R. J., & Luo, H. (2008). Ultrasound thrombolysis. *Ultrasonics*, *48*(4), 312-320.

[47] Newman, C. M. H., & Bettinger, T. (2007). Gene therapy progress and prospects: ultrasound for gene transfer. *Gene therapy*, *14*(6), 465-475.

[48] Walmsley, A. D. (1988). Applications of ultrasound in dentistry. *Ultrasound in medicine & biology*, *14*(1), 7-14.

[49] Tobis, J. M., Mallery, J., Mahon, D., Lehmann, K., Zalesky, P., Griffith, J. & Dwyer, M. L. (1991). Intravascular ultrasound imaging of human coronary arteries in vivo. Analysis of tissue characterizations with comparison to in vitro histological specimens. *Circulation*, *83*(3), 913-926.

[50] Volpicelli, G., Elbarbary, M., Blaivas, M., Lichtenstein, D. A., Mathis, G., Kirkpatrick, A. W. & Petrovic, T. (2012). International evidence-based recommendations for point-of-care lung ultrasound. *Intensive care medicine*,*38*(4), 577-591.

169

[51] Sofuni, A., Iijima, H., Moriyasu, F., Nakayama, D., Shimizu, M., Nakamura, K. & Itoi, T. (2005). Differential diagnosis of pancreatic tumors using ultrasound contrast imaging. *Journal of gastroenterology*, *40*(5), 518-525.

[52] Ali, M., Magee, D., & Dasgupta, U. (2008). Signal processing overview of ultrasound systems for medical imaging. *SPRAB12, Texas Instruments, Texas*.

[53] Hunt, J. W., Arditi, M., & Foster, F. S. (1983). Ultrasound transducers for pulse-echo medical imaging. *IEEE Transactions on Biomedical Engineering,* (8), 453-481.

[54] Havlice, J. F., & Taenzer, J. C. (1979). Medical ultrasonic imaging: An overview of principles and instrumentation. *Proceedings of the IEEE*, *67*(4), 620-641.

[55] Morgan, C. L., Trought, W. S., Clark, W. M., von Ramm, O. T., & Thurstone, F. L. (1978). Principles and applications of a dynamically focused phased array real time ultrasound system. *Journal of Clinical Ultrasound*, *6*(6), 385-391.

[56] Kossoff, G. (1979). Analysis of focusing action of spherically curved transducers. *Ultrasound in medicine & biology*, *5*(4), 359-365.

[57] Eggleton, R. C., & Johnston, K. W. (1975, February). Real time B-mode mechanical scanning system. In *Application of Optical Instrumentation in Medicine III* (pp. 96-100). International Society for Optics and Photonics.

[58] Wildes, D. G., Chiao, R. Y., Daft, C. M., Rigby, K. W., Smith, L. S., & Thomenius, K. E. (1997). Elevation performance of 1.25 D and 1.5 D transducer arrays. *IEEE*

Transactions on Ultrasonics, Ferroelectrics, and Frequency Control, 44(5), 1027-1037.

[59]   Thomenius, K. E. (1996, November). Evolution of ultrasound beamformers. In*Ultrasonics Symposium, 1996. Proceedings of the IEEE* (Vol. 2, pp. 1615-1622). IEEE.

[60]   Bajura, M., Fuchs, H., & Ohbuchi, R. (1992, July). Merging virtual objects with the real world: Seeing ultrasound imagery within the patient. In *ACM SIGGRAPH Computer Graphics* (Vol. 26, No. 2, pp. 203-210). ACM.

[61]   Fenster, A., Downey, D. B., & Cardinal, H. N. (2001). Three-dimensional ultrasound imaging. *Physics in medicine and biology*, *46*(5), R67.

[62]   Oralkan, Ö., Johnson, J., Karaman, M., Demirci, U., Kaviani, K., Lee, T. H., & Khuri-Yakub, B. T. (2002). Capacitive micromachined ultrasonic transducers: Next-generation arrays for acoustic imaging?. *IEEE Transactions on Ultrasonics, Ferroelectrics, and Frequency Control, 49*(11), 1596-1610.

[63]   Insana, M. F., Wagner, R. F., Garra, B. S., Brown, D. G., & Shawker, T. H. (1986). Analysis of ultrasound image texture via generalized Rician statistics.*Optical Engineering*, *25*(6), 256743-256743.

[64]   Meir, A., & Rubinsky, B. (2009). Distributed network, wireless and cloud computing enabled 3-D ultrasound; a new medical technology paradigm. *PloS one*, *4*(11), e7974.

171

[65] Basak, A., Ranganathan, V., & Bhunia, S. (2013, January). A wearable ultrasonic assembly for point-of-care autonomous diagnostics of malignant growth. In *Point-of-Care Healthcare Technologies (PHT), 2013 IEEE* (pp. 128-131).

[66] Szabo, T. L. (2004). *Diagnostic ultrasound imaging: inside out*. Academic Press.

[67] Harris, F. J. (2004). *Multirate signal processing for communication systems*. Prentice Hall PTR.

[68] Kim, G. D., Yoon, C., Kye, S. B., Lee, Y., Kang, J., Yoo, Y., & Song, T. K. (2012). A single FPGA-based portable ultrasound imaging system for point-of-care applications. *IEEE Transactions on Ultrasonics, Ferroelectrics, and Frequency Control, 59*(7), 1386-1394.

[69] Lee, H., Sohn, H. Y., Yoon, C., Yoo, Y. M., & Song, T. K. (2009, September). Software-based hand-held ultrasound color Doppler imaging system. In*Ultrasonics Symposium (IUS), 2009 IEEE International* (pp. 1844-1847).

[70] Hwang, J. J., Quistgaard, J., Souquet, J., & Crum, L. (1998). Portable ultrasound device for battlefield trauma. In *Ultrasonics Symposium, 1998. Proceedingsof the IEEE* (Vol. 2, pp. 1663-1667).

[71] Chiang, A. M., Chang, P. P., & Broadstone, S. R. (2000, October). PC-based ultrasound imaging system in a probe. In *Ultrasonics Symposium, 2000 IEEE*(Vol. 2, pp. 1255-1260).

[72] Schneider, F. K., Agarwal, A., Yoo, Y. M., Fukuoka, T., & Kim, Y. (2010). A fully programmable computing architecture for medical ultrasound machines. *IEEE Transactions on Information Technology in Biomedicine, 14*(2), 538-540.

[73] Kim, K. C., Kim, M. J., Joo, H. S., Lee, W., Yoon, C., Song, T. K., & Yoo, Y. (2013, July). Smartphone-based portable ultrasound imaging system: A primary result. In *Ultrasonics Symposium (IUS), 2013 IEEE International* (pp. 2061-2063).

[74] Huang, Q. H., Zheng, Y. P., Lu, M. H., & Chi, Z. R. (2005). Development of a portable 3D ultrasound imaging system for musculoskeletal tissues. *Ultrasonics*,*43*(3), 153-163.

[75] Fuller, M., Blalock, T. N., Hossack, J., & Walker, W. F. (2003, October). A portable, low-cost, highly integrated, 3D medical ultrasound system. *2003 IEEE Symposium on Ultrasonics,* (Vol. 1, pp. 38-41).

[76] Matrone, G., Quaglia, F., & Magenes, G. (2010, August). Modeling and simulation of ultrasound fields generated by 2D phased array transducers for medical applications. In *Engineering in Medicine and Biology Society (EMBC), 2010 Annual International Conference of the IEEE* (pp. 6003-6006).

[77] Austeng, A., & Holm, S. (2002). Sparse 2-D arrays for 3-D phased array imaging-design methods. *IEEE Transactions on Ultrasonics, Ferroelectrics, and Frequency Control, 49*(8), 1073-1086.

[78] Smith, S. W., Trahey, G. E., & Von Ramm, O. T. (1992). Two-dimensional arrays for medical ultrasound. *Ultrasonic Imaging*, *14*(3), 213-233.

[79] Light, E. D., Davidsen, R. E., Fiering, J. O., Hruschka, T. A., & Smith, S. W. (1998). Progress in two-dimensional arrays for real-time volumetric imaging. *Ultrasonic Imaging*, *20*(1), 1-15.

[80] Karaman, M., Wygant, I. O., Oralkan, Ö., & Khuri-Yakub, B. T. (2009). Minimally redundant 2-D array designs for 3-D medical ultrasound imaging. *IEEE Transactions on Medical Imaging*, *28*(7), 1051-1061.

[81] Jensen, J. A., Nikolov, S. I., Gammelmark, K. L., & Pedersen, M. H. (2006). Synthetic aperture ultrasound imaging. *Ultrasonics*, *44*, e5-e15.

[82] Hasegawa, H., & Kanai, H. (2011). High-frame-rate echocardiography using diverging transmit beams and parallel receive beamforming. *Journal of Medical Ultrasonics*, *38*(3), 129-140.

[83] DIARRA, B., Liebgott, H., Tortoli, P., & Cachard, C. (2012). Sparse array techniques for 2D array ultrasound imaging. *no. April*, 1591-1596.

[84] Johnson, J., Karaman, M., & Khuri-Yakub, B. T. (2005). Coherent-array imaging using phased subarrays. Part I: basic principles. *IEEE Transactions on Ultrasonics, Ferroelectrics, and Frequency Control, 52*(1), 37-50.

[85] Synnevåg, J. F., Austeng, A., & Holm, S. (2007). Adaptive beamforming applied to medical ultrasound imaging. *IEEE Transactions on Ultrasonics, Ferroelectrics, and Frequency Control*, *54*(8), 1606-1613.

[86] Rasmussen, M. F., & Jensen, J. (2014). Comparison of 3-D synthetic aperture phased-array ultrasound imaging and parallel beamforming. *IEEE Transactions on Ultrasonics, Ferroelectrics, and Frequency Control, 61*(10), 1638-1650.

[87] Bonavita, J. A., Mayo, J., Babb, J., Bennett, G., Oweity, T., Macari, M., & Yee, J. (2009). Pattern recognition of benign nodules at ultrasound of the thyroid: which nodules can be left alone?. *American Journal of Roentgenology*, *193*(1), 207-213.

[88] Noble, J. A., & Boukerroui, D. (2006). Ultrasound image segmentation: a survey. *IEEE Transactions on Medical Imaging, 25*(8), 987-1010.

[89] Dai, S., Han, M., Wu, Y., & Gong, Y. (2007, July). Bilateral back-projection for single image super resolution. In *Multimedia and Expo, 2007 IEEE International Conference* (pp. 1039-1042).

[90] Farsiu, S., Robinson, M. D., Elad, M., & Milanfar, P. (2004). Fast and robust multiframe super resolution. *IEEE Transactions on Image processing, 13*(10), 1327-1344.

[91] Glasner, D., Bagon, S., & Irani, M. (2009, September). Super-resolution from a single image. In *Computer Vision, 2009 IEEE 12th International Conference* (pp. 349-356).

[92] Parker, K. J. (2012). Superresolution imaging of scatterers in ultrasound B-scan imaging. *The Journal of the Acoustical Society of America*, *131*(6), 4680-4689.

[93] Clement, G. T., Huttunen, J., & Hynynen, K. (2005). Superresolution ultrasound imaging using back-projected reconstruction. *The Journal of the Acoustical Society of America*, *118*(6), 3953-3960.

[94] Tsakallakis, M., & Bourbakis, N. (2013, November). A wearable ultrasound multi-transducer array system for abdominal organs monitoring. In *Bioinformatics and Bioengineering (BIBE), 2013 IEEE 13th International Conference* (pp. 1-5).

[95] Tsakalakis, M., & Bourbakis, N. G. (2014, November). Ultrasound Image Despeckling/Denoising Based on a Novel Multi-transducer Architecture. In *Bioinformatics and Bioengineering (BIBE), 2014 IEEE International Conference* (pp. 62-68).

[96] Park, S. C., Park, M. K., & Kang, M. G. (2003). Super-resolution image reconstruction: a technical overview. *Signal Processing Magazine, IEEE*, *20*(3), 21-36.

[97] Arsenault, H. H., & April, G. (1976). Properties of speckle integrated with a finite aperture and logarithmically transformed. *JOSA*, *66*(11), 1160-1163.

[98] Weng, L., Reid, J. M., Shankar, P. M., & Soetanto, K. (1991). Ultrasound speckle analysis based on the K distribution. *The Journal of the Acoustical Society of America*, *89*(6), 2992-2995.

[99] Joel, T., & Sivakumar, R. (2013). Despeckling of ultrasound medical images: A survey. *Journal of Image and Graphics*, *1*(3), 161-164.

[100] Gehlbach, S. M., & Sommer, F. G. (1987). Frequency diversity speckle processing. *Ultrasonic imaging*, *9*(2), 92-105.

[101] Adam, D., Beilin-Nissan, S., Friedman, Z., & Behar, V. (2006). The combined effect of spatial compounding and nonlinear filtering on the speckle reduction in ultrasound images. *Ultrasonics*, *44*(2), 166-181.

[102] He, P. (1997). Spatial compounding in 3D imaging of limbs. *Ultrasonic imaging*,*19*(4), 251-265.

[103] Rohling, R., Gee, A., & Berman, L. (1997). Three-dimensional spatial compounding of ultrasound images. *Medical Image Analysis*, *1*(3), 177-193.

[104] Khare, A., Khare, M., Jeong, Y., Kim, H., & Jeon, M. (2010). Despeckling of medical ultrasound images using Daubechies complex wavelet transform. *Signal Processing*, *90*(2), 428-439.

[105] Lazrag, H., & Naceur, M. S. (2012, March). Despeckling of intravascular ultrasound images using curvelet transform. In *Sciences of Electronics, Technologies of Information and Telecommunications (SETIT), 2012 6th International Conference* (pp. 365-369).

[106] Hiremath, P. S., Akkasaligar, P. T., & Badiger, S. (2010). Speckle reducing contourlet transform for medical ultrasound images. *Int J Compt Inf Engg*, *4*(4), 284-291.

[107] Eskicioglu, A. M., & Fisher, P. S. (1995). Image quality measures and their performance. *IEEE Transactions on Communications, 43*(12), 2959-2965.

177

[108] Achim, A., Bezerianos, A., & Tsakalides, P. (2001). Novel Bayesian multiscale method for speckle removal in medical ultrasound images. *IEEE Transactions on Medical Imaging, 20*(8), 772-783.

[109] Sattar, F., Floreby, L., Salomonsson, G., & Lovstrom, B. (1997). Image enhancement based on a nonlinear multiscale method. *IEEE transactions on image processing*, *6*(6), 888-895.

[110] Taxt, T., & Jiřík, R. (2004). Superresolution of ultrasound images using the first and second harmonic signal. *IEEE Transactions on Ultrasonics, Ferroelectrics, and Frequency Control, 51*(2), 163-175.

[111] Clement, G. T., Huttunen, J., & Hynynen, K. (2005). Superresolution ultrasound imaging using back-projected reconstruction. *The Journal of the Acoustical Society of America*, *118*(6), 3953-3960.

[112] Parker, K. J. (2012). Superresolution imaging of scatterers in ultrasound B-scan imaging. *The Journal of the Acoustical Society of America*, *131*(6), 4680-4689.

[113] Jensen, J. A. (1996). Field: A program for simulating ultrasound systems. In *10TH NORDICBALTIC CONFERENCE ON BIOMEDICAL IMAGING, VOL. 4, SUPPLEMENT 1, PART 1: 351--353*.

[114] Jensen, J. A., & Svendsen, N. B. (1992). Calculation of pressure fields from arbitrarily shaped, apodized, and excited ultrasound transducers. *IEEE Transactions on Ultrasonics, Ferroelectrics, and Frequency Control, 39*(2), 262-267.

178

[115] Papoulis, A. (1975). A new algorithm in spectral analysis and band-limited extrapolation. *IEEE Transactions on Circuits and Systems, 22*(9), 735-742.

[116] Irani, M., & Peleg, S. (1991). Improving resolution by image registration.*CVGIP: Graphical models and image processing*, *53*(3), 231-239.

[117] Zomet, A., Rav-Acha, A., & Peleg, S. (2001). Robust super-resolution. In*Computer Vision and Pattern Recognition, 2001. CVPR 2001. Proceedings of the 2001 IEEE Computer Society Conference* (Vol. 1, pp. I-645).

[118] Pham, T. Q., Van Vliet, L. J., & Schutte, K. (2006). Robust fusion of irregularly sampled data using adaptive normalized convolution. *EURASIP Journal on Applied Signal Processing*, *2006*, 236-236.

APPENDIX A

In the following appendix the mathematical equations for the overlapped regions among the transducers are given. The Appendix is divided into two parts. In the first one, the equations of the overlapped regions in the case of 2D circular phased array transducers are presented, while in the second the equations of the overlapped regions in the case of common 2D phased array transducers are described. The design of the proposed system, as well as the proposed methodology was based on the overlapped regions of the multiple sensors. Keeping that in mind, knowing the total volume of the overlapped regions is of great significance. The bigger those regions are the better image quality can be achieved after applying the proposed methodology.

A.1 Mathematical Equations: Circular Phased Array Transducers

In this section, an algorithmic-based mathematical model that represent the overlapping areas and volumes formed by 2x2 circular array transducers is presented. The number of overlaps that are going to be used during image formation and volume reconstruction requires further examination. The calculation of the overlapped area can be approximated through the following algorithmic steps.

180

1. Knowing the exact positions and the technical characteristics of the transducers the depths in which new overlaps are about to be introduced can be calculated. In this trend we divide the axial (z) direction into layers (Figure A- 1)

2. We calculate all the overlapped areas in each layer as a function of the z.

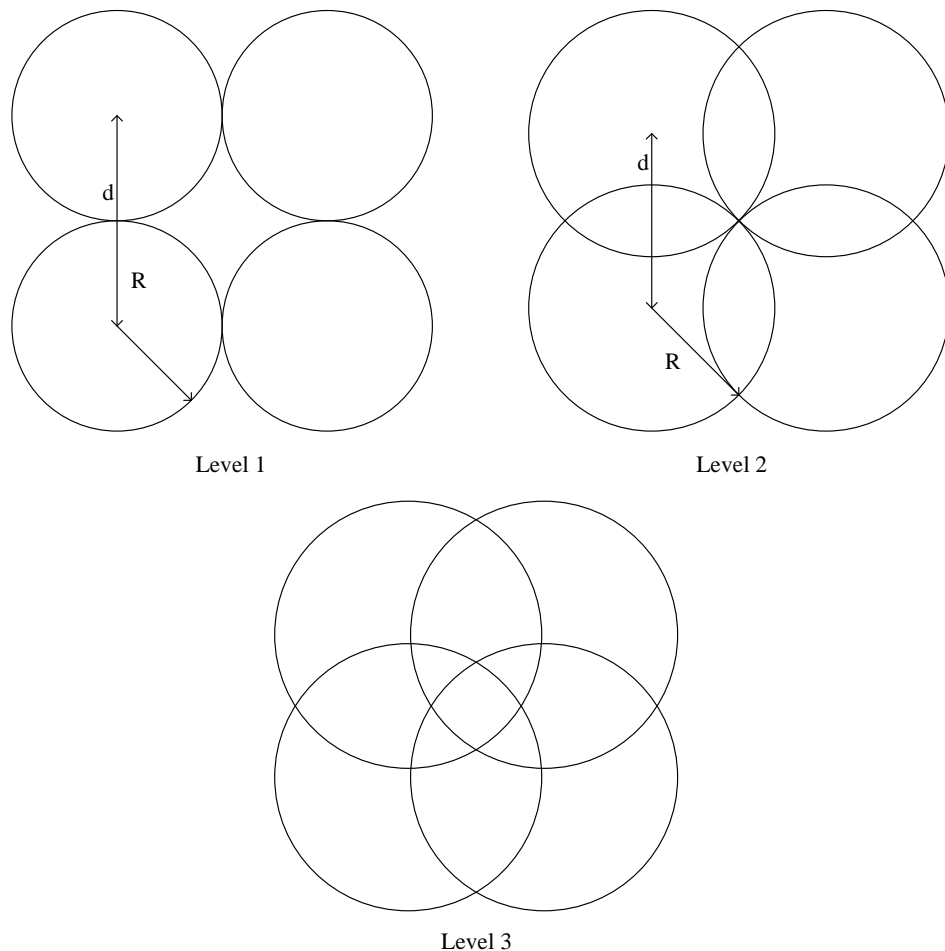3. Integrating from one layer to another in respect to z we obtain the overlapped volume between these layers.

Level 1   Level 2

Level 3

Figure A- 1: The three distinct layers of our approach a) Level 1, b) Level 2 and c)

Level 3

181

The radius of each created circle in each level and the corresponding depth should be:

Level 1: R= d∕2, h_1

Level 2: R= d∕√2, h_2

Level 3: the radius at the maximum recorded depth, h_{max}

The first step is to find the area created by two intersecting circles. This is a simple problem already examined. In order to calculate this overlapped area the area of the circular segment (region Acs in Figure A- 2 a)) needs to be calculated. The area of the circular segment is given from the formula:

$$A_{cs}(R, T_H) = R^2 cos^{-1}\left(\frac{T_H}{R}\right) - T_H\sqrt{R^2 - T_H^2} \qquad \text{(A-1)}$$
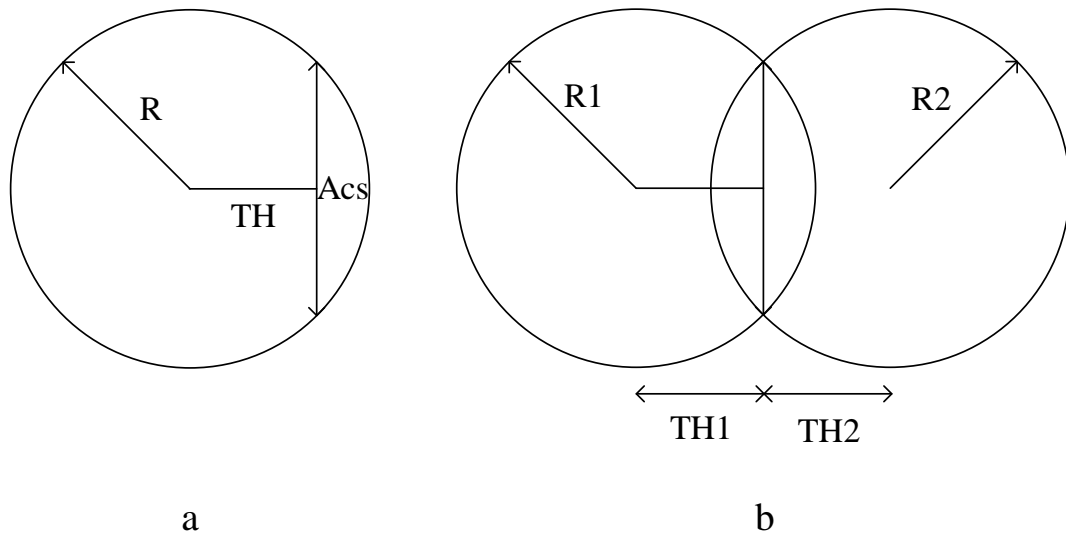

Figure A- 2: a) Representation of a circular segment and b) representation of the intersection of two circles (combination of two circular segments)

182

Thus the total area restricted by two intersecting circles (Figure A- 2 b)) formatted by the cones in depth z into the human body should be:

$$A_{ci} = A_{cs}(R_1, T_{H1}) + A_{cs}(R_2, T_{H2}) \tag{A-2}$$

Where i = 1,2,3,4 and represent one of the 4 overlapped regions in Figure A- 1 Level 2. Due to the assumption that all the transducers will be identical, they will present identical characteristics. Consequently all the intersections observed in Figure A- 1 Level 2 will have the same area. Therefore:

$$R_1 = R_2 = R, \qquad T_{H1} = T_{H2} = T \tag{A-3}$$

$$T_H = \frac{1}{2}\sqrt{d} \tag{A-4}$$

$$A_{ci} = 2R^2 cos^{-1}\left(\frac{\frac{1}{2}\sqrt{d}}{R}\right) - \sqrt{d}\sqrt{R^2 - \frac{1}{4}d} \tag{A-5}$$

Expressing the radius R of the circles in each layer as a function of depth (z) and angle φ and plugging in into the equation A-2 the overlapped area formed by to circles in level 2 can be calculated. Due to the symmetry of the design, all the overlapped areas in level 2 will have the manifest the same area given by the formula:

$$A_{ci}(z) = 2(z * tan\varphi)^2 cos^{-1}\left(\frac{\frac{1}{2}\sqrt{d}}{z*tan\varphi}\right) - \sqrt{d'}\sqrt{(z * tan\varphi)^2 - \frac{1}{4}d} \tag{A-6}$$

Integrating $A_{ci}(z)$ over z from level 1 (which is the depth in which the area begins to form) to level 2 the overlapped volume formed by the known field of view of two consecutive sensors can be calculated. Because of symmetry the volume will be the same

183

for all of the seven overlaps produced by the four sensors and the corresponding formula is given below:

$$V_{ci} = \int_{h1}^{h2} A_{ci}(z)\, dz = 2\int_{h1}^{h2}(z*tan\varphi)^2 cos^{-1}\left(\frac{\frac{1}{2}\sqrt{d}}{z*tan\varphi}\right) dz -$$

$$\sqrt{d}\int_{h1}^{h2}\sqrt{(z*tan\varphi)^2 - \frac{1}{4}d}\, dz \tag{A-7}$$

Regarding the third and the last level in this particular model design, all possible areas of intersection are depicted in Figure A- 3 a). The procedure followed for this case is described bellow:

1　Calculation of the intersecting points P1-P4.

2　Knowing these points we can calculate the area of circular segments generated by the intersection of circles (Figure A- 3 b)). Then, region 4 can be calculated as the addition of the 4 generated circular segments and the rectangular area illustrated in Figure A- 3 c).

3　Due to the symmetry and applying simple subtraction the area of all the other regions can be calculated.

4　Finally, integrating over z from level 2 to level 3 the corresponding volumes can be computed.
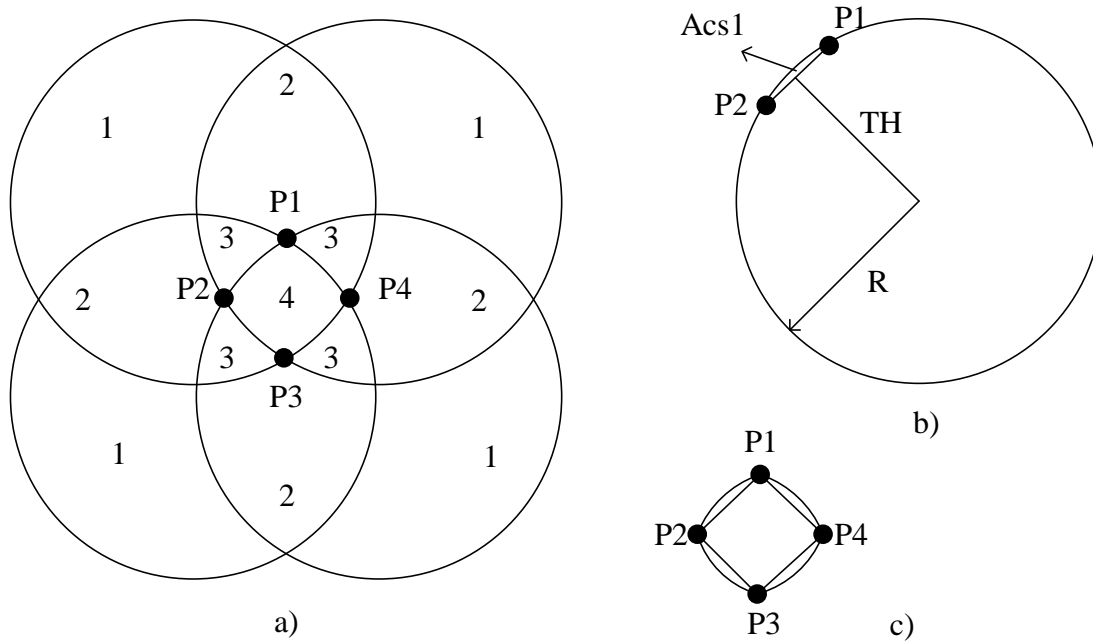
Figure A- 3: a) Overlapped regions for level 3, b) area of the circular segment created by the points P1 and P2 and c) close look of region 4 and the inscribed square.

The functions for the 4 circles at a certain depth are:

$$C_1: x^2 + y^2 = R^2 \tag{A-8}$$

$$C_2: (x - d)^2 + y^2 = R^2 \tag{A-9}$$

$$C_3: x^2 + (y - d)^2 = R^2 \tag{A-10}$$

$$C_4: (x - d)^2 + (y - d)^2 = R^2 \tag{A-11}$$

Solving the above system we get the four points of intersection which are:

$$P_1 = \left(\frac{d}{2}, d \quad -\frac{1}{2}\sqrt{4R^2 - d^2} \right) \tag{A-12}$$

$$P_2 = \left(d \quad -\frac{1}{2}\sqrt{4R^2 - d^{\,2}}, \frac{d}{2} \right) \tag{A-13}$$

185

$$P_3 = \left(\sqrt{R^2 - \frac{d}{4}^2}, \frac{d}{2} \right) \tag{A-14}$$

$$P_4 = \left(\frac{d}{2}, \sqrt{R^2 - \frac{d}{4}^2} \right) \tag{A-15}$$

Distances P1P2, P2P3, P3P4, P4P1 can be computed as a function of z taking into consideration that R= z*tanφ.

$$P_1P_2 = P_2P_3 = P_3P_4 = P_4P_1 = D = \sqrt{2(z * tan\varphi)^2 + \frac{d}{2} - 2d\sqrt{(z * tan\varphi)^2 - \frac{d}{4}}}$$

$$(A-16)$$

Distance TH in Figure A- 3 b) is computed:

$$T_H = \sqrt{(z * tan\varphi)^2 - \frac{(D)^2}{2}} \tag{A-17}$$

Applying in the formula for the circular segment we have the areas for Acs1 = Acs2 = Acs3 = Acs4 = Acs

Thus, the area for region 4 in Figure A- 3 a) is given:

$$A_4 = A_{P1P2P3P4} = 4A_{cs} + (D)^2 \tag{A-18}$$

Integrating from level 2 to level 3 in respect to z the corresponding volume is calculated:

$$V_4 = \int_{h2}^{h\max} A_4 \, dz = \int_{h2}^{h\max} 4A_{cs} + (D)^2 \tag{A-19}$$

Everything that is needed for the above equation is given. All the rest areas can be found by subtraction.

186

A.2 Mathematical Equations: 2D Phased Array Transducers

In this section the algorithmic-based mathematical model to represent the overlapping areas and volumes formed by 2x2 2D phased array transducer configuration is presented. The calculation of the overlapped areas can be achieved following the same reasoning with the previous section. In this case the calculations are much simpler. The procedure presented here has be conducted in order to describe the overlapped regions that can be generated using 2D phased array transducers in the configuration proposed in chapter 4 and illustrated again in Figure A- 4. Depending on the distance among the transducers, as well as on the achieved field of view of the transducers different volumes of overlapped regions can be produced. In this section the mathematical formulas that describe these volumes are explained.
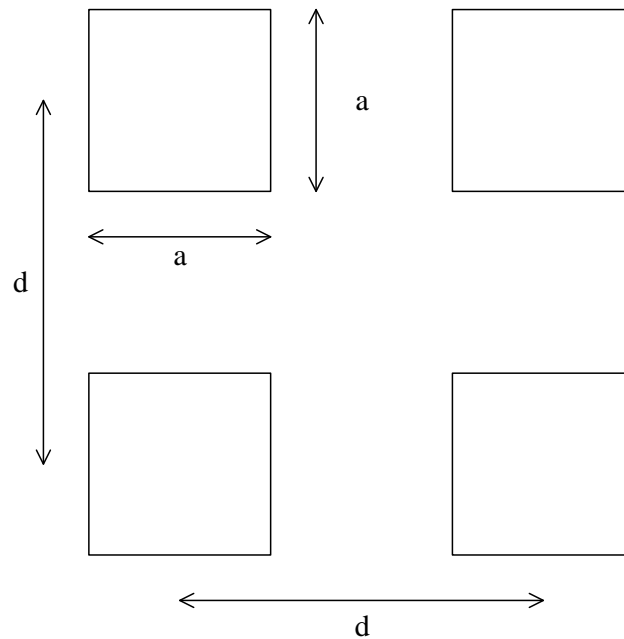

Figure A- 4: Configuration of the transducers for the case of 2D phased array ones

187

Following the same reasoning the different levels for this case are depicted in
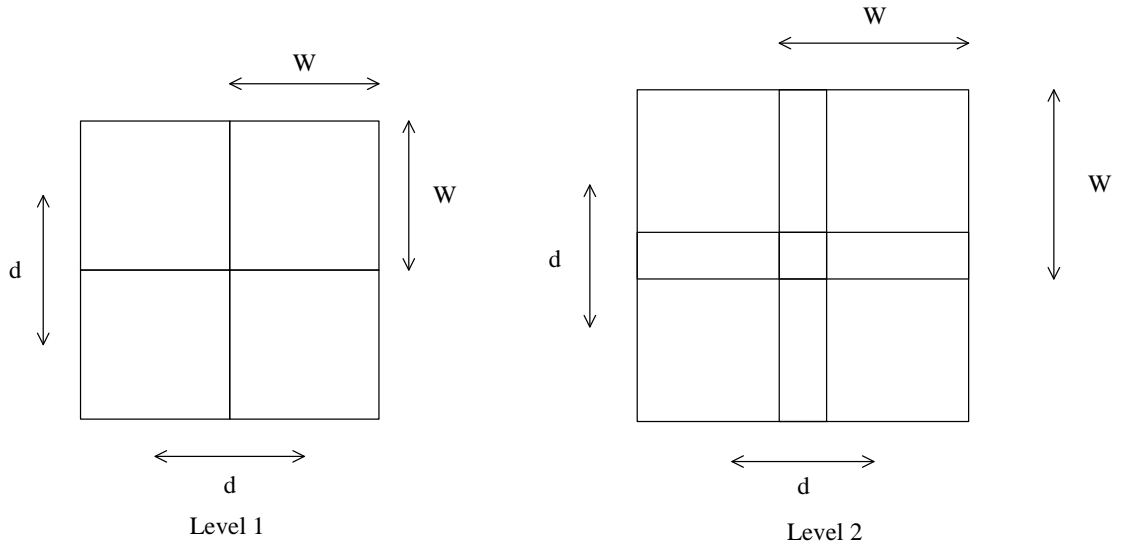

Level 1

Level 2

Figure A- 5 while the dimensions of the formatted areas along with the corresponding depths are given bellow:

Level 1: W= d, h_1
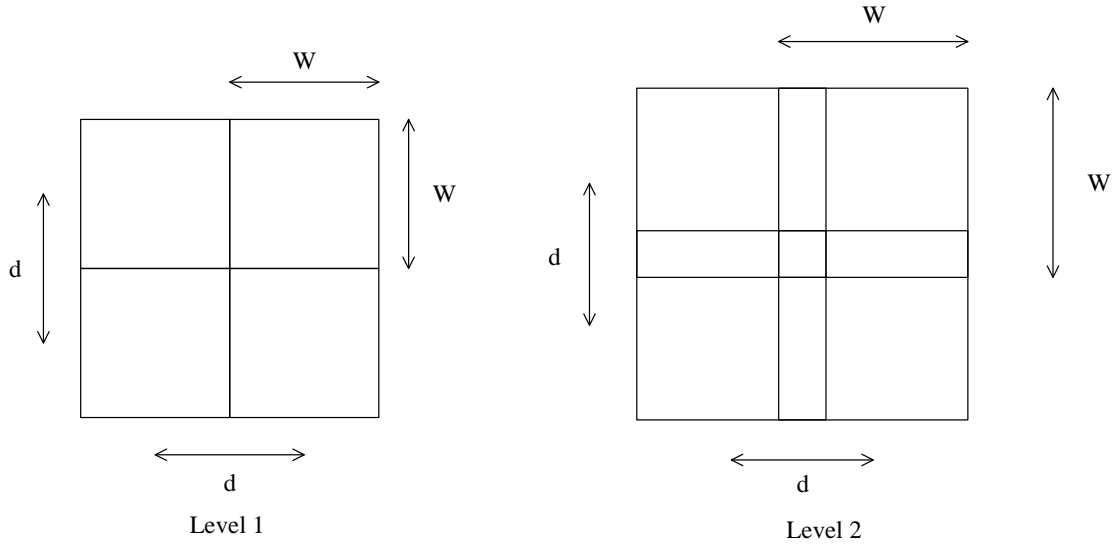
Level 2: W at the maximum depth, h_{max}

188

Figure A- 5: The two distinct layers of overlapped surfaces for the 2D phased array

transducers case

All the overlapped regions generated from Level 1 and bellow are depicted in the following figure. $W1 = W2 = W$ due to the fact that the FOV of the transducers used is the same for both azimuthal and elevation direction. The width of the formatted rectangle is given depending on the depth by the formula:

$$W1 = W2 = W = z * tan\varphi = z * tan\theta \tag{A-20}$$

189

1	2	1
2	4	2
1	2	1

Figure A- 6: Overlapped regions from Level 1 and below

Starting again by calculating the area produced by two consecutive transducers given in
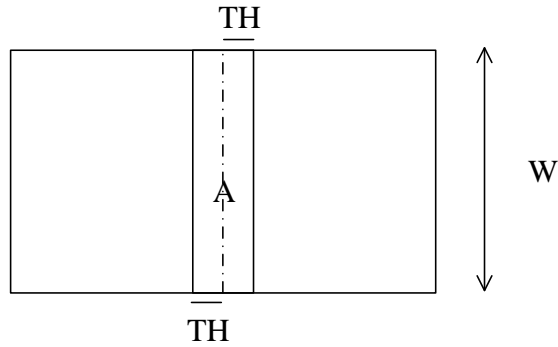

Figure A- 7: Overlapped region for two consecutive transducers

$$TH = (z - h1) * tan\theta \qquad (A-21)$$

Where $(h1) = \frac{d}{2} * tan\theta$. The total area of A is then given using the formula:

$$A = 2 * TH * W = 2 * z * tan^2(\theta) * (z - h1) = 2 * z^2 * tan^2(\theta) - 2 * z * h1 *$$

$$tan^2(\theta) \qquad (A-22)$$

190

The corresponding volume can be easily calculated by integrating from level 1 to level 2

$$V = \int_{h1}^{h\max} A \, dz \tag{A-23}$$

The next step is to compute area of the region 4 (A4) of the Figure A- 6.

$$A_4 = (2 * \text{TH}) * (2 * \text{TH}) = 4 * tan^2(\theta) * (z - h1)^2 \tag{A-24}$$

The corresponding volume can be easily calculated by integrating from level 1 to level 2

$$V_4 = \int_{h1}^{h\max} A_4 \, dz \tag{A-24}$$

The rest areas can be easily computed from simple subtraction. Regions depicted with the symbol 2 in Figure A- 6 can be calculated

$$A_2 = A - A_4 \tag{A-25}$$

The corresponding volume is finally given:

$$V_2 = \int_{h1}^{h\max} A_2 \, dz \tag{A-26}$$

At this point any volume of the produced overlapped regions can be calculated knowing the characteristics and the configuration of the transducers. This can be extremely helpful during the design. Designers might want to maximize the overlapped regions in order to exploit the advantages of the proposed methodology. These formulas may help them towards this direction.

191